3–3 Mineralization

Placer gold is known to occur in Sungai Puteh, some of the tributaries of Sungai Sebuluh and in a few other streams close to Pangkalan Tebang. Prospecting in the past by local prospectors was mainly confined to panning and some pitting and trenching particularly in the vicinity of Sungai Pad and near Pangkalan Tebang. At Bukit Pelanduk just north of the surveyed area a few prospecting pits and trenches in silicified Pedawan Formation can still be seen. During the present survey, gold mineralization was discovered in Sungai Matung and cinnabar in Sungai Seripoh Kechil. Subordinate amounts of cinnabar and realgar were also commonly observed in panned concentrates containing gold-grains. Minor pyrite and pyrrhotite disseminations were also frequently observed in altered intrusives and in the rocks of the Pedawan Formation near its contact with the intrusives.

Sungai Nguyu – Sungai Pad Area

The area is underlain by weakly silicified rocks of the Pedawan Formation containing some quartz veinlets and drusy quartz in sandstone which is interbedded with shale. Floats of large quartz crystals were commonly observed in the stream sediments in the area. Some of the panned concentrate samples contain appreciable amounts of gold with minor realgar and cinnabar.

The placer gold was derived most probably from the quartz veins in the weakly silicified rocks which were observed to contain also subordinate disseminated pyrite.

Sungai Sinyi Area

The area is underlain by altered intrusive dikes and the Pedawan Formation. The Pedawan Formation close to its contact with the intrusive bodies are often weakly silicified and in places contain quartz stringers. Some of the panned concentrate samples from along Sungai Sinyi contain appreciable amounts of gold grains with minor cinnabar and realgar. Analysis of samples of the silicified shale and sandstone of the Pedawan Formation shows the presence of gold. The source of gold mineralization in the area is most likely near the contact between the altered intrusive bodies and the Pedawan Formation, and in quartz veins in the silicified Pedawan Formation. Gold mineralization is also corroborated by 3 stream sediment samples highly anomalous for Au.

Sungai Matung Area

The area is underlain by shale of the Pedawan Formation and an altered intrusive dike. Stream sediment samples from the Sungai Matung do not indicate any anomalous values for most of the elements analysed. Panned concentrate samples however, show appreciable amounts of gold grains. Panning of the weathered bedrock of shale in a sheared zone with quartz veinlets at one place showed the presence of gold. Floats of vein quartz and metamorphosed sandstone

with quartz veinlets and pyrite dissemination were commonly observed in the stream. It is clear from field observation and panning that the gold mineralization is related to quartz veining in a ENE shear zone which runs parallel to Sungai Matung.

Sungai Puteh Area

The area is underlain by an altered intrusive and many dikes, tuff and tuff-breccia, and the Pedawan Formation. Disseminations of pyrite and occasionally pyrrhotite were observed in the altered intrusive rocks. Pyrrhotite is common in silicified tuff and tuff-breccia. The panned concentrate samples contain pyrite, magnetite, zircon and occasionally minor amounts of cinnabar and realgar, but only one sample contains gold. Exposures of highly silicified rocks up to several m wide with closely spaced subparallel quartz veinlets and pyrrhotite disseminations were encountered at a few places in the Sungai Sebejig, an upper tributary of Sungai Puteh. Analysis of a few rock samples gave values for Cu of up to 298 ppm and Ag of 14.7 ppm. Au was only detected. Results of stream sediment samples generally also show the area to be mildly anomalous for base metals, Cu, Pb, Zn, and Mo.

Sungai Seripoh Kecil Area

The area is underlain by the Pedawan Formation of alternating, thinly-bedded hornfelsic shale and sandstone. A thin lens of medium to coarse clastic limestone was also encountered in the stream. Panned concentrate samples contain abundant cinnabar, some realgar, magnetite and zircon. Results of stream sediment samples also show the area to be anomalous for Hg.

Bedrock cinnabar mineralization exists in the area but was not encountered during the field survey.

Other Areas

In other areas, some pyrite dissemination and occasionally pyrrhotite were observed in altered intrusive rocks and in rocks of the Pedawan Formation near the contacts with the intrusives. Magnetite is abundant in panned concentrates from the SW part of the area but not in the area east of Sungai Pedi. Pyrite and zircon are common and cinnabar and realgar rare.

3–4 Discussion

The Pedawan Formation in the SE part of the area is dominated by a calcareous sequence which indicates a shallower marine environment of deposition than the rest of the formation to the west. The Gunung Begah – Gunung Blan intrusive is the southern most stock of the NNE alignment of intrusives in the Bau area and may be differentiated from the Gunung Api and Gunung Badud intrusives by its intense alteration and finer grained texture. This and the asso-

ciated tuff and tuff-breccia, suggest that the Gunung Begah – Gunung Blan intrusive was most probably emplaced at a very shallow depth and in parts extrusive. Apparently because of this, the intrusive was also intensely altered whereas the Gunung Api and Gunung Badud intrusives appear relatively fresh. Dikes for a similar reason also suffered intense alteration. The NNE fault and the regional strike of the Pedawan Formation were important structures controlling the shapes and sites of emplacement of the intrusives.

Mildly anomalous values for Cu, Pb and Mo may be correlated with the Gunung Begah – Gunung Blan intrusive. From field observations and results of the geochemical survey, gold mineralization appears to be related mainly to the dikes and is associated with quartz veining near the contacts of the dikes in the Sungai Sebuloh – Sungai Sinyi area and fault zones as in Sungai Matung and possibly the Sungai Nguyu – Sungai Pad area. Minor mercury enrichment accompanies gold mineralization and is observed as cinnabar grains in some of the panned concentrate samples. Probable bedrock mercury mineralization in the Sungai Seripoh – Sungai Jugan area is indicated by anomalous values in stream sediments and abundant cinnabar in panned concentrate samples from Sungai Seripoh Kecil.

Based on the results, it is concluded that only gold and possibly mercury mineralization is of potential economic importance in the area. Two areas are considered to merit immediate follow-up work for gold: (i) The Sungai Sinyi area of about 1.5 km^2 which include Sungai Pad, Sungai Nguyu, Sungai Sinyi and Sungai Ulu Sebuloh, and (ii) The Sungai Matung Area of about 0.5 km^2.

PART Ⅱ GEOPHYSICAL SURVEY

CHAPTER 1 GENERAL INFORMATION

1–1 Objective

A geophysical survey using the Spectral Induced Polarization method was undertaken over a few known old mine workings (Au and stibnite bearing quartz/calcite veins) in order to examine the applicability of this method in detecting such mineralization and its continuity in depth.

By means of the spectral responses to magnitude and phase, it is theoretically possible to identify the kind of mineral, or type of deposit which exists. Another advantage of this method over the conventional IP method is that it also allows reliable acquisition of deep, low resistivity zones by the de-coupling of the electromagnetic field.

1–2 Survey Area

The Spectral IP Survey was carried out over three old mine workings (Tai Ton B, Bidi and Bidi South Ore Deposits) located 5 km south of the Bau town. The Tai Ton B Ore Deposit is found in a very steep and rugged limestone hill whereas the other two are in limestone flats (Fig. II–1).

Six survey lines with a total length of 3,300 meters were surveyed. Line A over the Tai Ton B ore deposit was oriented in the direction N50°E perpendicular to the strike of ore deposit. Over the Bidi ore deposit, two survey lines (100 m apart, Lines B and C) were set in the direction N80°W perpendicular to a row of small old mine pits. Over the Bidi South ore deposit, three survey lines (Lines D, E and F) 100 m and 120 m apart were oriented in the direction N10°W, perpendicular to a row of old mine pits. The station spacing of each survey line was 50 m. The dipole-dipole electrode configuration was adopted and an electrode separation factor of n = 1 to 5 was computed for the results.

Area (Ore Deposit)	Name of Line	Length (m)	Number of Measuring Points	Direction of Line
Tai Ton B	Line A	550	35	N50°E
Bidi	Line B Line C	550 550	35 35	N80°W N80°W
Bidi South	Line D Line E Line F	550 550 550	35 35 35	N10°W N10°W N10°W
	Total	3,300 m	210 points	

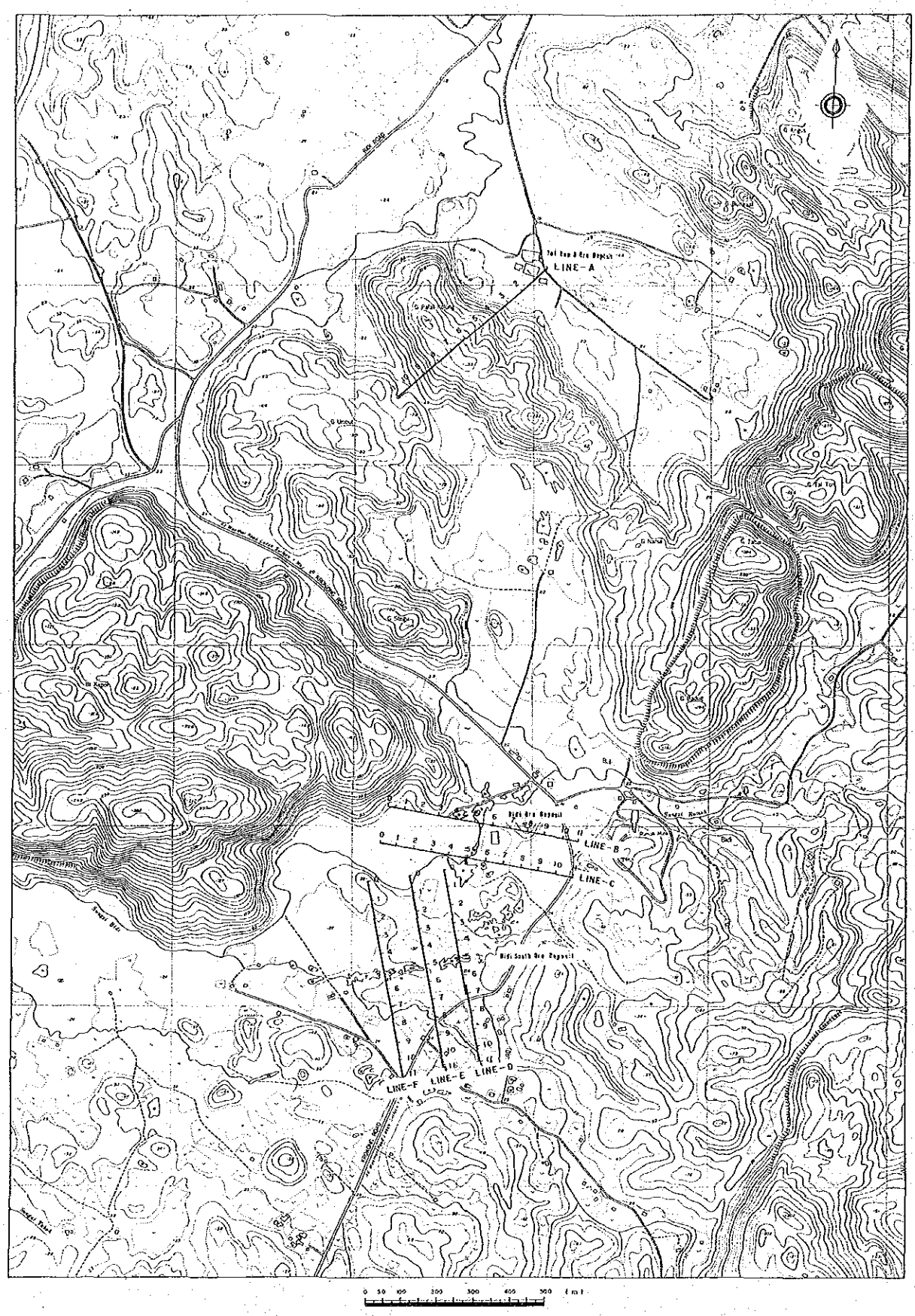

Fig. Ⅱ-1 Location Map of Spectral IP Survey Lines

1–3 Survey Method

The Spectral IP method enables the measuring of the spectral responses to magnitude and phase, using a wide range of frequencies from 0.001 to 1000 Hz.

This method has the advantage over the conventional IP method, as it has the ability to discriminate the anomalous IP source from the frequency responses of the stratum and the ore body. On the other hand, the conventional IP method only measures the apparent resistivity and percent frequency effect (PFE) of two frequencies.

The frequency range most often used is from 0.1 to 100 Hz for practical reasons. In this survey, a system of the Zonge Engineering & Research Organization, U.S., using the frequency range of 0.125 Hz to 88 Hz was employed. Current of three fundamental frequencies, of 0.125 Hz, and 8 Hz were introduced into the ground. A Fourier analysis for these frequencies was performed to obtain their third, fifth, seventh, ninth and eleventh harmonics, and to check the IP responses.

The survey technique for the Spectral IP method is basically not very different from the technique of the conventional IP method, in that both use the dipole-dipole electrode configuration in the frequency domain. However, in the Spectral IP method, it is necessary to synchronize the signals in both the transmitter and receiver, as the Spectral IP survey uses the magnitude and phase of each frequency. In order to accomplish proper timing of the signals, the transmitter and receiver should be connected by a communication wire which is laid parallel to the survey line, 25 m apart.

Layout of Potential Electrodes

Non-polarizable potential electrodes were used. These electrodes consists of saturated copper sulphate solution contained in a porous pot with a copper electrode. The layout is as shown in Figure II–2. This arrangement enables better noise rejection in the differential preamplifier, as a zero electric potential point is established at point (B) which is exactly the same distance from points (A) and (C).

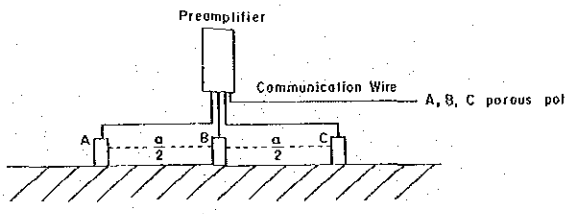

Fig. II-2 Layout of Potential Electrodes and Preamplifier

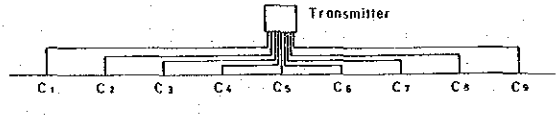

Fig. II-3 Layout of Current Electrodes

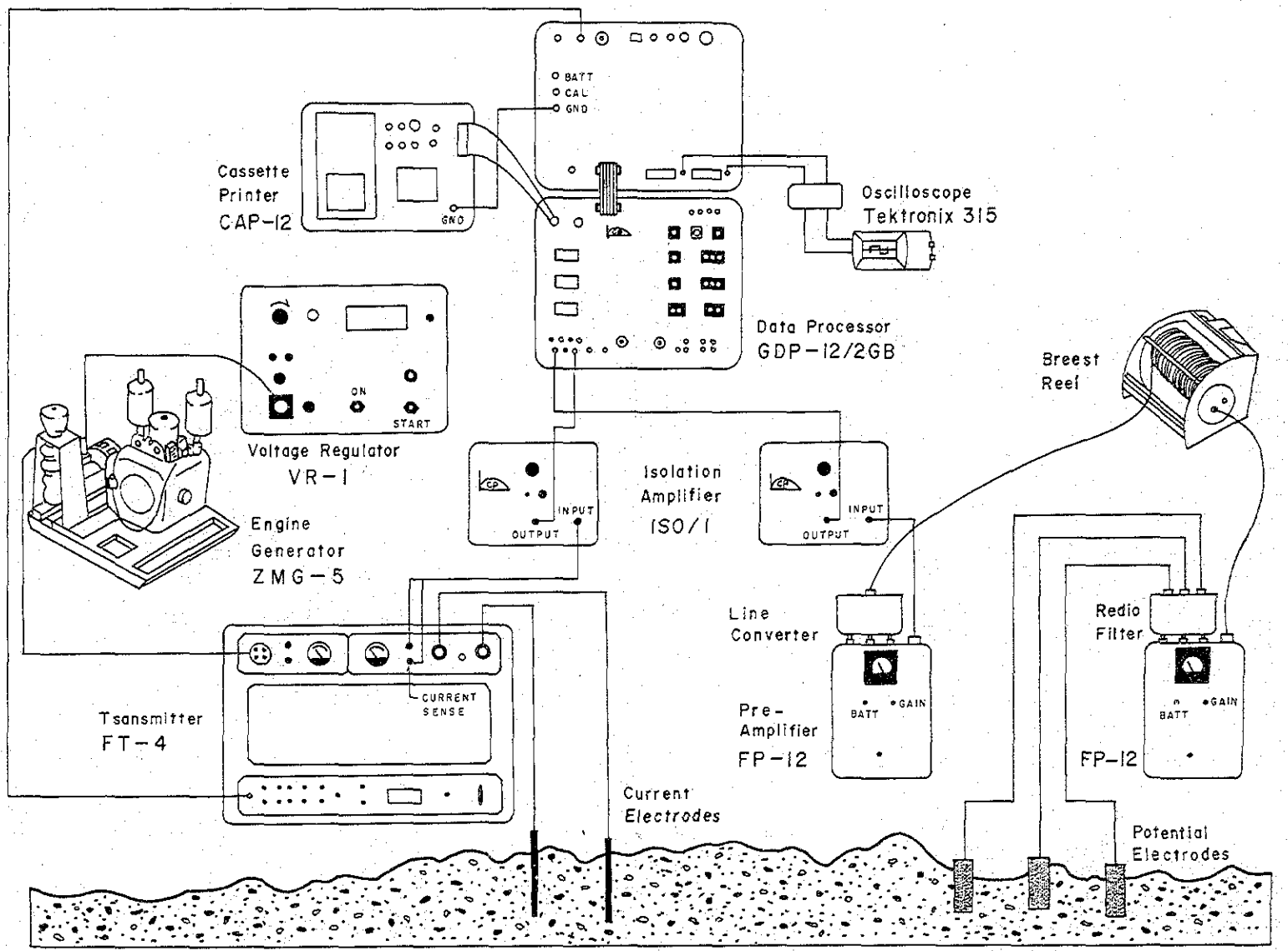

Fig. Ⅱ-4 Block Diagram of Spectral IP Survey Instruments

Layout of Current Electrodes

When the current electrodes are laid out, the future mobility and operational efficiency of the electrodes are considered. Normally, 7 or 9 electrodes are planted before actual measurement and the connections are changed at the transmitter, as required (Fig. II–3). In this survey, a configuration of up to 8 electrodes was used. The electrodes consist of four sheets of alminium foil, each 30 cm x 30 cm in size. Normally, 4 electrodes were used but if the contact resistance was very high, the number of electrodes was doubled.

1–4 Measuring Equipment

The equipment used in this survey is manufactured by Zonge Engineering and Research Organization Co., Arizona, U.S.A. The component parts of this equipment are described in following table and a typical measurement configuration is shown in Figure II–4.

Table Ⅱ-1 Spectral IP Survey Instruments

Data Processor	GDP-12/2GB	1 piece
Pre-amplifier	FP-12	2 pieces
Isolation Amplifier	ISO/1	2 pieces
Cassette Printer	CAP-12	1 piece
Oscilloscope	Tektronix 315	1 piece
Transmitter	FT-4 (Geotronics)	1 piece
Engine Generator	ZMG-5	1 piece
Voltage Regulator	VR-1	1 piece

CHAPTER 2 DATA PROCESSING AND DATA ANALYSIS

In the Spectral IP method, the magnitude and the phase of the signal are measured. The results are plotted as the spectrum versus the frequency, or the Cole-Cole diagram. Apparent resistivity, 3-point decoupled phase, etc. are shown as pseudo-sections which are the same as that of the conventional IP method.

The Theory of Spectral IP Method

The theory of Spectral IP is summarized in Figure II–5 where (a), shows a small section of a mineralized rock, which has both blocked and un-blocked pore passages. If this is depicted in an equivalent circuit, then it appears like (b), (c) shows the time domain responses, while Z and ϕ are the measuring values in spectral IP.

In Figure II–6, the concepts of in-phase and out-of-phase are shown. When the arbitrary amplitude rectangular waveforms are transmitted, the signals with the phase-shift of ϕ and an amplitude of V are obtained at the receiver.

The sampling sequence for in-phase and quadrature measurement are shown in the graphs in the lower part of Figure II–6. The relation between frequency effect and phase angle is shown in Figure II–7. In this figure the Cole-Cole diagram is adopted, with the vertical axis showing negative out-of-phase factors and the horizontal axis showing positive in-phase factors. The magnitude (M_1) is at 0.1 Hz, and (M_2) at 1 Hz, and the phase angles are ϕ_1 and ϕ_2 respectively. Frequency effects and in-phase factors are approximately directly proportional to each other and the phase angle and out-of-phase factors are directly proportional to each other. The dotted line in the figure shows the results of the measurement, with the lower frequencies occurring to the right, and the higher frequencies occurring to the left.

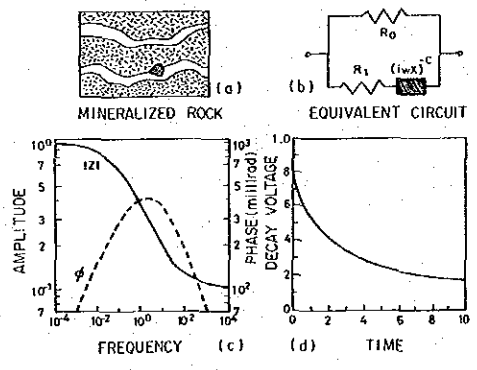

Fig. II-5 Spectral IP Effect

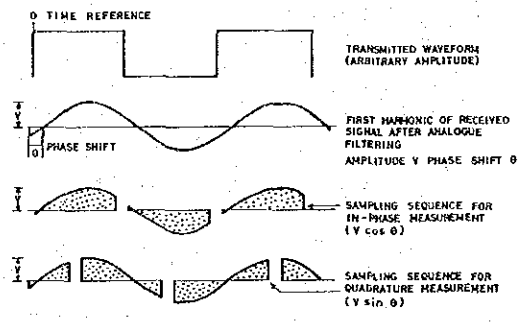

Fig. II-6 Transmitted and Received Waveforms

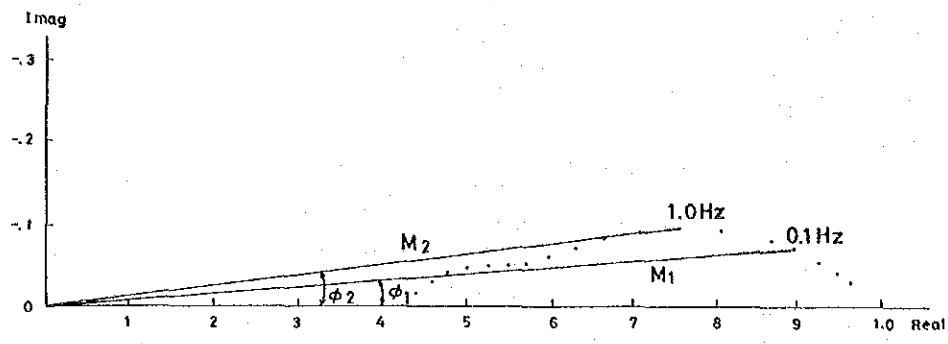

$$PFE = \frac{M_1 - M_2}{M_2} \times 100\% \qquad (0.1 \text{to} 1.0 \text{Hz decade})$$

Fig. Ⅱ-7 Relation between Frequency Effect and Phase Shift

2–1 Data Processing

Data from field measurements give phase shift and magnitude of eighteen frequencies, from 0.125 Hz to 88 Hz. These signals were recorded and input into the Data Processor (GDP-12/2GB), where the real and imaginary parts of each frequency, the resistivity values of the three fundamental frequencies (0.125, 1, and 8 Hz), the value of the three point de-coupled and the percent frequency effect (PFE) were calculated. The results were printed out and could also be stored on magnetic tape-cassette if necessary. Other relevant data were also stored and could be printed out; these include the current supplied, SEM, survey location, notch filter setting, and stacking number.

After data processing, a pseudo-section was generated. Terrain correction was applied if necessary, to the apparent resistivity.

A daily calibration measurement was taken, prior to any field measurements. The values received in this measurement were then removed from subsequent signal measurements at each point in order to be sure that only the correct earth signal was being calculated.

Generally, when a dipole-dipole electrode array is used, the topography strongly affects the apparent resistivity values. The tendency is that topographic highs produce correspondingly higher apparent resistivity values, and topographic lows produce correspondingly lower apparent resistivity values.

As Line A is set across a hill, the elevation change of Line A is very large and terrain correction was applied. The other five survey lines are located in a flat area and hence no correction was required.

The result of the terrain correction to Line A are shown in Figure II–8.

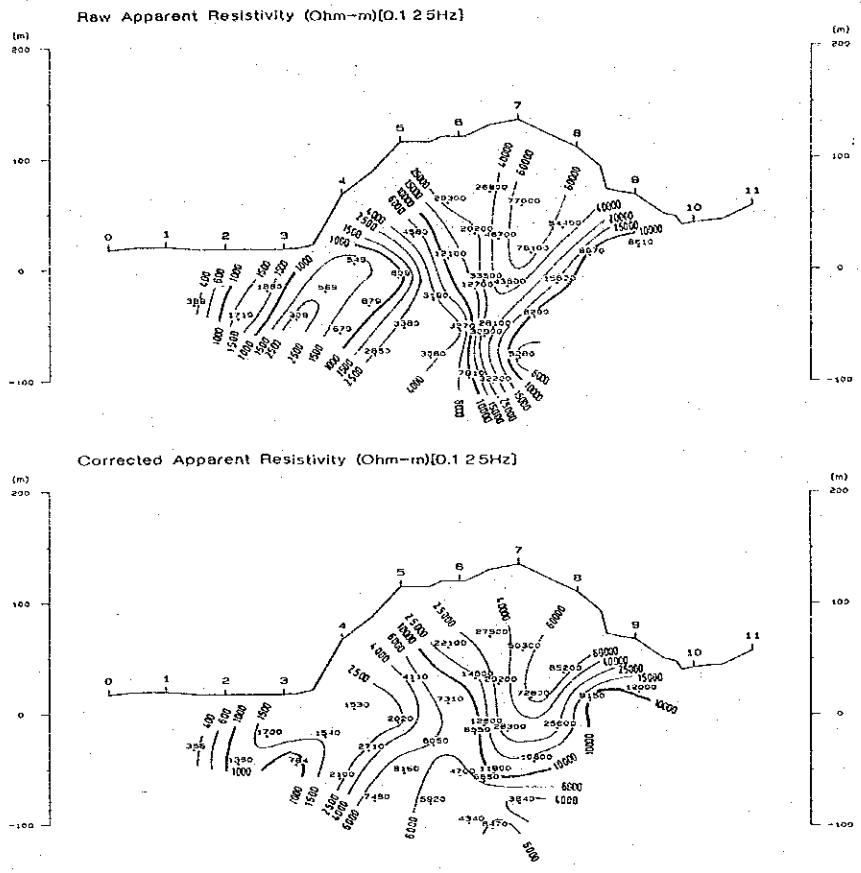

Fig. Ⅱ-8 Example of Terrain Correction (Line A)

2–2 Results of Laboratory Measurement

In order to evaluate the results of the resistivities and spectral responses of magnitude and phase of the rocks which are found in the survey area, a total of 27 superficial rock and ore samples mainly from the survey area were collected. These samples were sent to Japan to be analysed for their properties. Figure II–9 shows the test measurement installation. The results of these measurements and the spectral responses for magnitude and phase are shown in Table II–2 and Figures II–10–1 to II–10–7.

It may not be accurate to try to represent the resistivity and spectral responses for phase and magnitude of these surface samples as being the same as the sub-surface rocks in the same area. However, it is important to know the types and qualities of the local rocks when the Spectral IP anomalies are analysed.

The results of the laboratory measurements are summarized in Table II–3.

Table Ⅱ-2 IP Properties of Ore and Rock Samples

No.	Sample No.	Resistivity (Ohm-m)	Raw Phase (-mrad)	3pt Decoupled (-mrad)	P.F.E. (%)	Rock name	Sample Location
1	AR–0084	37	660	691	129	Stibnite rich, native arsenic ore	Tai Ton A Ore Deposit
2	AR–0032d	52	609	655	107	Py-Sb-calcite ore	G. Tongga ore Deposit
3	Bidi–2	27	532	551	94.6	Stibnite, native arsenic ore	Bidi Ore Deposit
4	AR–0008	292	313	300	55.7	Py-Sb-calcite ore	G. Krian Ore Deposit
5	Bidi–1	1570	194	193	30.4	Stibnite bearing arsenic, calcite ore	Bidi Ore Deposit
6	AR–0069d	1930	52.1	49.7	8.2	Sarabauite and stibnite ore	Lucky Hill A Ore Deposit
7	A–10	12800	2.62	2.18	0.41	Limestone	Tai Ton B Ore Deposit
8	A–7.5	16400	2.1	1.95	0.29	Limestone	Tai Ton B Ore Deposit
9	A–6	24300	2.03	1.86	0.33	Limestone	Tai Ton B Ore Deposit
10	A–3.5	15100	6.74	6.61	0.95	Limestone	Tai Ton B Ore Deposit
11	B–4	5060	8.44	6.6	1.29	Limestone	Bidi Ore Deposit
12	B–5	7100	2.26	1.32	0.41	Limestone	Bidi Ore Deposit
13	B–7	16900	1.73	1.76	0.27	Limestone	Bidi Ore Deposit
14	C–5.5	15400	3.92	4.23	0.5	Limestone	Bidi Ore Deposit
15	C–7.5	17500	0.59	–0.13	0.32	Limestone	Bidi Ore Deposit
16	D–0.5	32500	0.29	–0.08	0.98	Limestone	Bidi South Ore Deposit
17	D–1	14100	1.79	1.74	0.2	Limestone	Bidi South Ore Deposit
18	D–2.5	15000	1.3	1.46	0.15	Limestone	Bidi South Ore Deposit
19	D–5	22300	2.1	1.66	0.31	Limestone	Bidi South Ore Deposit
20	E–3.5	13400	0.91	0.91	0.18	Limestone	Bidi South Ore Deposit
21	E–5.5	20200	1.56	1.67	0.22	Limestone	Bidi South Ore Deposit
22	F–0	29000	2.77	3.08	0.39	Limestone	Bidi South Ore Deposit
23	F–1.5	16900	1.18	1.7	0.19	Limestone	Bidi South Ore Deposit
24	F–3.5	15600	0.43	0.8	0.03	Limestone	Bidi South Ore Deposit
25	B–5.5	8400	3.07	2.55	0.4	Calcite	Bidi Ore Deposit
26	A–6.3	11600	4.37	2.63	0.58	Calcite	Tai Ton B Ore Deposit
27	AR–0055	11800	10.7	10	1.4	Quartz Porphyry	Bidi Ore Deposit

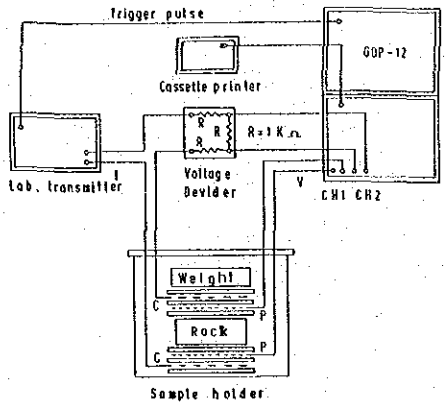

Fig. Ⅱ-9 Block Diagram of Laboratory Measurement

Table Ⅱ-3 Characteristics of Ore and Rock Samples

	Ore	Rock (Limestone, Calcite, Quartz porphyry)
Resistivity	Low (30 to 2,000Ωm)	High (more than 5,000Ωm)
Raw Phase (0.125 Hz)	More than -50 mrad (-52.1 to -660 mrad)	Less than -11 mrad
Phase Spectrum	Flat or decreases slowly as the frequency increases.	Increases as the frequency increases.
Magnitude	Decreases as the frequency increases. When the raw phase at 0.125 Hz is large, its slope becomes large.	Flat
Cole-Cole Diagram	When the raw phase at 0.125 Hz is large, curve starts from (0.7, -0.7) showing a slope of 45°. As the raw phase become small, curve starts near (1,0) and its slope becomes almost flat.	Concentrates near (1.0)

The limestone, the host rock of the ore deposits, shows high resistivity and low IP effect. If there exists ore deposits, it is expected that low resistivity and high IP anomalies are observed.

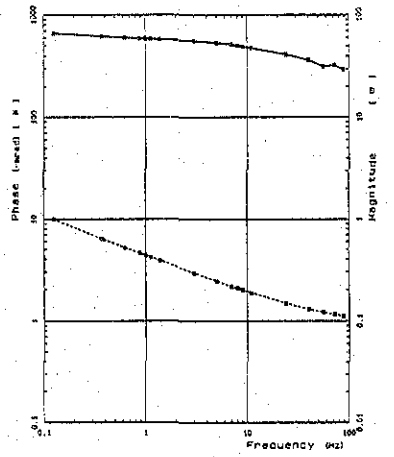

PHASE & MAGNITUDE RESPONSE

ROCK NAME : Stibnite rich. native arsenic ore

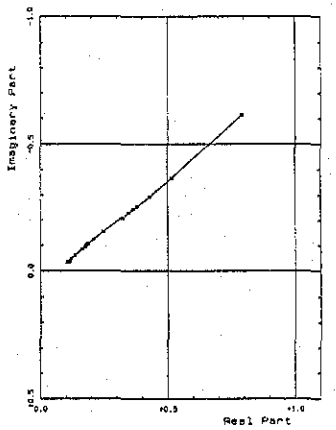

COLE-COLE DIAGRAM

(a) AR-0084

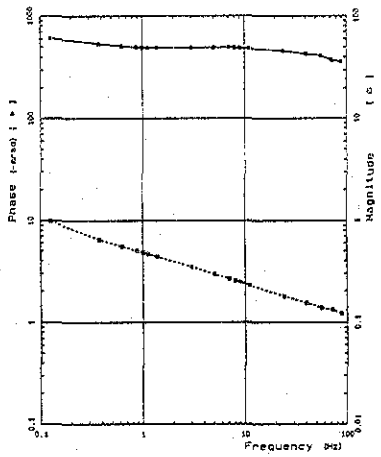

PHASE & MAGNITUDE RESPONSE

ROCK NAME : Py-Sb-calcite ore

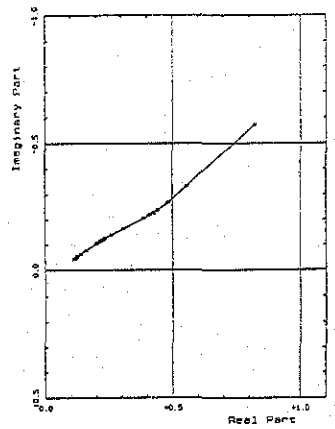

COLE-COLE DIAGRAM

(b) AR-0032d

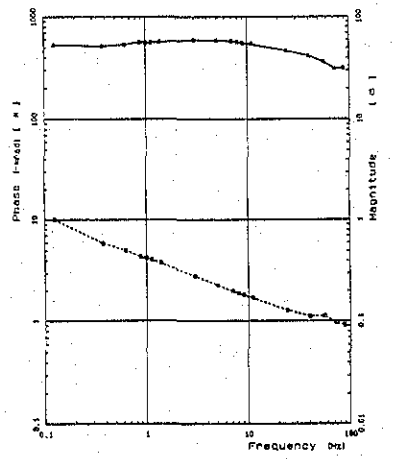

PHASE & MAGNITUDE RESPONSE

ROCK NAME : Stibnite, native arsenic ore

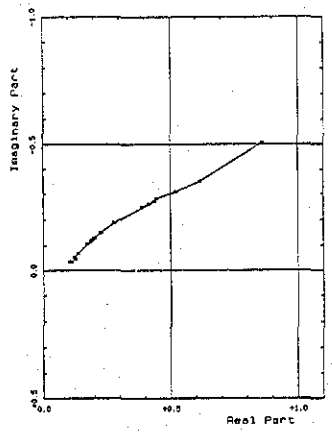

COLE-COLE DIAGRAM

(c) Bidi-2

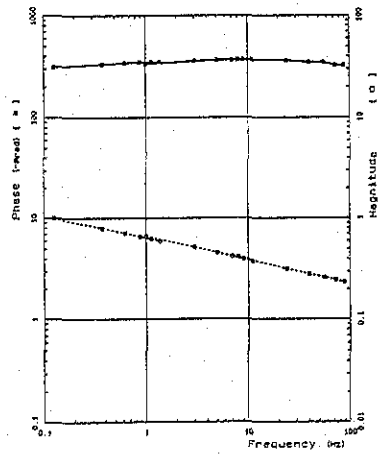

PHASE & MAGNITUDE RESPONSE

ROCK NAME : Py-Sb-calcite ore

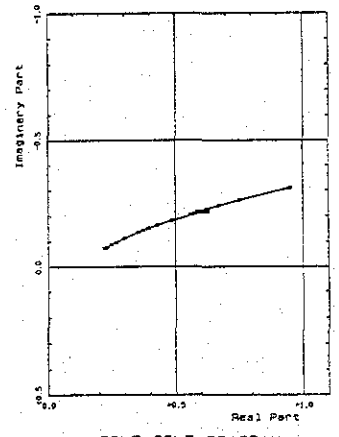

COLE-COLE DIAGRAM

(d) AR-0008

Fig. Ⅱ-10-1 Frequency Response of Ore Sample

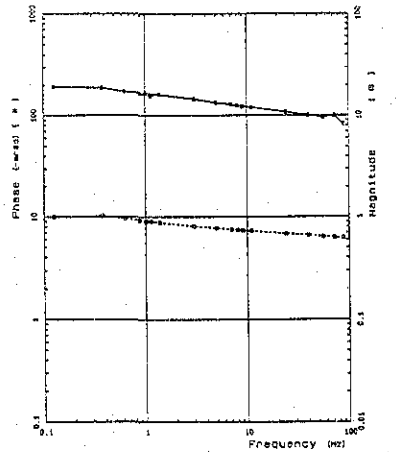

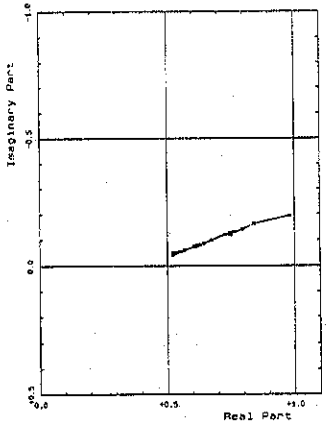

(a) Bidi-1

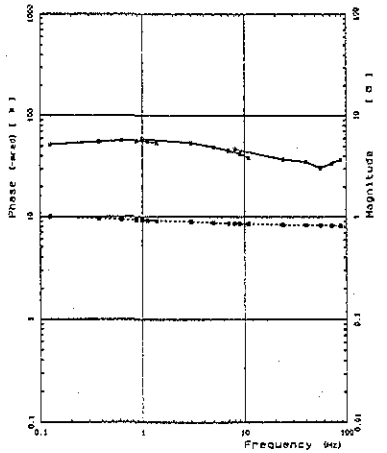

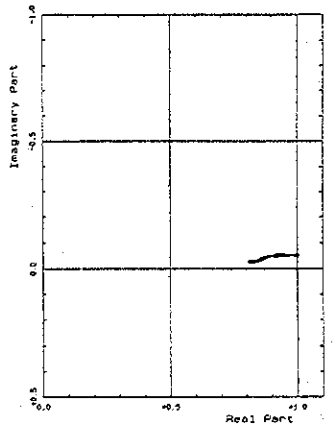

(b) AR-0069d

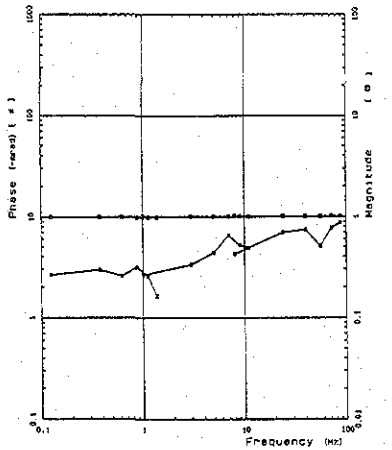

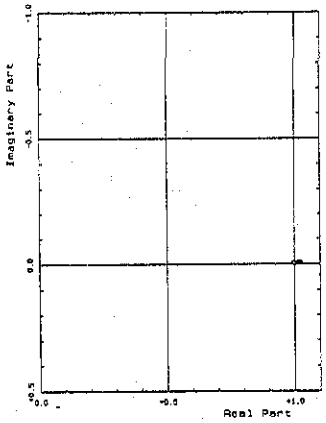

(c) A-10

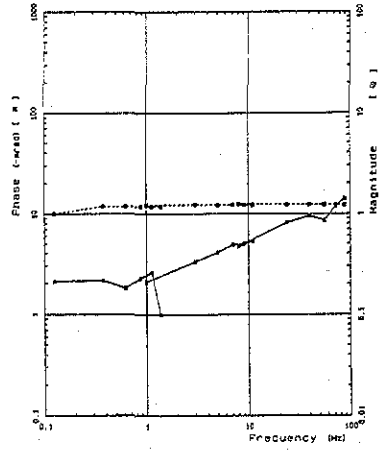

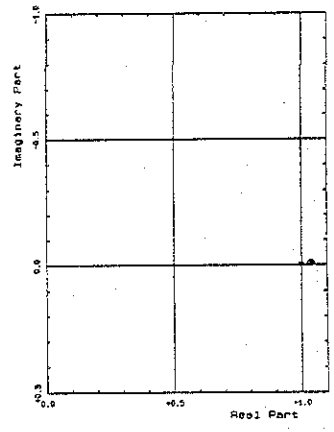

(d) A-7.5

Fig. Ⅱ-10-2 Frequency Response of Ore Sample

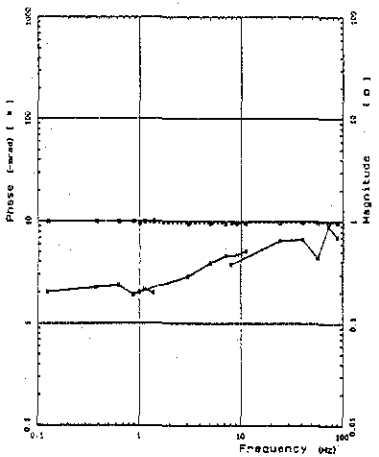

PHASE & MAGNITUDE RESPONSE
ROCK NAME : Limestone

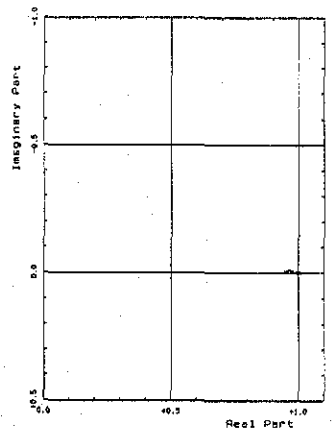

COLE-COLE DIAGRAM

(a) A-6

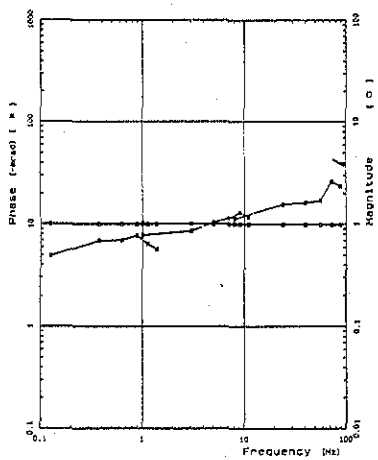

PHASE & MAGNITUDE RESPONSE
ROCK NAME : Limestone

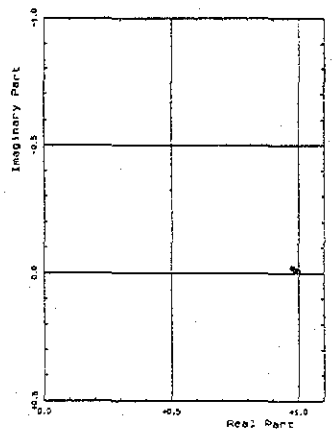

COLE-COLE DIAGRAM

(b) A-3.5

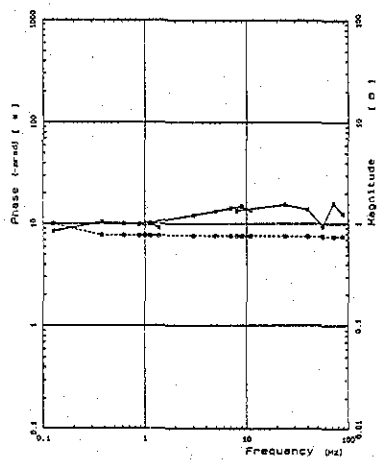

PHASE & MAGNITUDE RESPONSE
ROCK NAME : Limestone

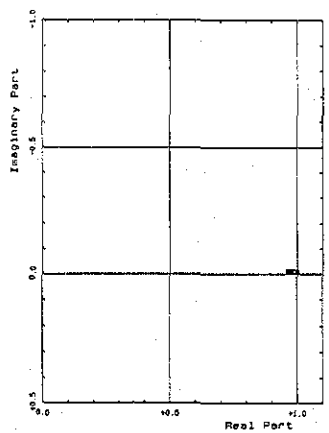

COLE-COLE DIAGRAM

(c) B-4

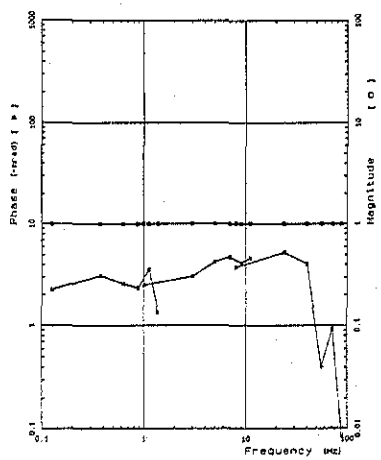

PHASE & MAGNITUDE RESPONSE
ROCK NAME : Limestone

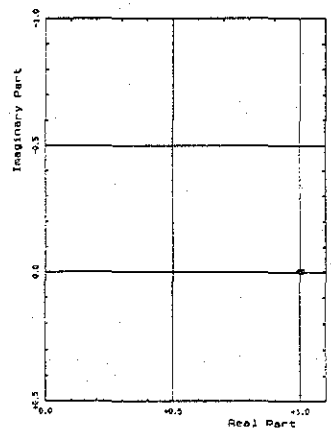

COLE-COLE DIAGRAM

(d) B-5

Fig. Ⅱ-10-3 Frequency Response of Ore Sample

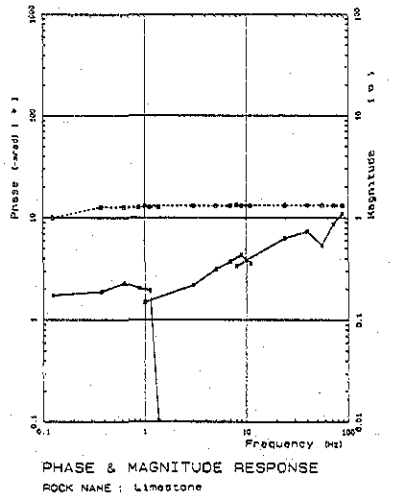

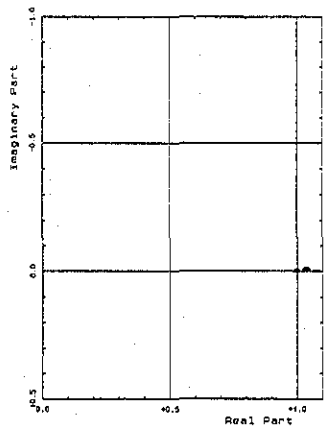

(a) B−7

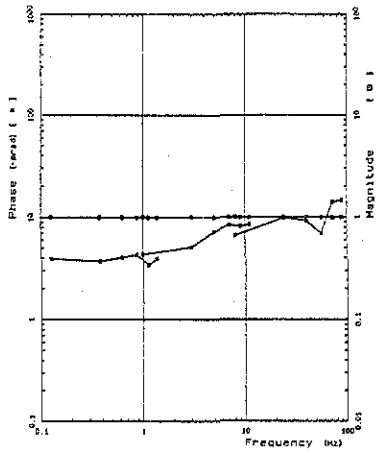

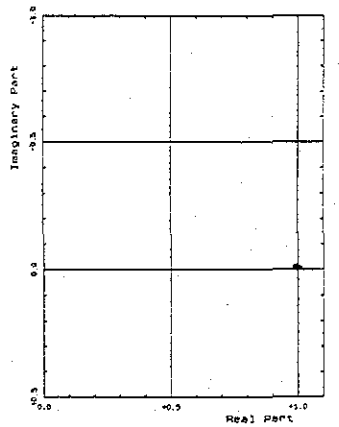

(b) C−5.5

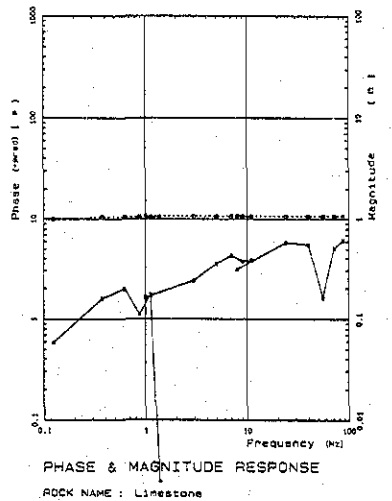

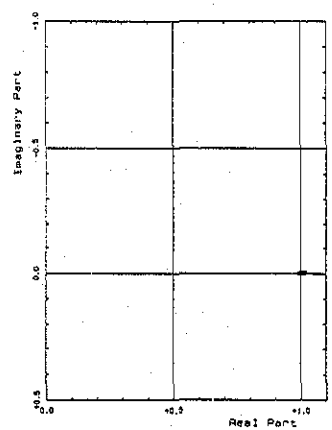

(c) C−7.5

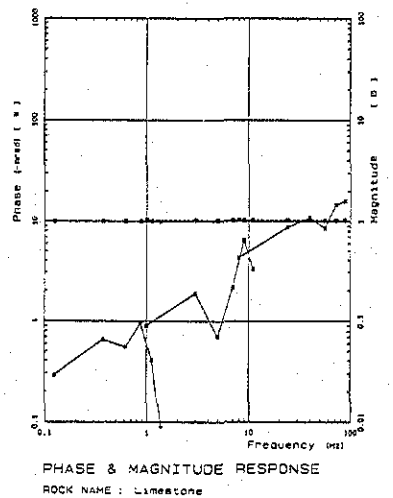

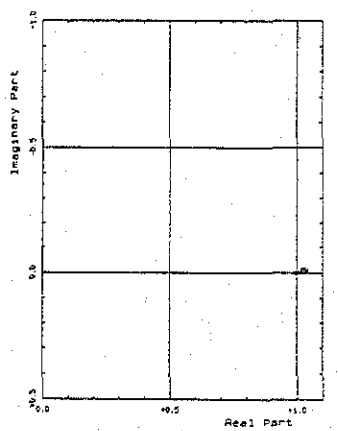

(d) D−0.5

Fig. Ⅱ-10-4 Frequency Response of Ore Sample

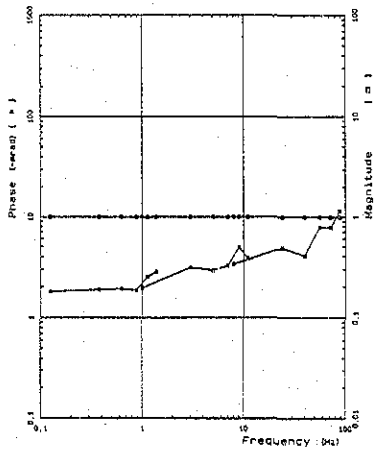

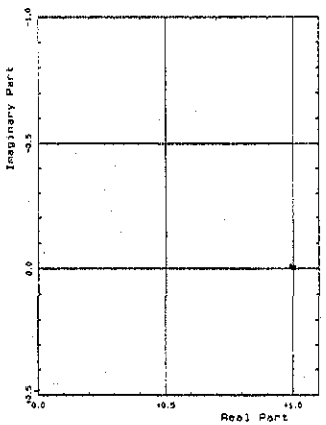

(a) D-1

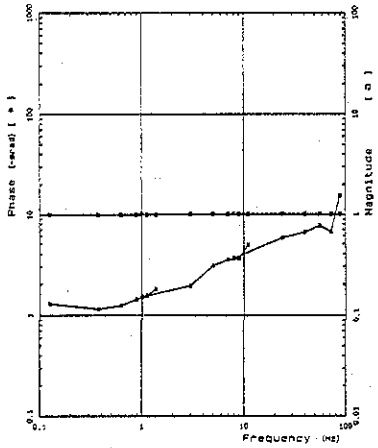

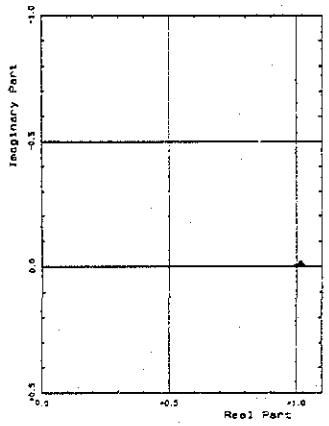

(b) D-2.5

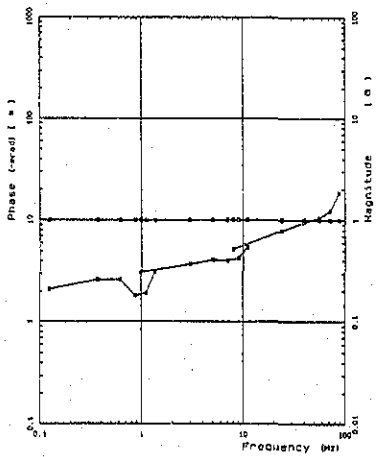

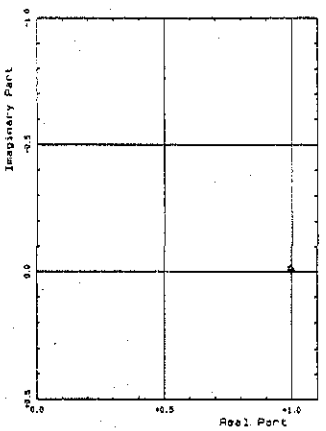

(c) D-5

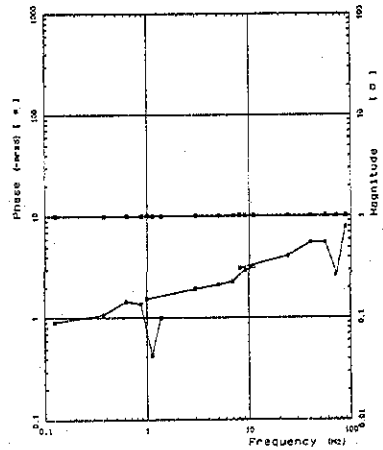

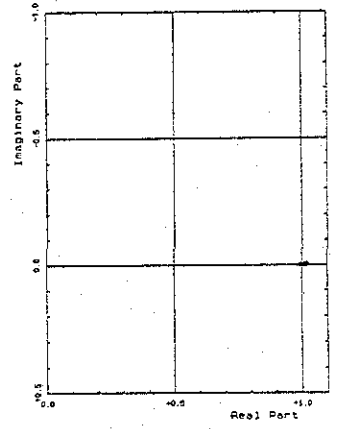

(d) E-3.5

Fig. Ⅱ-10-5 Frequency Response of Ore Sample

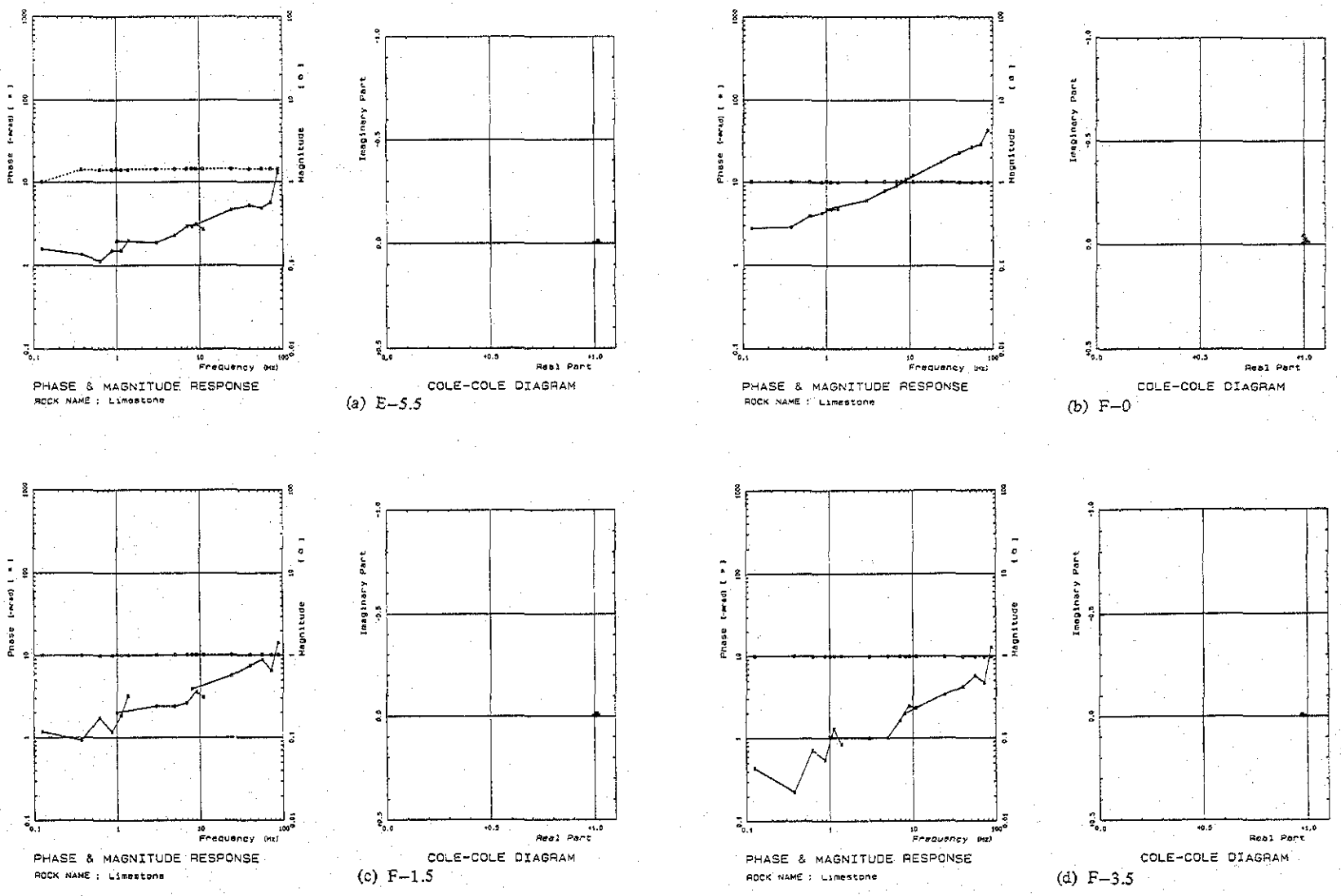

Fig. Ⅱ-10-6 Frequency Response of Ore Sample

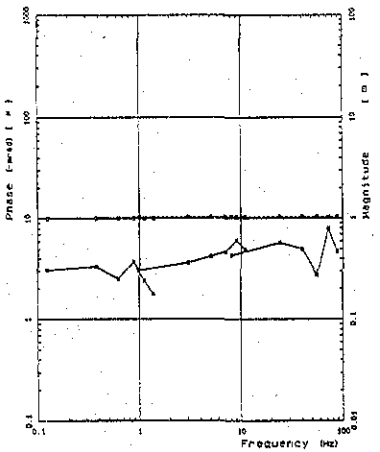

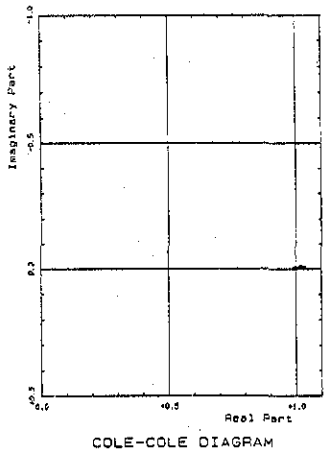

(a) B–5.5

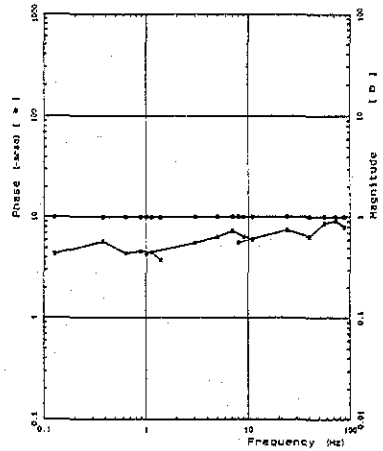

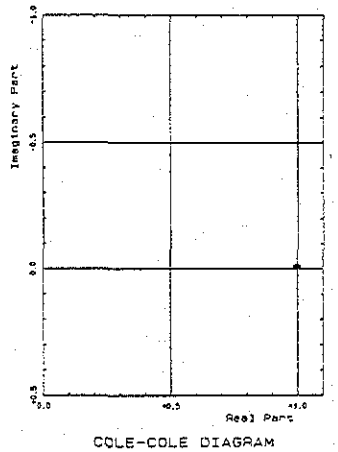

(b) A–6.3

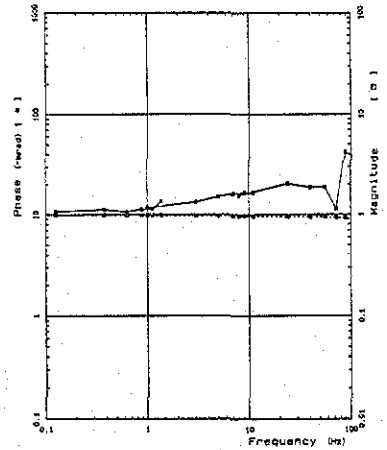

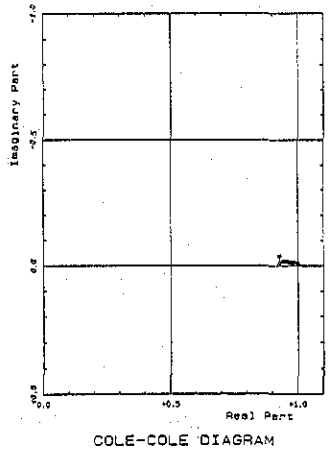

(c) AR–0055

Fig. Ⅱ-10-7 Frequency Response of Rock Sample

One of the ore deposits consists mainly of a calcite vein with stibnite. According to the results of the laboratory measurement, resistivity and IP effects tend to become high and low respectively as the content of calcite in the ore sample increases. It is considered that minerals which cause high IP effects are mainly stibnite and arsenopyrite.

2–3 Data Analysis

From the field measurements obtained, section, plan and spectral diagrams were drawn, and the results analysed for IP anomalies. The treatment include deriving the following diagrams:

(1) Plan diagram and section diagram of apparent resistivity (0.125 Hz).

(2) Plan diagram and section diagram of PFE (0.125–1 Hz).

(3) Section diagram of raw phase (15 frequencies)

(4) Cole-Cole Diagram

(5) Phase spectral response diagram.

(6) Magnitude spectral response diagram.

(7) Three-point decoupled phase diagram.

The ordinate method of analysis for (1) and (2) were applied. From diagrams (3)–(7), IP anomalous sourves can be identified through their spectral responses.

Three-point decoupled phase is an approximated phase in direct current using 0.125, 0.375 and 0.625 Hz. Assuming that phase is represented as the second order polynomial of frequency, and then phase ϕ may be represented by the equation $\phi = af^2 + bf + c$, where c is the phase which can become a frequency close to a direct current called the 3-point decoupled phase of the frequency, a and b are constants and f the frequency. c is given by the following equation:

$$c = \frac{15}{8}\phi_{0\cdot125} - \frac{10}{8}\phi_{0\cdot375} + \frac{3}{8}\phi_{0\cdot625}$$

where $\phi_{0\cdot125}$, $\phi_{0\cdot375}$ and $\phi_{0\cdot625}$ are the phases at 0.125, 0.375 and 0.625 Hz respectively.

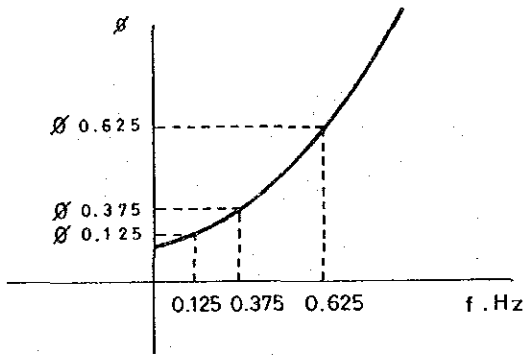

Fig. Ⅱ-11 Three-point Decoupled Phase Shift

CHAPTER 3 RESULTS OF DATA ANALYSIS AND DISCUSSION

3–1 Results of Data Analysis

All observed values in this Spectral IP survey are presented as Spectral IP pseudo-sections, phase spectral diagrams, magnitude spectrum diagrams, Cole-Cole diagrams and raw phase pseudo-sections.

Based on the spectrum between 0.125 Hz and 8 Hz, the Spectral IP data observed are classified into five types as described in Table II–4.

Table Ⅱ-4 Classification of Spectral IP Data

	Type I	Type II	Type III	Type IV	Type V
Phase Spectrum (0.125–8 Hz)	Peak near 1 Hz or flat	Flat or right-side-up	Right-side-up (its slope is greater than type II)	Negative coupling	Right-side-up (its slope is very large)
Magnitude Spectrum (0.125–8 Hz) and its slope	Right-side-down	Right-side down	Almost flat	Right-side down	Right-side down
	Large	Small		Small	Small
Cole-Cole Diagram (0.125–8 Hz) and length of horizontal curve	Left-side-down or flat	Flat	Flat	Downward curve	Upward curve
	Long	Short	Very Short		
Raw Phase at 0.125 Hz	High (more than – 40 mrad)	Low (–10 mrad to –20 mrad)	Very Low (less than –10 mrad)	Very Low (–10 mrad to 10 mrad)	Very Low (less than –10 mrad)
Coupling type	Normal	Normal	Normal	Negative	Normal (partially negative)

Type I is a very strong spectral IP anomaly which may be caused by a large amount of sulphide minerals, and is detected below station No. 4 and No. 6 of Line B and below No. 4 and No. 5 of Line C.

Type II is a very weak spectral IP anomaly, detected at depth below station No. 3.5 of Line A and near the surface at No. 5.5 of Line F. This anomaly may be caused by a small amount of sulphide minerals.

Type III, IV and V correspond to barren rock. Type IV shows a negative coupling anomaly which is thought to occur where there exists a boundary of high resistivity contrast or where there exists a conductive body within a highly resistive rock. Type V appears around the Type IV negative coupling anomaly. Type III appears to represent the standard spectrum of barren rocks such as limestone and calcite.

3–1–1 Tai Ton B Ore Deposit

The spectral IP pseudo-section, spectrum diagram and raw phase pseudo-sections of Line A are shown in Figures II–12, II–13, and II–14–1 to II–14–5, respectively.

As shown in Figure II–12, a very weak IP anomaly of more than –10 mrad is detected at depth below Station No. 4 but there are no distinct anomalies corresponding to ore bodies. The values at points plotted by means of a dipole-dipole array, may not represent the physical properties at these points due to the rugged topography. The above-mentioned weak IP anomaly may correspond to the known Tai Ton B ore body.

In the apparent resistivity pseudo-section (Fig. II–12), high resistivity of more than 5,000 Ωm, below Station No. 8, is dominant in the south from Station No. 4.5 onwards and low resistivity of less than 2,000 Ωm (355 Ωm below No. 1.5) in the north. Negative couplings are observed at No. 4 to depth (see Fig. II–13), which may reflect this resistivity contrast. It is inferred that the southern high resistivity corresponds to limestone with calcite vein and the low resistivity in the north may be caused by different rock units.

In the raw phase pseudo-section, a very weak raw phase anomaly of higher than –5 mrad is observed between Station No. 7 and 9. This weak anomaly may correspond to the extension of small ore veins which are found just SE of the survey line.

Spectral type II characteristics appear at depth below No. 3.5, where a very weak spectral IP anomaly is detected.

Spectral type III characteristics are predominant over the survey line except for the central part where type IV and V characteristics are observed.

3–1–2 Bidi Ore Deposit

The results along lines B and C over this old mine working are shown in Figures II–15 to II–18, and Figures II–19–1 to II–20–5.

A very strong spectral IP anomaly appears below Station No. 4.5 of Line B and continues in depth, dipping to the east and also shows a low resistivity of less than 2,000 Ωm and a high phase of more than –80 mrad. This anomaly is of the Spectral Type I. Laboratory data suggest that body causing anomaly is an ore vein with abundant stibnite and rare arsenopyrite.

A small spectral IP anomaly is detected to the west of an above-mentioned anomaly with a phase of –20 mrad and a resistivity of about 2,000 Ωm. This may be caused by a similar ore body of calcite with little stibnite.

A strong near-surface spectral IP anomaly appears at Station No. 4.5 on Line C, and corresponds to a low resistivity and high phase anomaly. This continues to about 100 m deep and dips to the west. The resistivity and phase of this anomaly is lower than 1,000 Ωm and higher than −40 mrad respectively and can be classified as Spectral Type I but is slightly weaker than the anomaly on line B. This anomaly may be caused by a similar ore body as that of Line B except that the dips are different. The ore bodies are indicated to be of limited lateral extent.

Negative couplings appear in the surroundings of these anomalies. These may be due to conductive SIP anomalous sources in resistive host rock (limestone).

As in the raw phase pseudo-sections (Figures II−19−1 to II−19−5 and Figures II−20−1 to II−20−5), similar patterns are shown even when the frequency was increased. There may be no effects of electro-magnetic (EM) coupling because of the highly resistive host rock.

The spectral characteristics at the margin of above-mentioned strong SIP anomalies are similar to those of type II. The spectral IP anomalous source of type II is considered to contain less stibnite and more calcite than of type I.

Low apparent resistivities of less than 1,000 Ωm is observed at both ends of Lines B and C which correspond to the overburden.

3−1−3 Bidi South Ore Deposit

The SIP results along lines D, E and F over this old mine working are shown in Figures II−21 to II−26 and Figures II−27−1 to II−32−3.

A very weak spectral IP anomaly, which may correspond to the ore deposit, appears near the surface at Station No. 5.5 of Line F and shows an inverse V shape. This anomalous source of the Spectral Type II is very small and may not continue in depth. It is probably a calcite vein with very little stibnite. There is a very weak indication below Station No. 5 on Line E, but it is doubtful that it indicates an ore deposit.

The results suggested that the ore body of this working had been totally mined out or the Spectral IP method is unsuitable for detecting an ore body rich in calcite and very poor in sulphide contents.

There is a remarkable resistivity contrast at Station No. 8 on Line D, with a high in the north and a low in the south where the very weak SIP anomaly is detected. The contrast corresponds to the boundary between the Bau limestone and shale of Pedawan Formation. A vertical fault may exist at No. 8 and a weak anomaly may be due to clay or pyrite with this fault.

In the raw phase pseudo-sections of Line D (Figures II−27−1 to −5), the effect of EM

coupling can be seen easily at the southern part where the contours become parallel to ground surface as the frequency increases. Besides Line D, there are no effects of EM coupling in this area.

3–2 Discussion

Laboratory studies of ore and rock samples from the Tai Ton area suggest that calcite vein with abundant stibnite is largely responsible for the strong spectral IP anomaly detected in the area surveyed. The results also show that spectral types observed may be classified into five types:

(1) Type I which corresponds to a strong spectral IP anomaly showing low resistivity of less than 2,000 ohm-m and high phase of more than –40 mrad. This may be caused by an ore body containing abundant stibnite and little calcite.

(2) Type II which corresponds to a very weak spectral IP anomaly showing relatively low resistivity and low phase of between –10 mrad and –20 mrad. Type II anomalous source may be an ore body containing stibnite of less than that of type I but rich in calcite.

(3) Type III, IV and V which correspond mainly to barren limestone host rock and partially barren calcite and shale.

The spectral IP characteristics of each area are as follows:

(1) Tai Ton B ore deposit

A very weak spectral IP anomaly (Type II) was determined at depth below Station No. 3.5 on Line A. There is a possibility that this type II anomaly is caused by calcite vein with little or some stibnite.

High resistivity of the southwestern side from No. 5 corresponds to massive limestone and low resistivity of the northeastern side may be due to different rock units.

(2) Bidi ore deposit

A very strong spectral IP anomaly (Type I) observed below Station No. 4.5 on Line B may be caused by an ore body with abundant stibnite and little calcite. This ore body continues in depth and dips to the east.

A strong spectral IP anomaly (Type I), appearing below Station No. 4.5 on Line C, is a shallow anomaly and may be due to an ore body with a little or some stibnite. This ore body does not continue in depth and dips to the west.

(3) Bidi South ore deposit

A very weak spectral IP (Type II), detected near surface below Station No. 5.5 on Line F, may be caused by a small and shallow ore body with little stibnite.

As there are no other anomalies indicating possible ore body besides this anomaly, it is

suggested that either the ore deposit had been completely mined out or the spectral IP method may not be suitable for detecting any ore body of calcite vein with very little stibnite.

A remarkable resistivity contrast below Station No. 8 on Line D may correspond to the boundary between the Bau Limestone and shale of the Pedawan Formation which is also suggested to be a vertical fault.

In conclusion it may be said that from the spectral IP survey undertaken, it is possible to estimate the location, shape and continuity in depth of the Bidi Ore Deposit. The method appears to be suitable for studying this type of ore deposit which is rich in stibnite.

It is recommended that a spectral or conventional IP survey be conducted over the northern side of the Bidi Ore Deposit Area west of Station No. 4.5 on Line B in order to understand the northern limit of the anomaly. Drilling should be carried out to a depth of about 100 m between Station No. 5 and No. 7 on Line B in order to check the characteristics and the continuity of the ore body causing the anomaly.

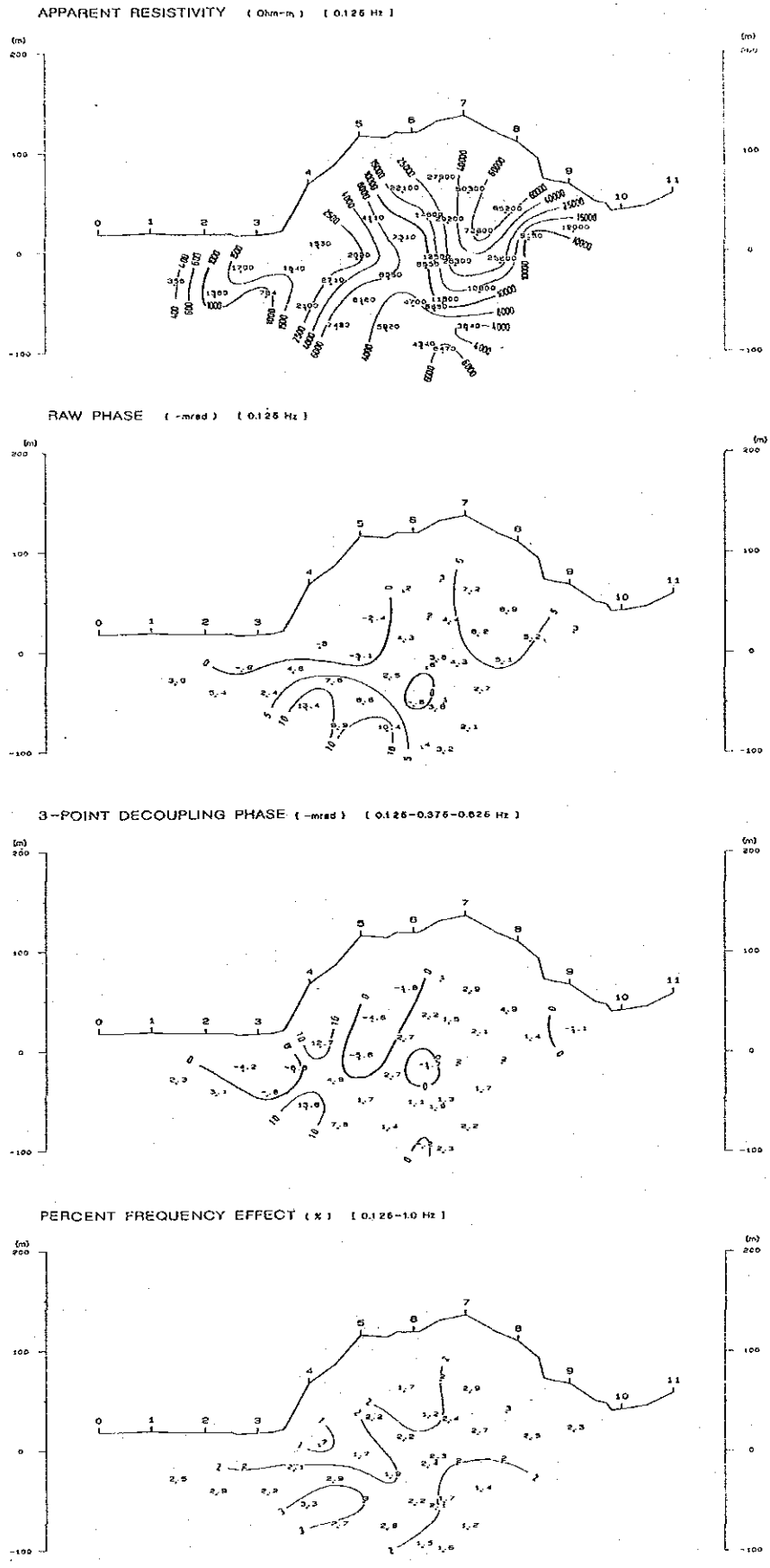

Fig. Ⅱ-12 Spectral IP Pseudo-Section of Line A

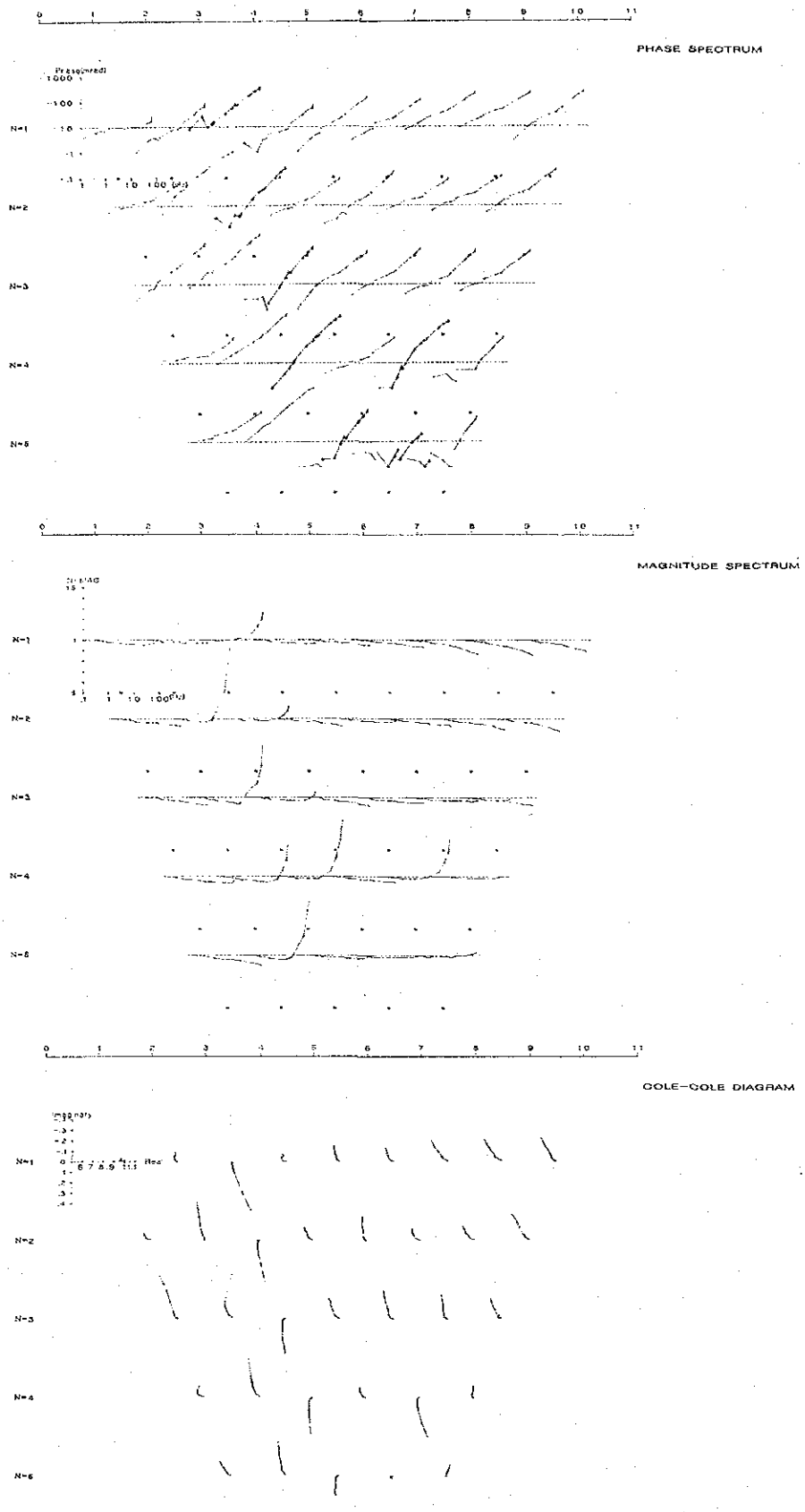

Fig. Ⅱ-13 Spectrum Diagram of Line A

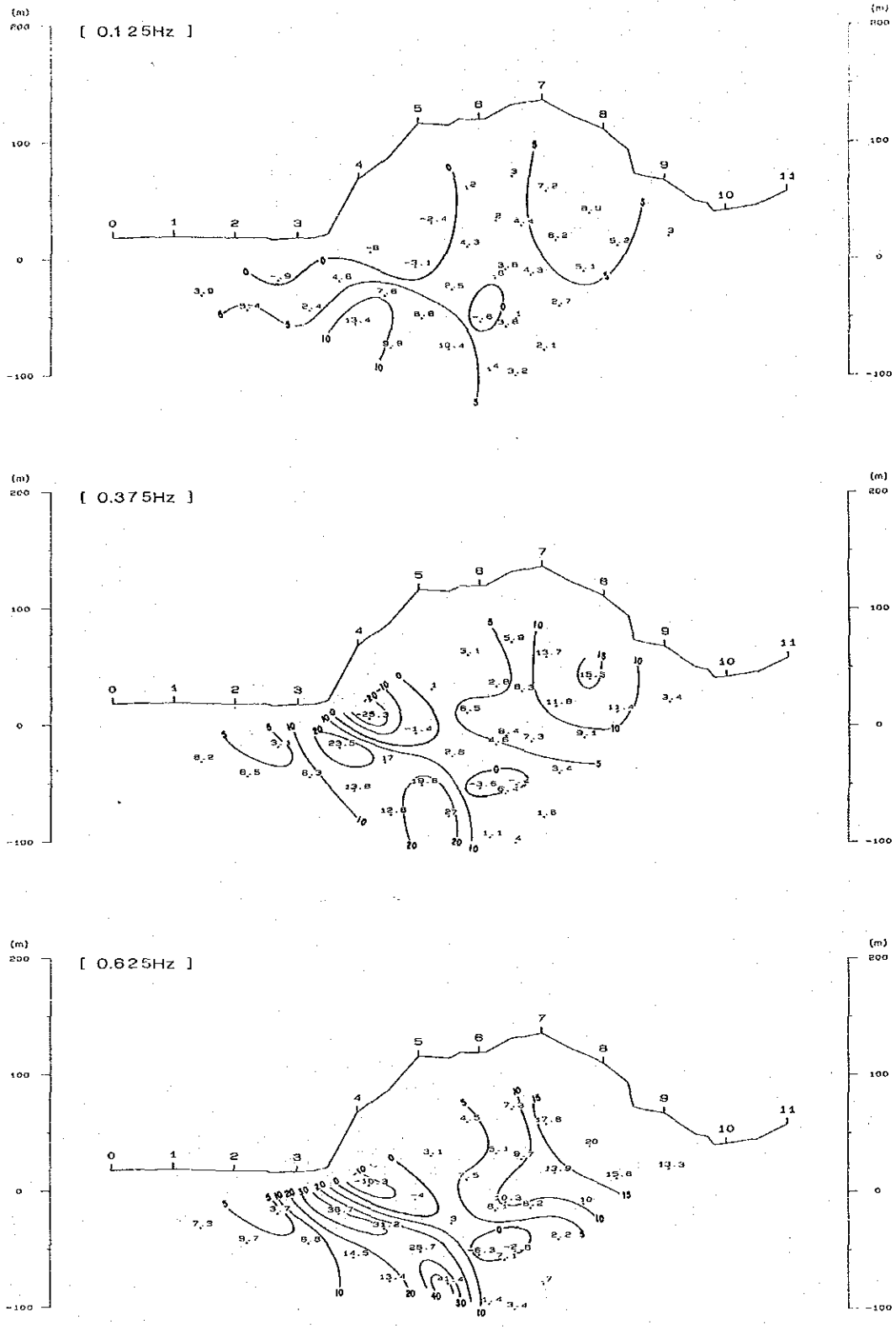

Fig. Ⅱ-14-1 Raw Phase Pseudo-Section of Line A (1)

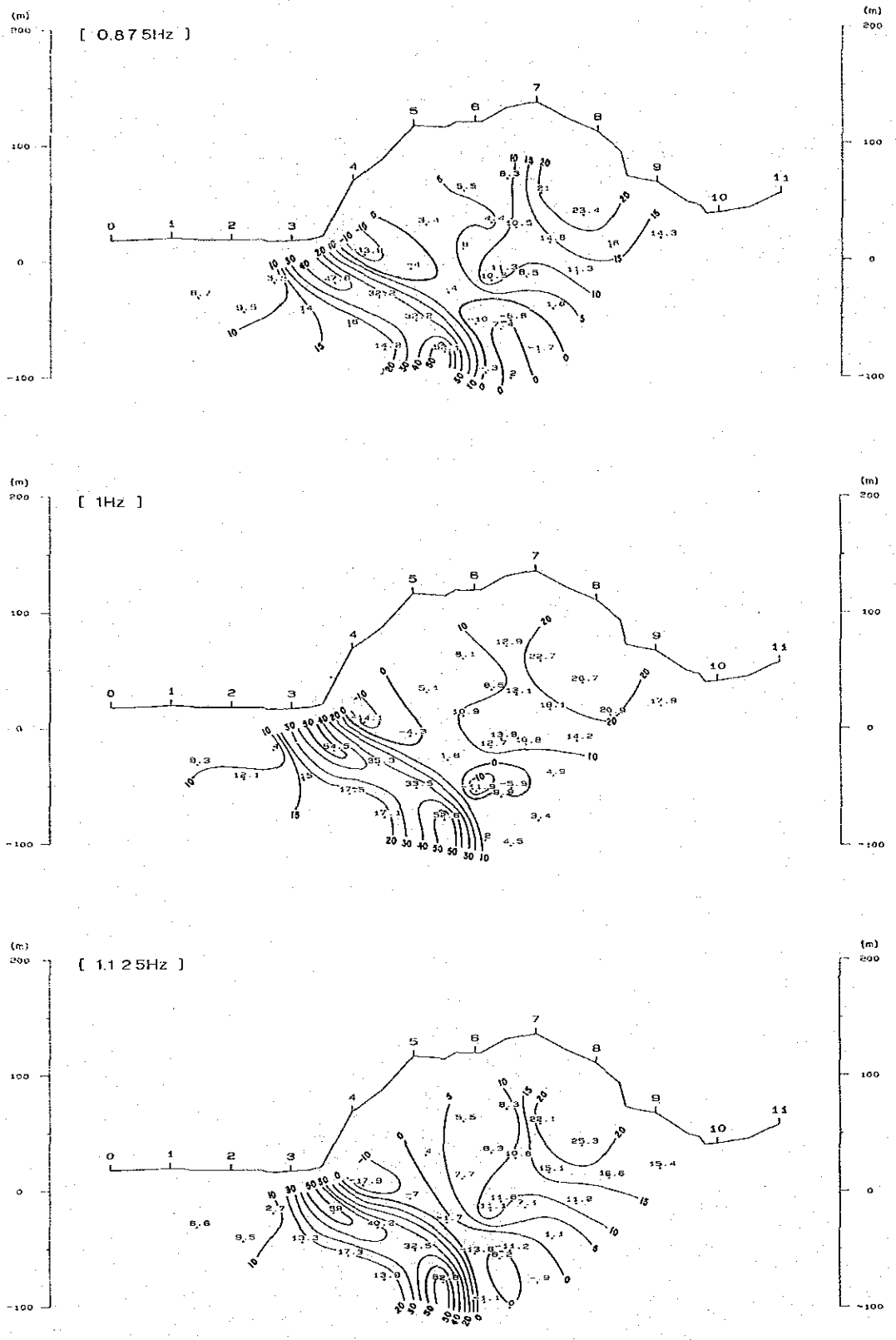

Fig. Ⅱ-14-2 Raw Phase Pseudo-Section of Line A (2)

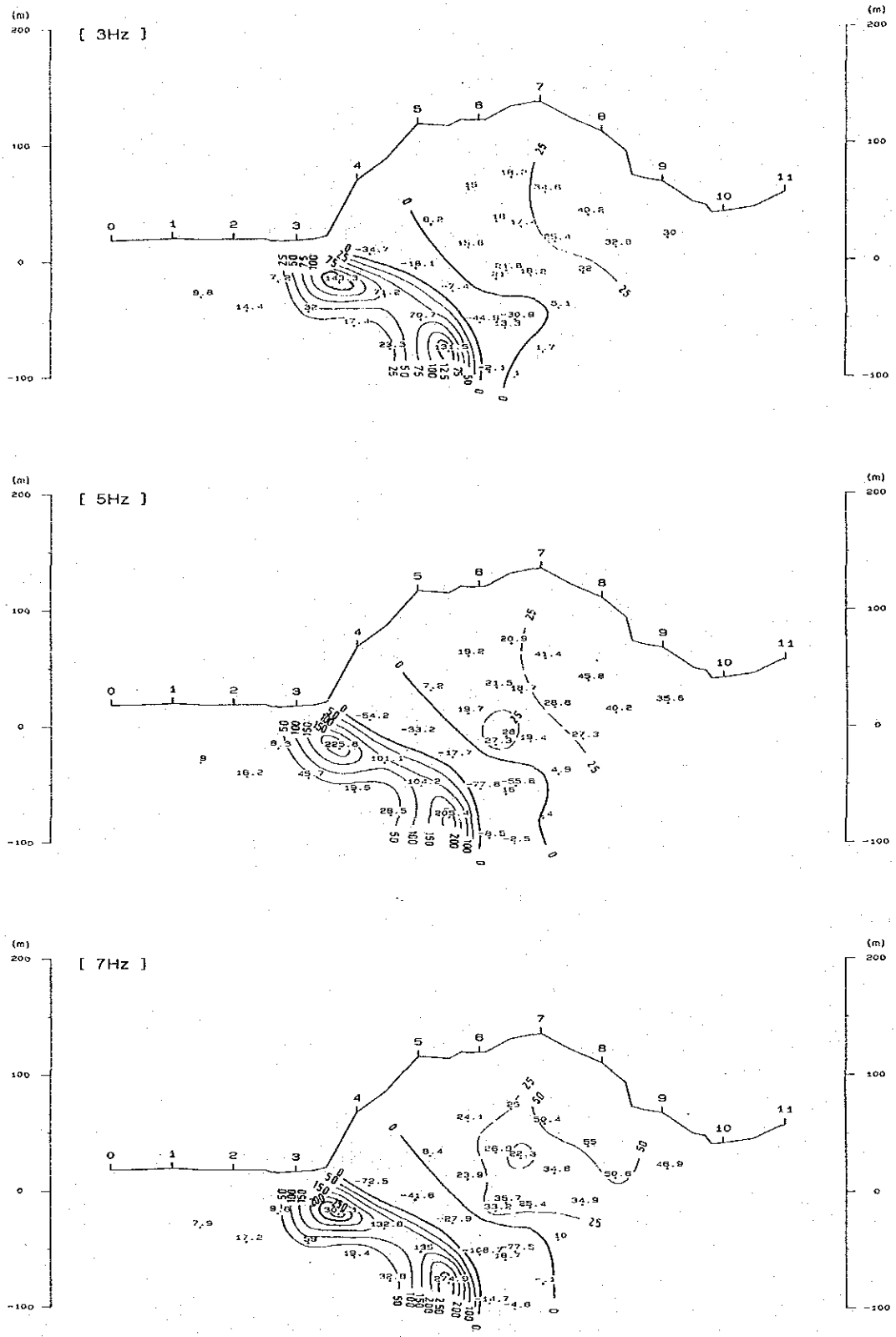

Fig. Ⅱ-14-3 Raw Phase Pseudo-Section of Line A (3)

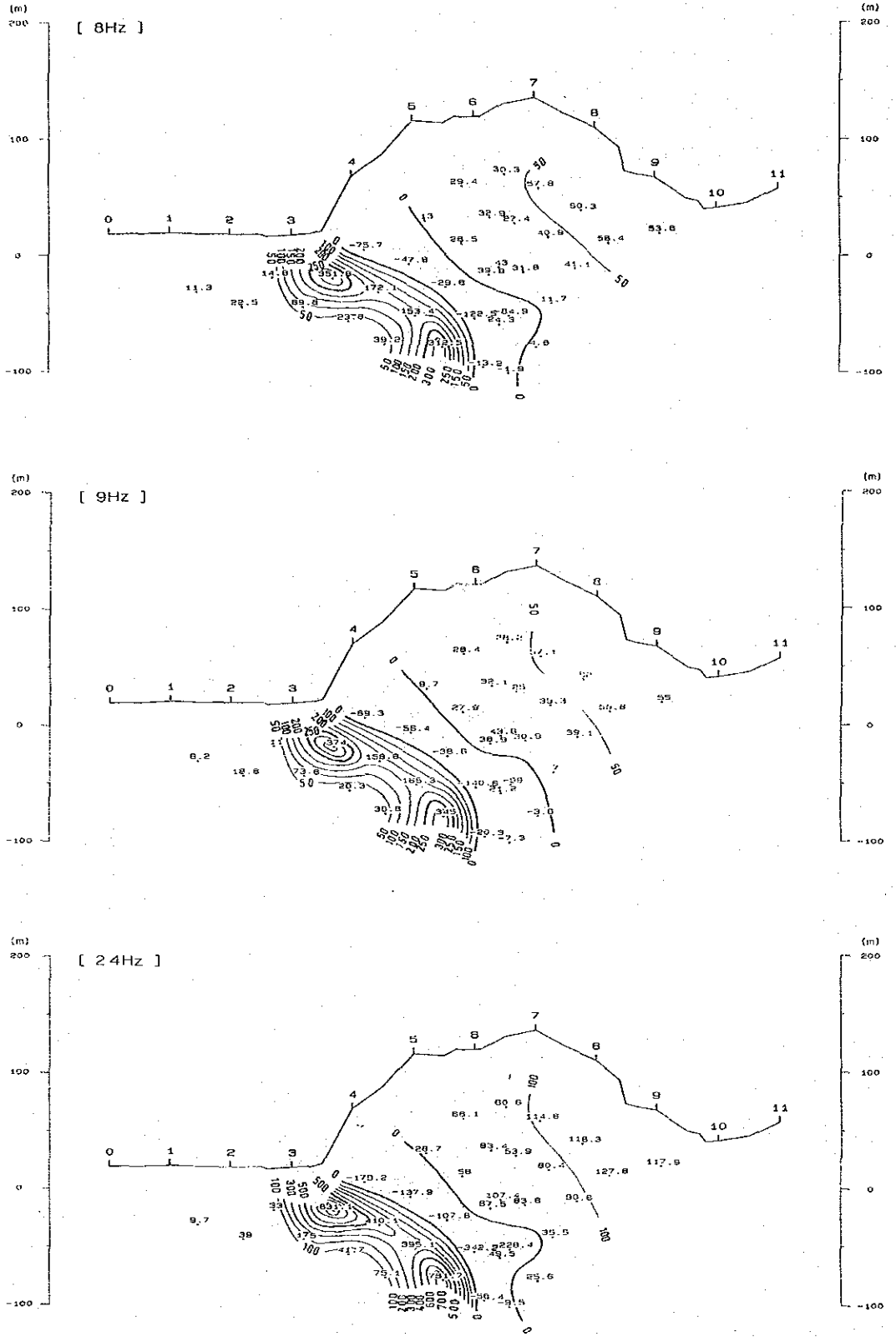

Fig. Ⅱ-14-4 Raw Phase Pseudo-Section of Line A (4)

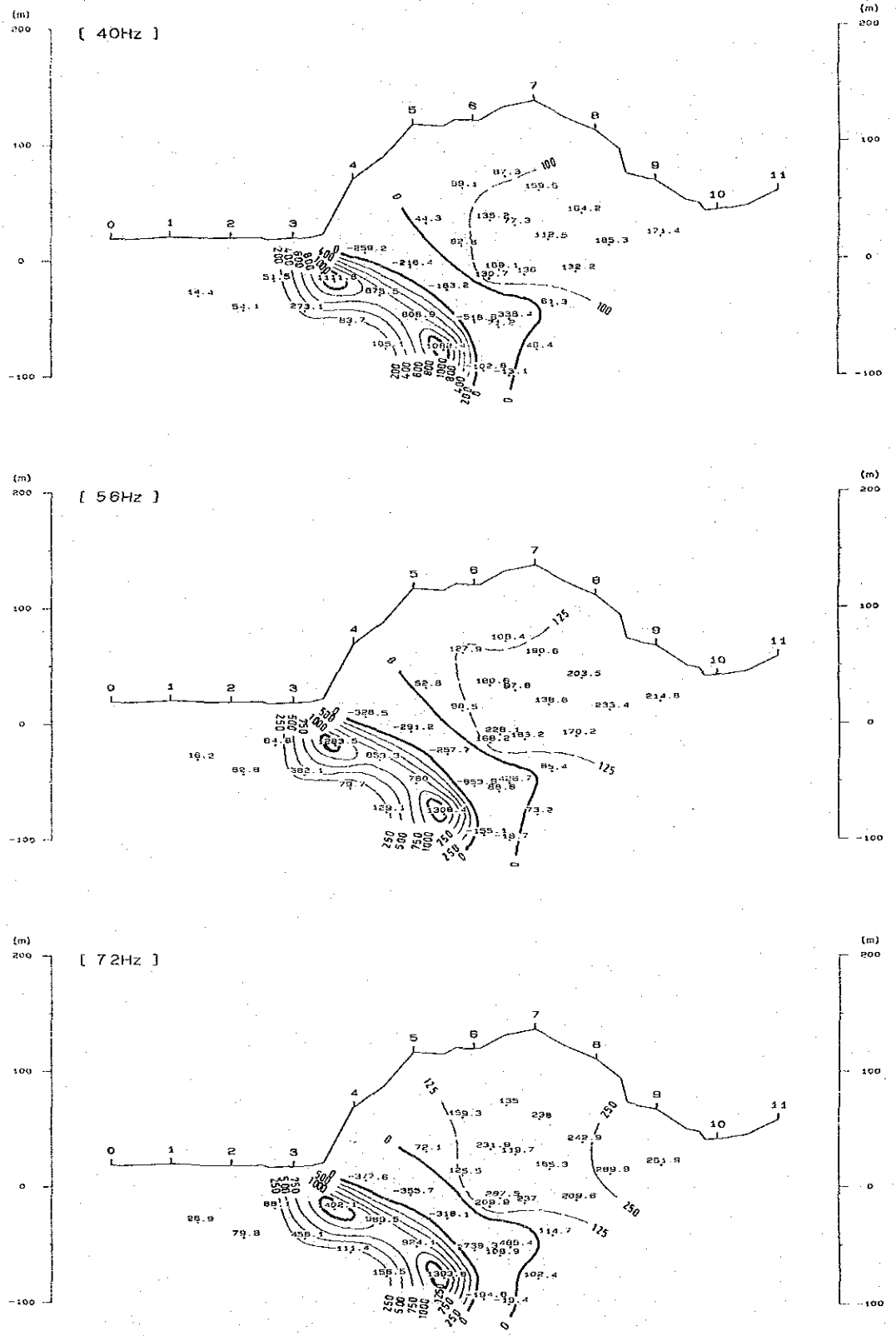

Fig. Ⅱ-14-5 Raw Phase Pseudo-Section of Line A (5)

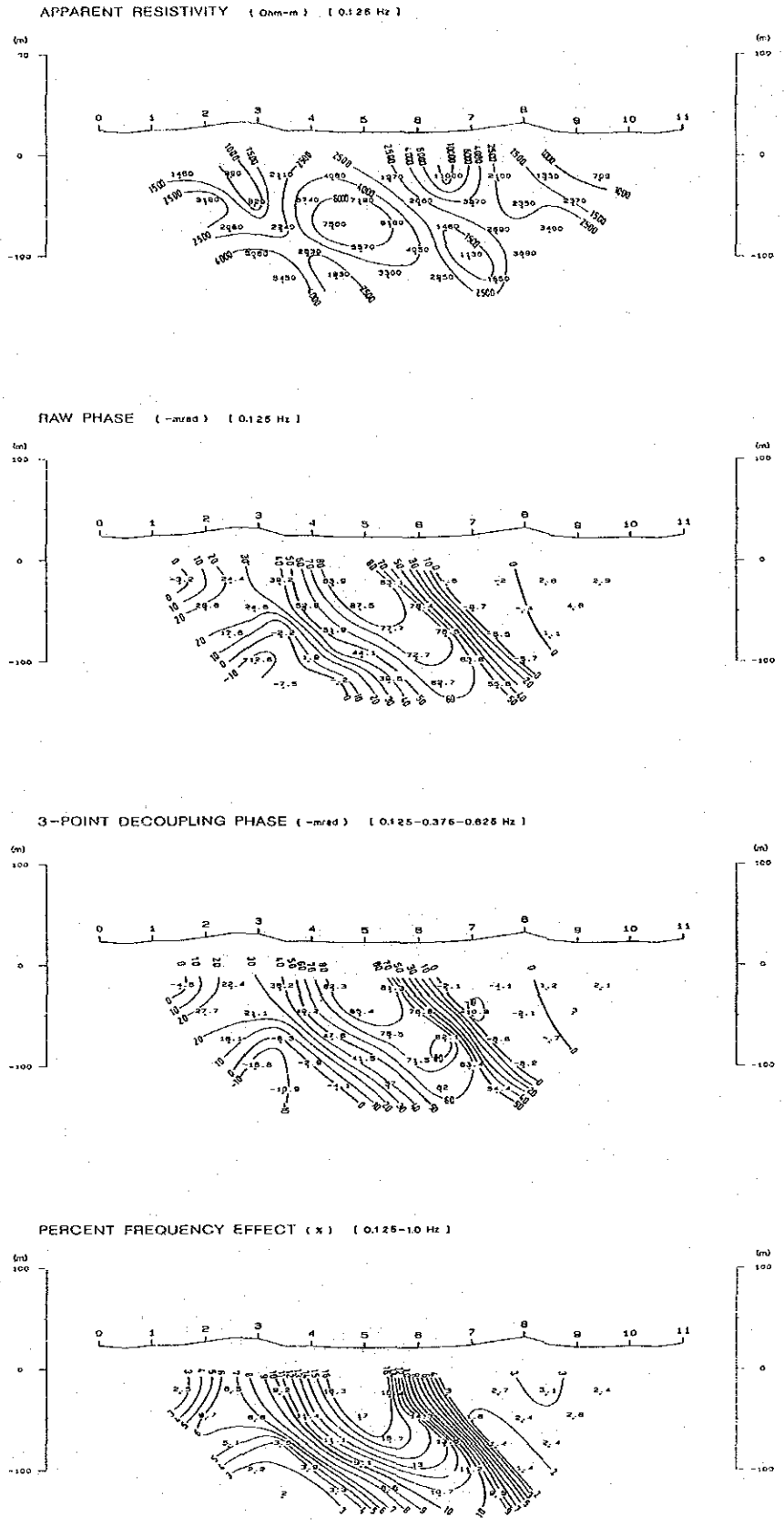

Fig. Ⅱ-15 Spectral IP Pseudo-Section of Line B

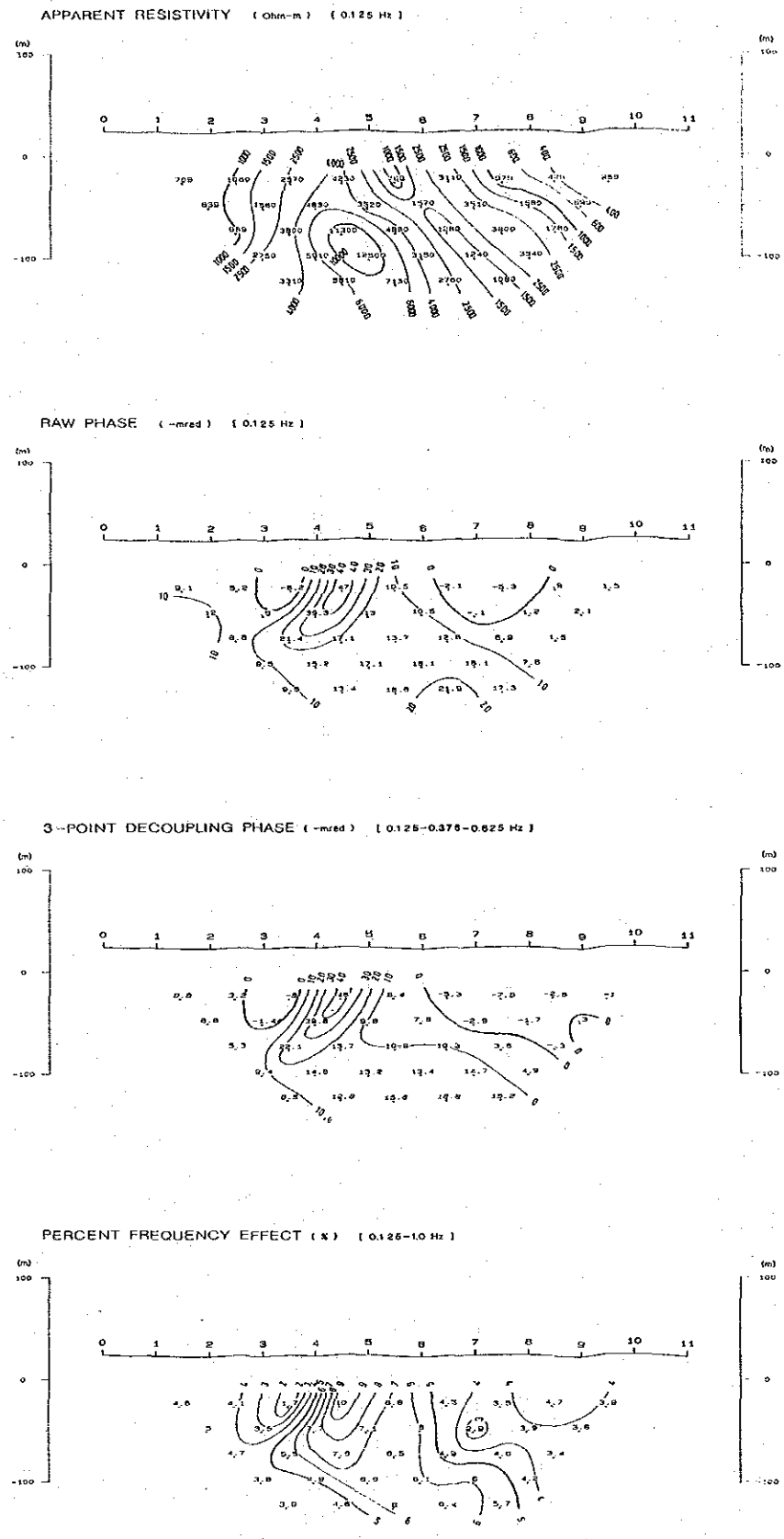

Fig. Ⅱ-16 Spectral IP Pseudo-Section of Line C

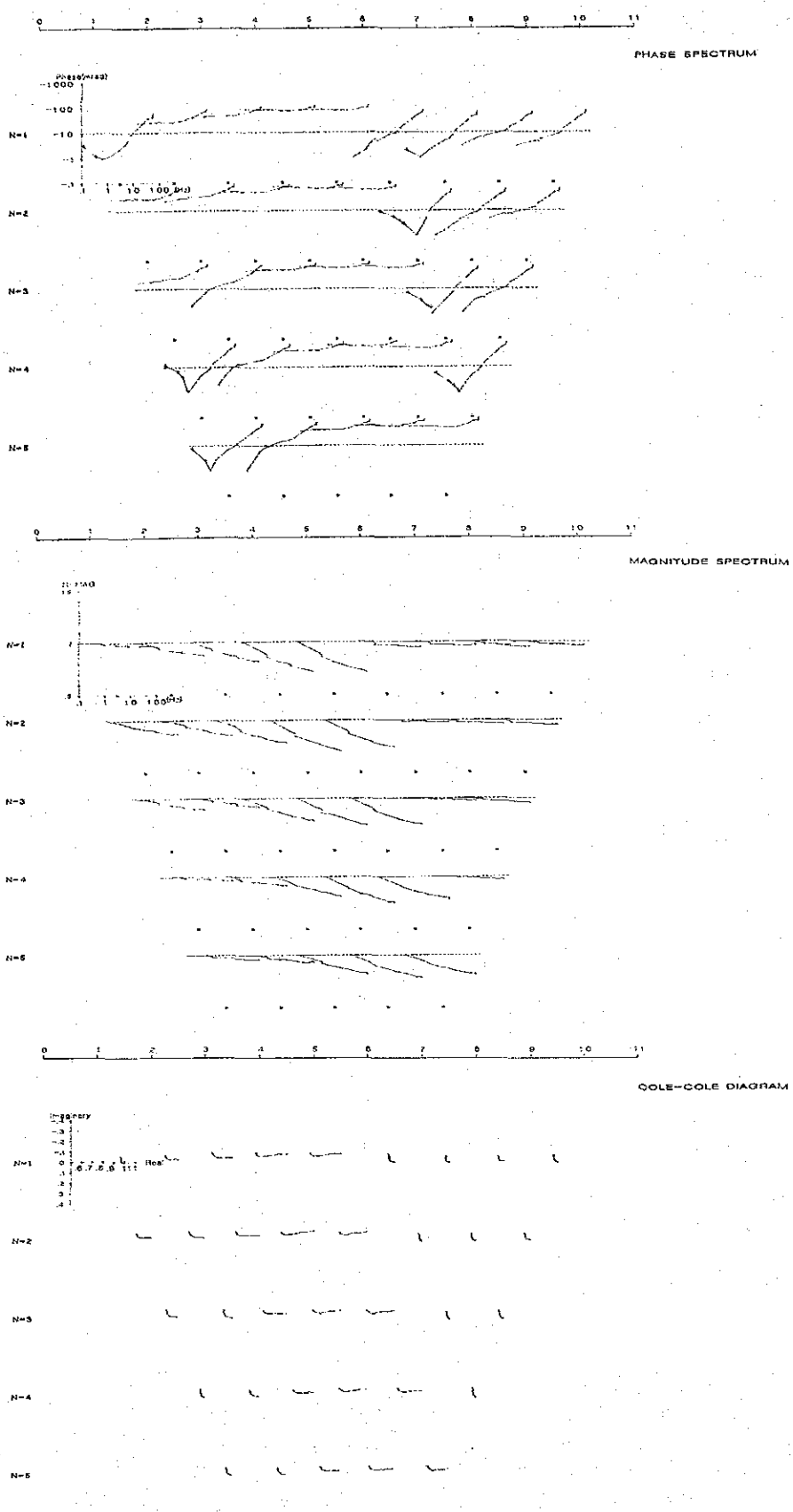

Fig. Ⅱ-17 Spectrum Diagram of Line B

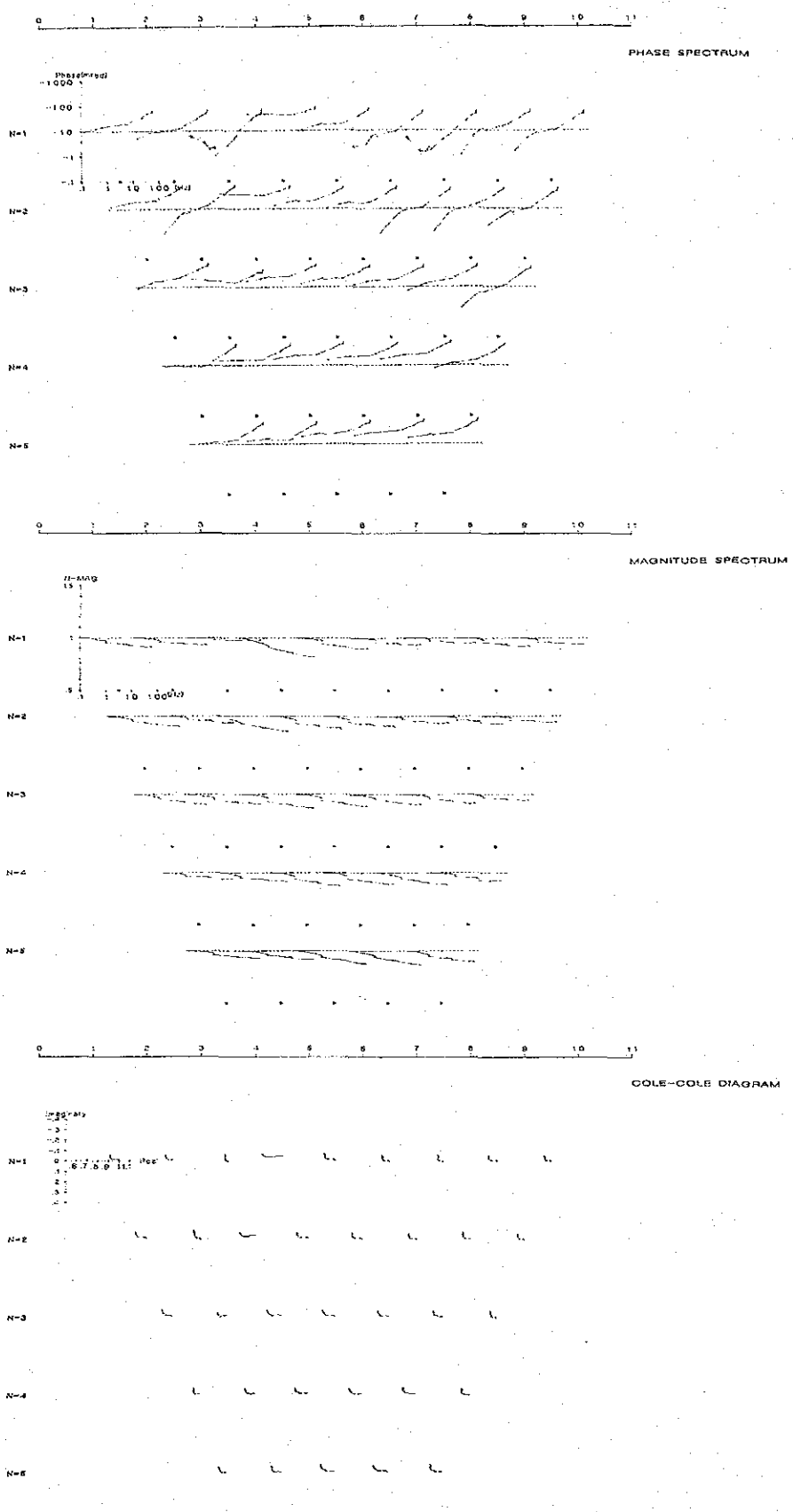

Fig. Ⅱ-18 Spectrum Diagram of Line C

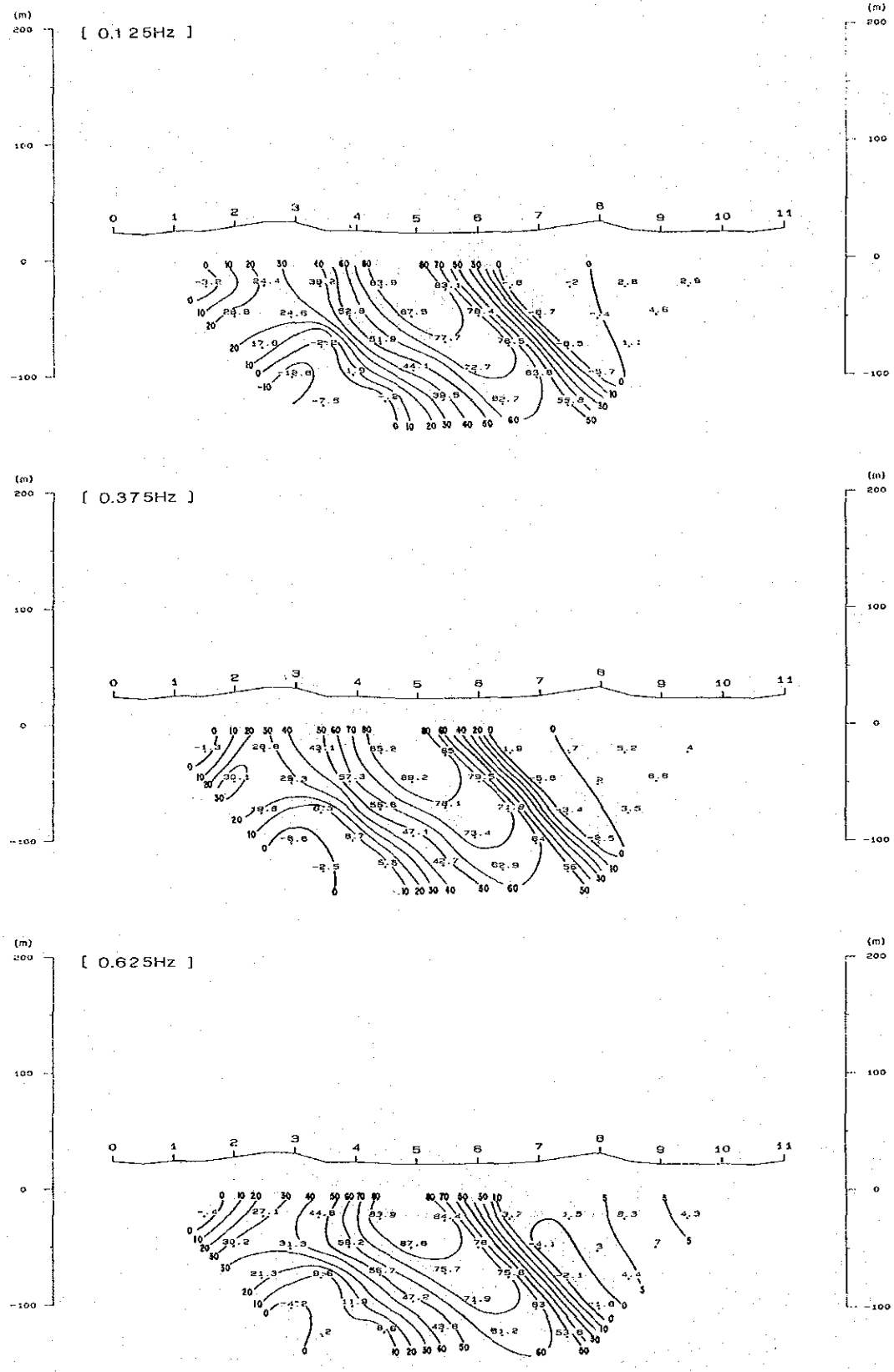

Fig. Ⅱ-19-1 Raw Phase Pseudo-Sectien of Line B (1)

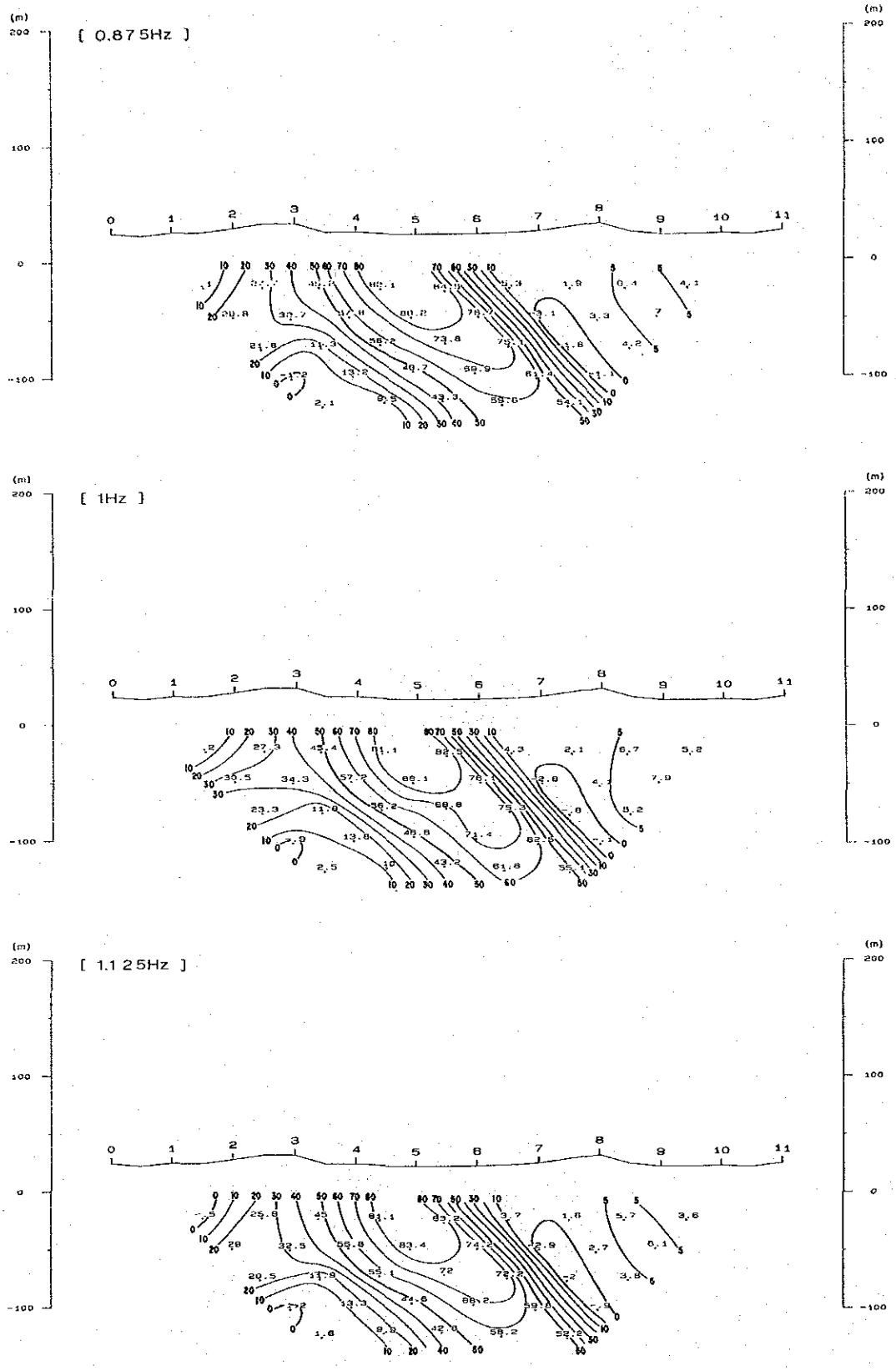

Fig. Ⅱ-19-2 Raw Phase Pseudo-Section of Line B (2)

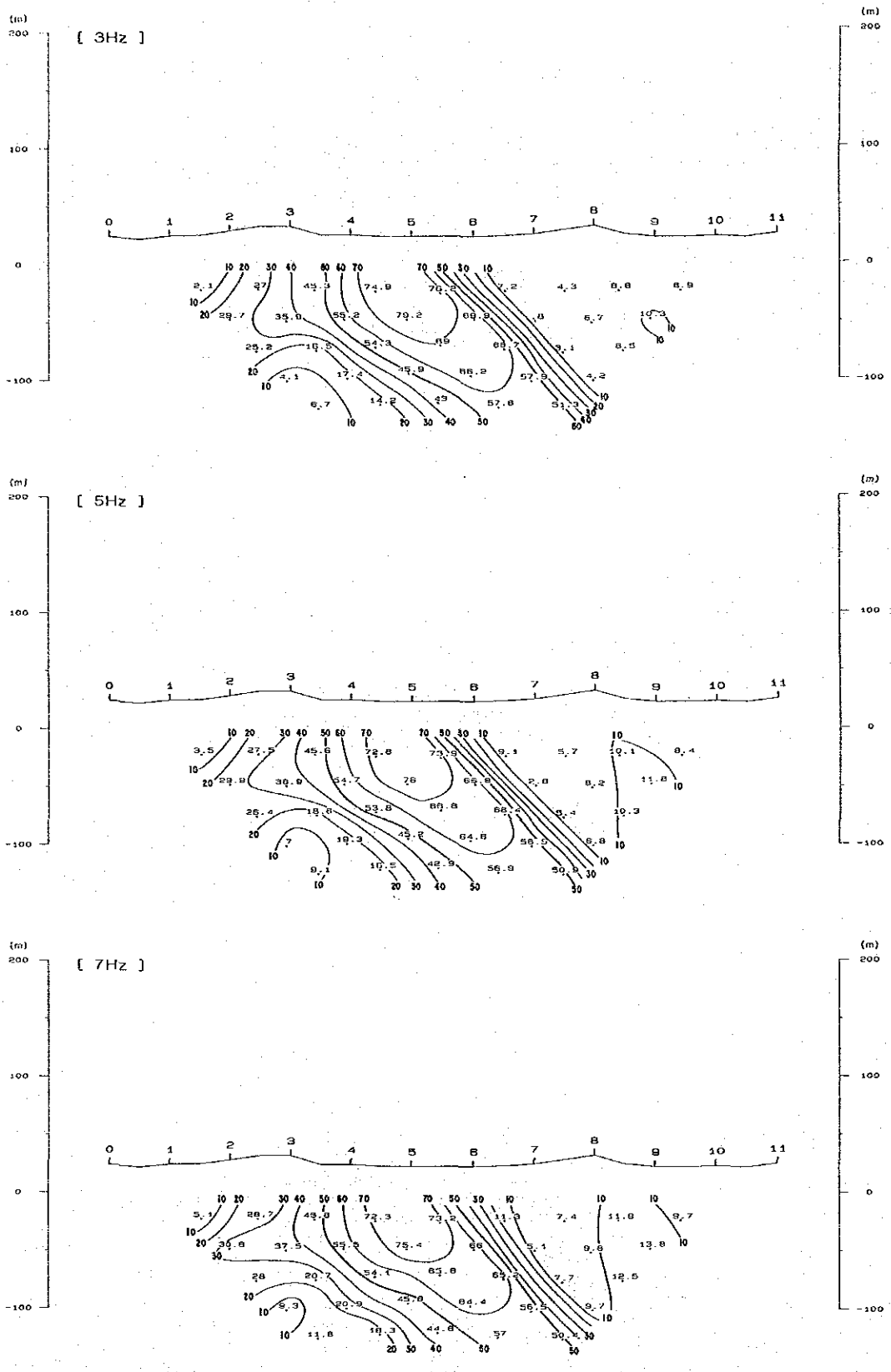

Fig. Ⅱ-19-3 Raw Phase Pseudo-Section of Line B (3)

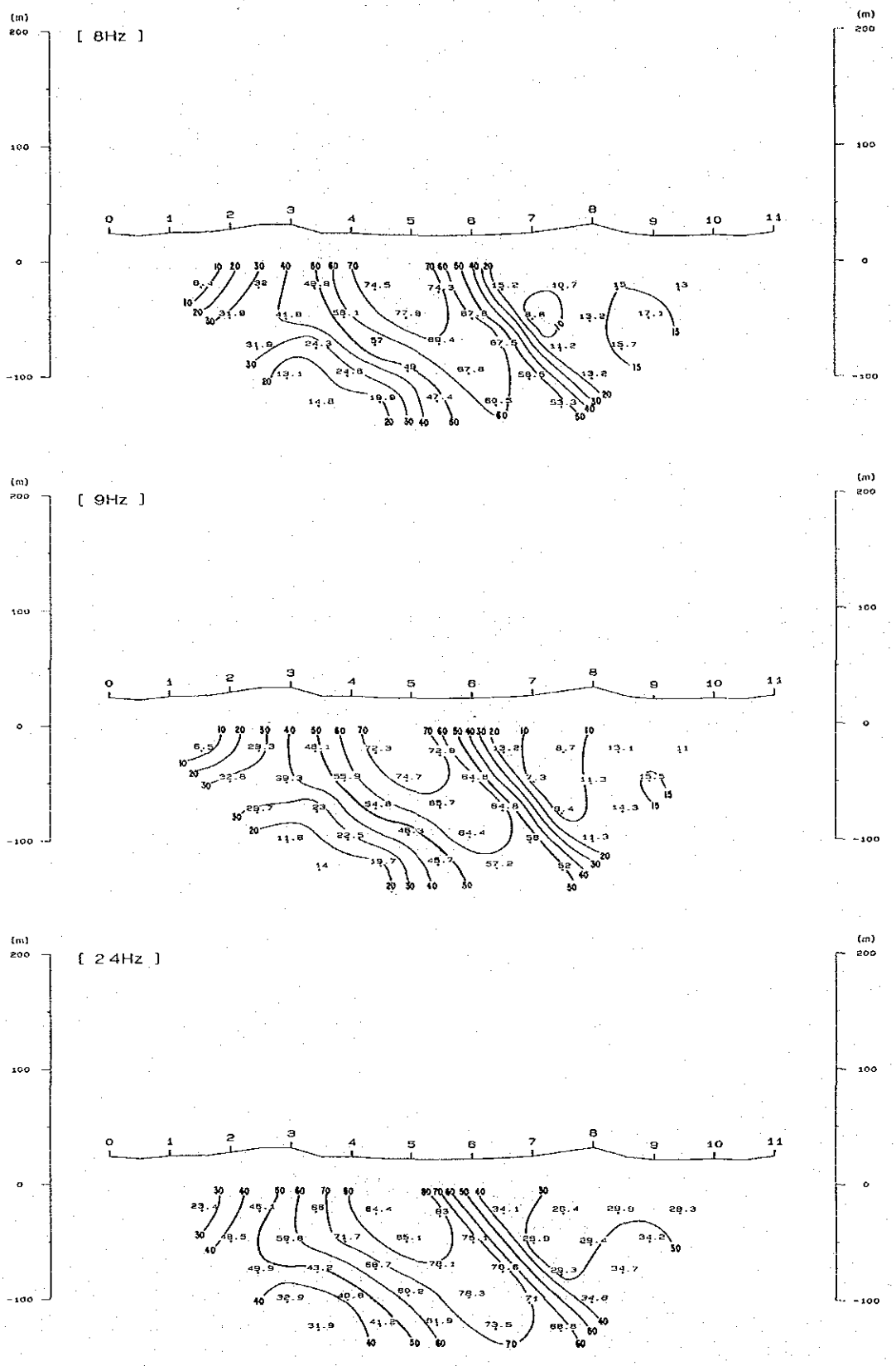

Fig. Ⅱ-19-4 Raw Phase Pseudo-Sectien of Line B (4)

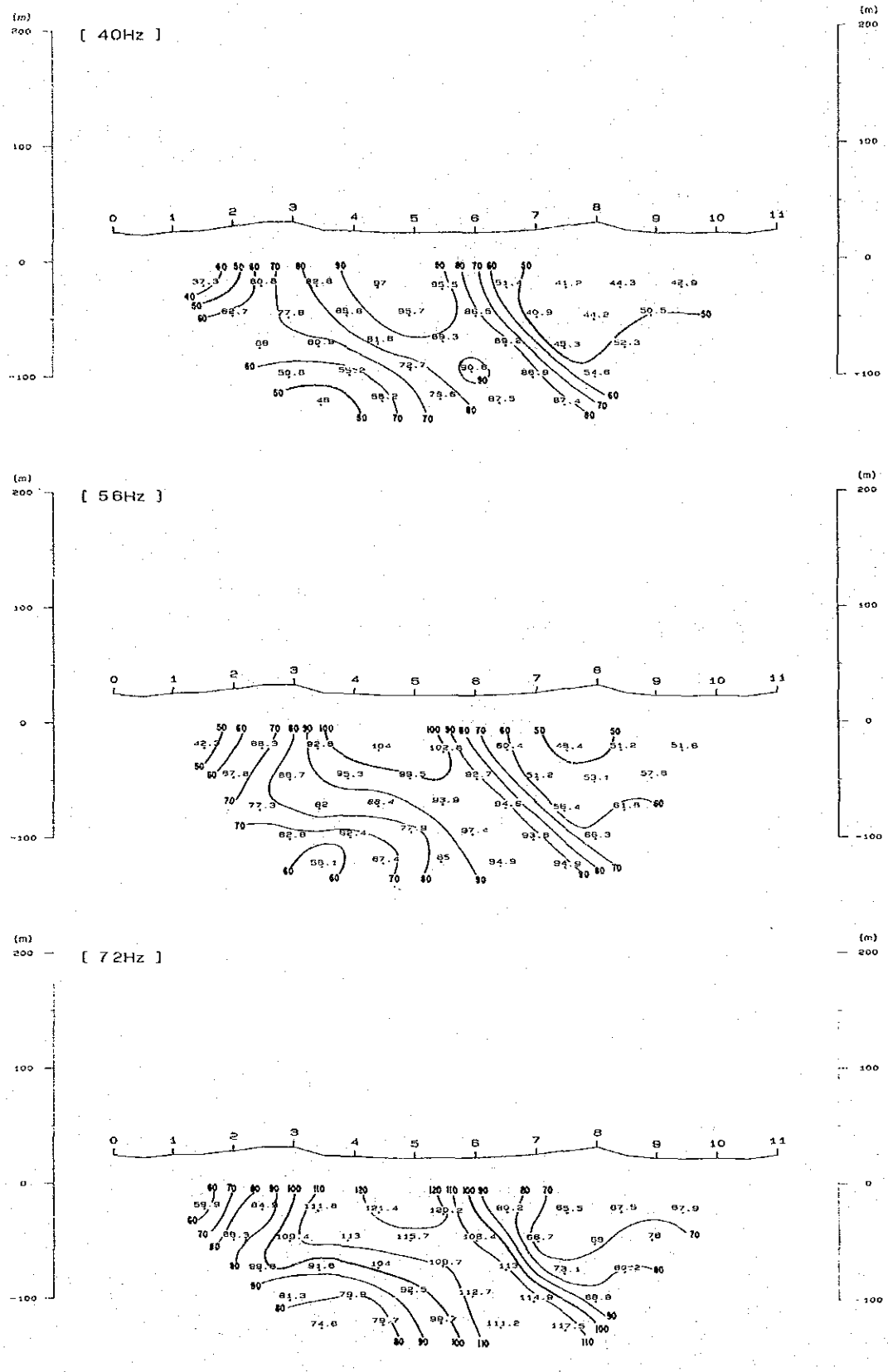

Fig. Ⅱ-19-5 Raw Phase Phase Pseudo-Section of Line B (5)

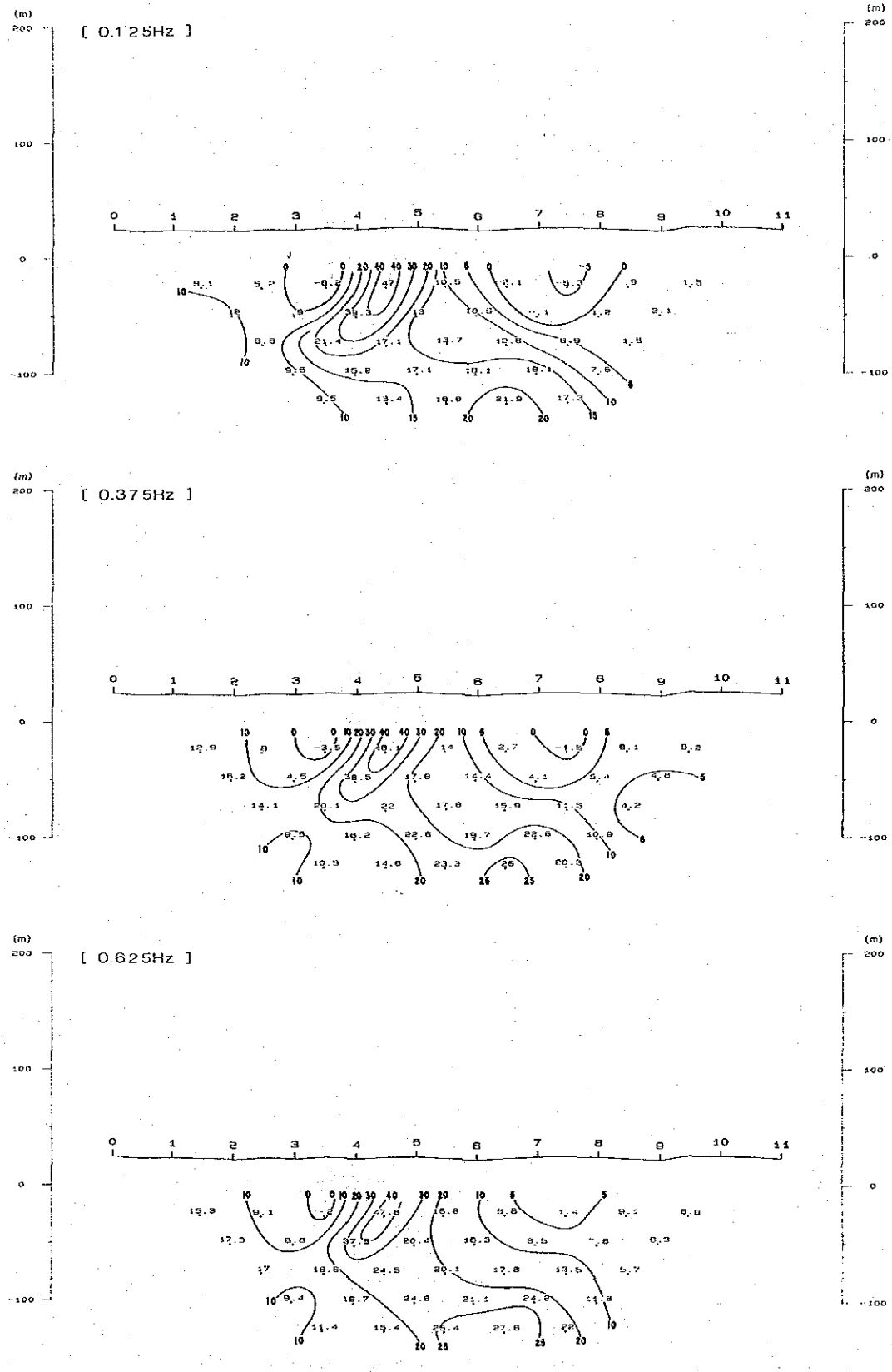

Fig. Ⅱ-20-1 Raw Phase Pseudo-Section of Line C (1)

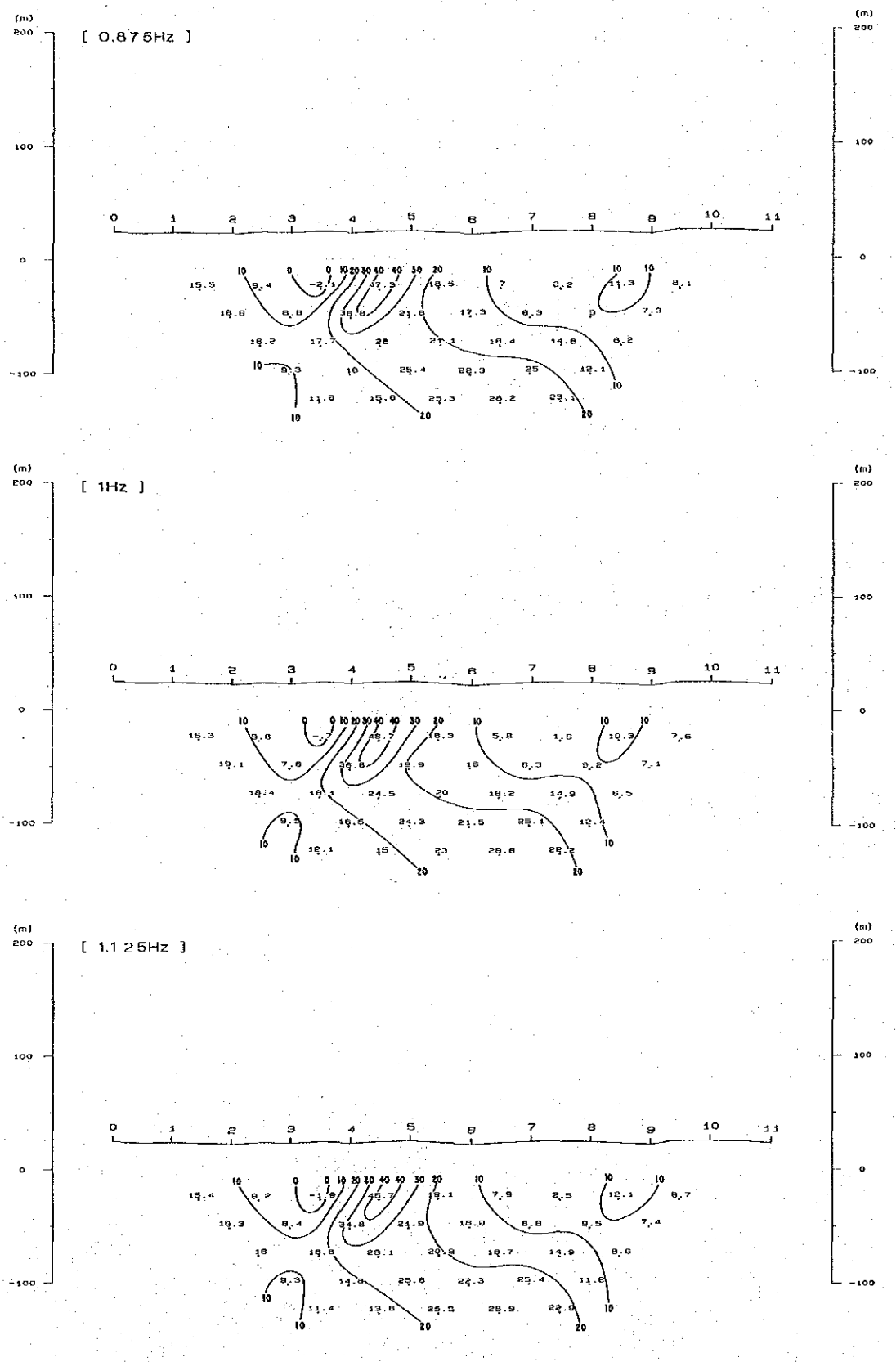

Fig. Ⅱ-20-2 Raw Phase Pseudo-Section of Line C (2)

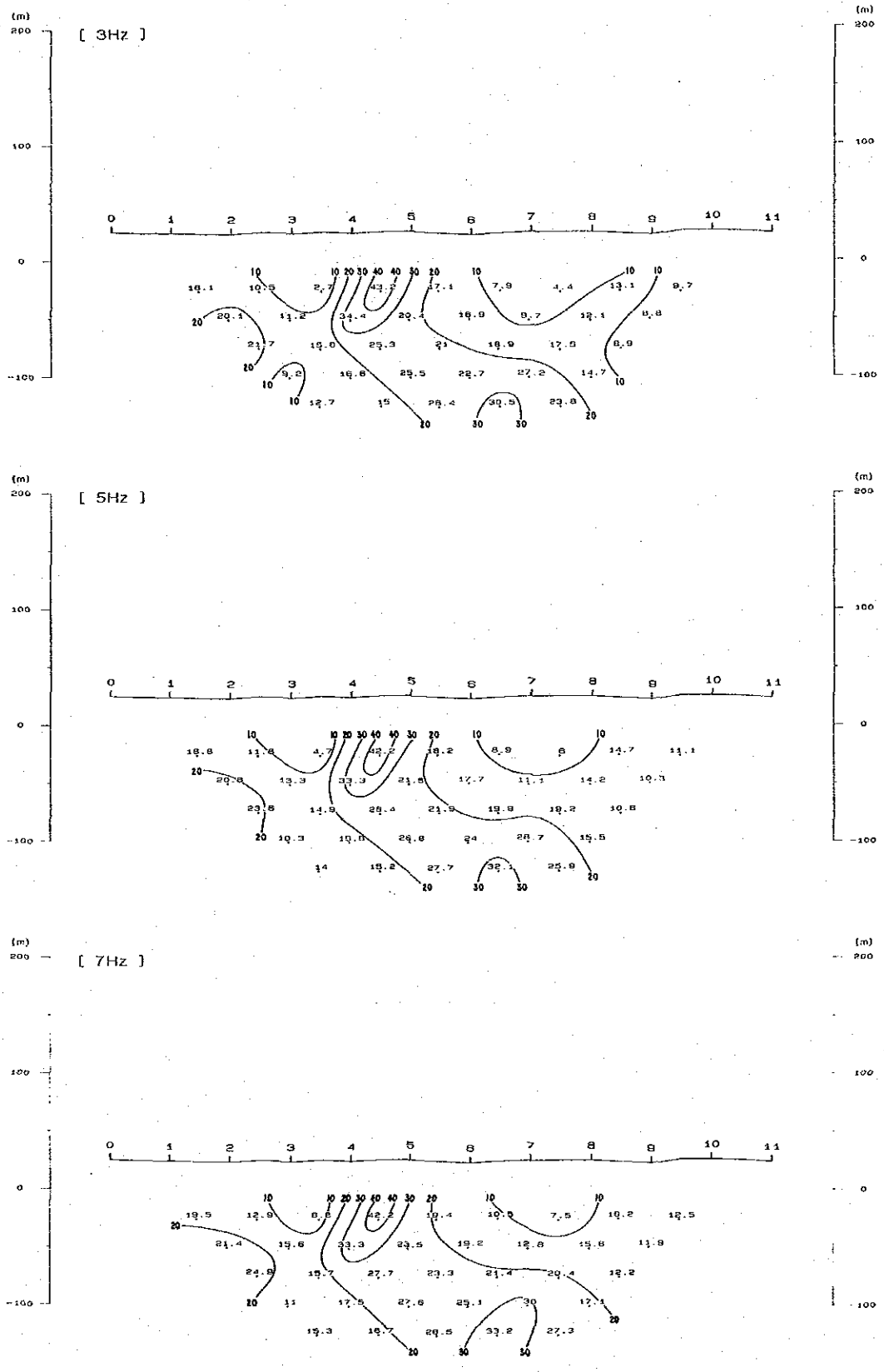

Fig. Ⅱ-20-3 Raw Phase Pseudo-Section of Line C (3)

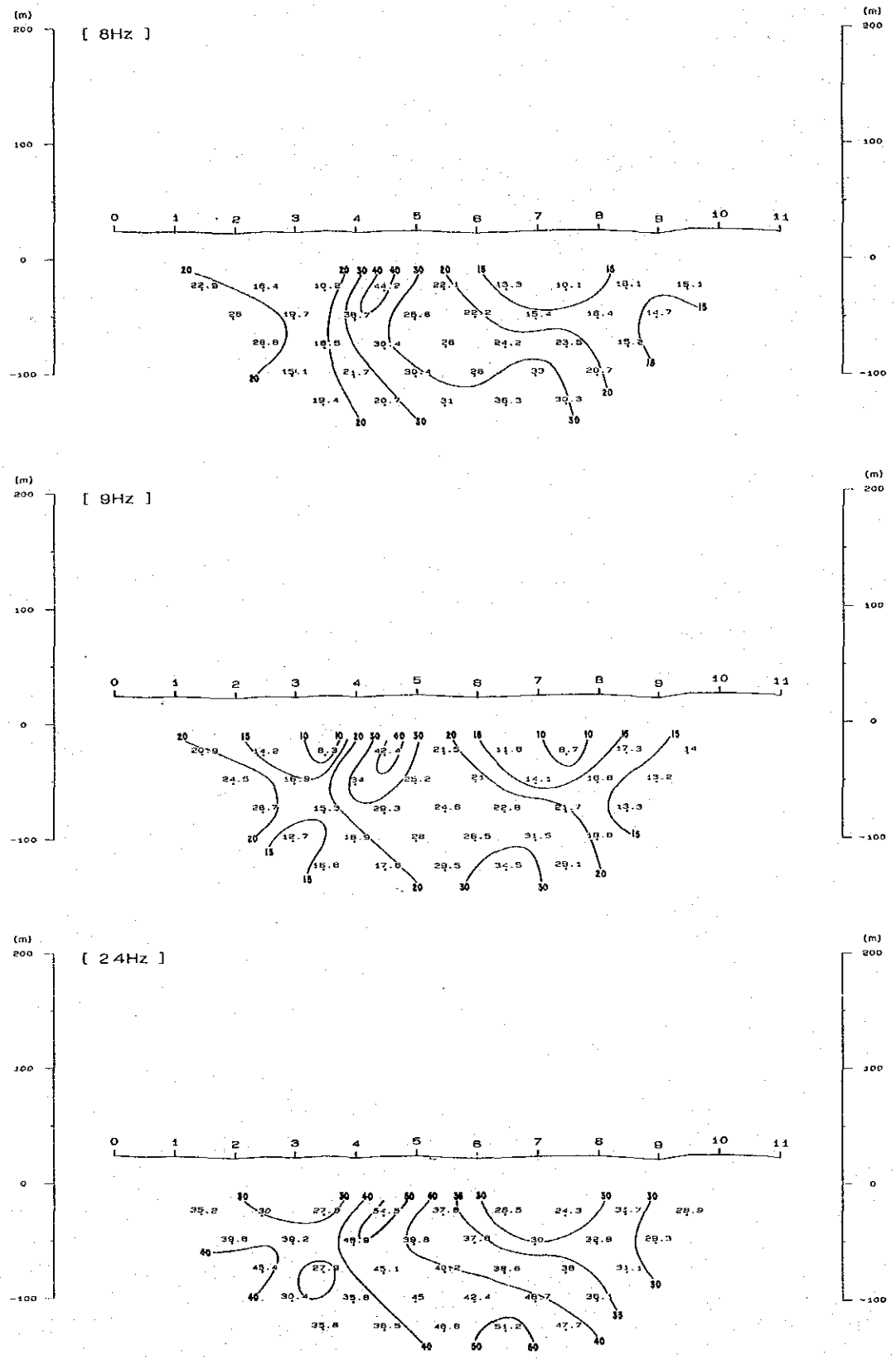

Fig. Ⅱ-20-4 Raw Phase Pseudo-Section of Line C (4)

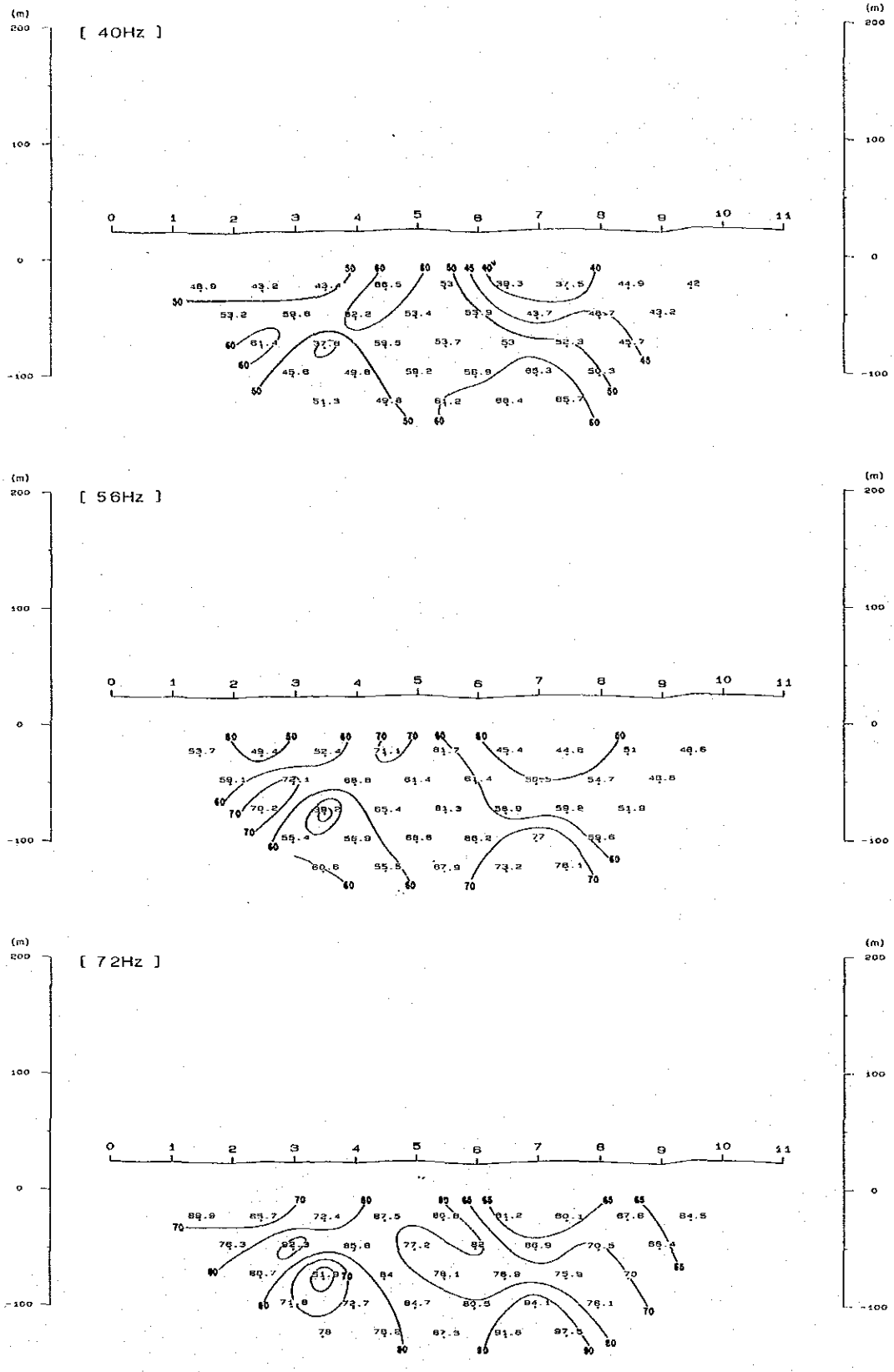

Fig. Ⅱ-20-5 Raw Phbse Pseudo-Section of Line C (5)

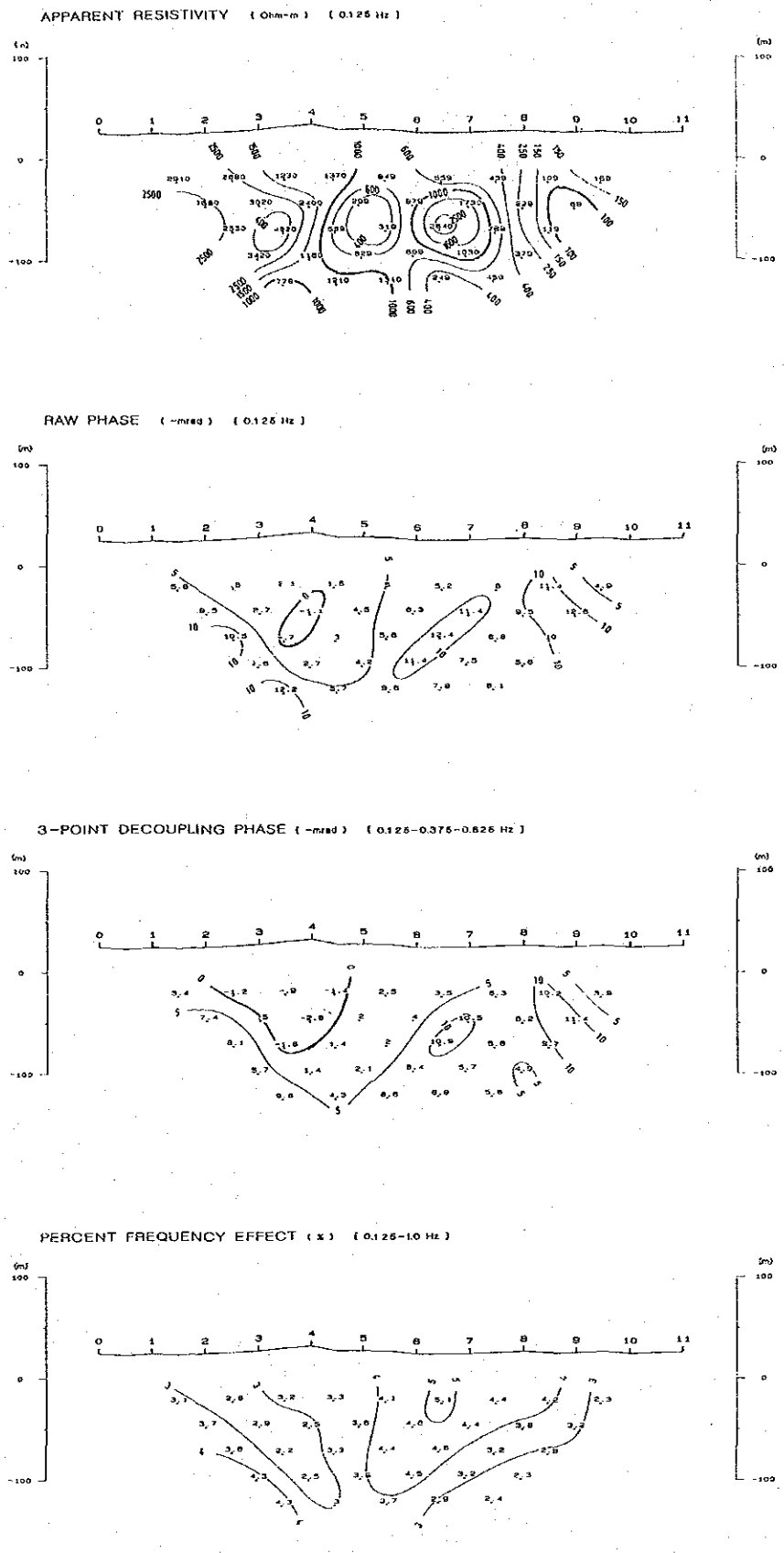

Fig. Ⅱ-21 Spectral IP Pseudo-Section of Line D

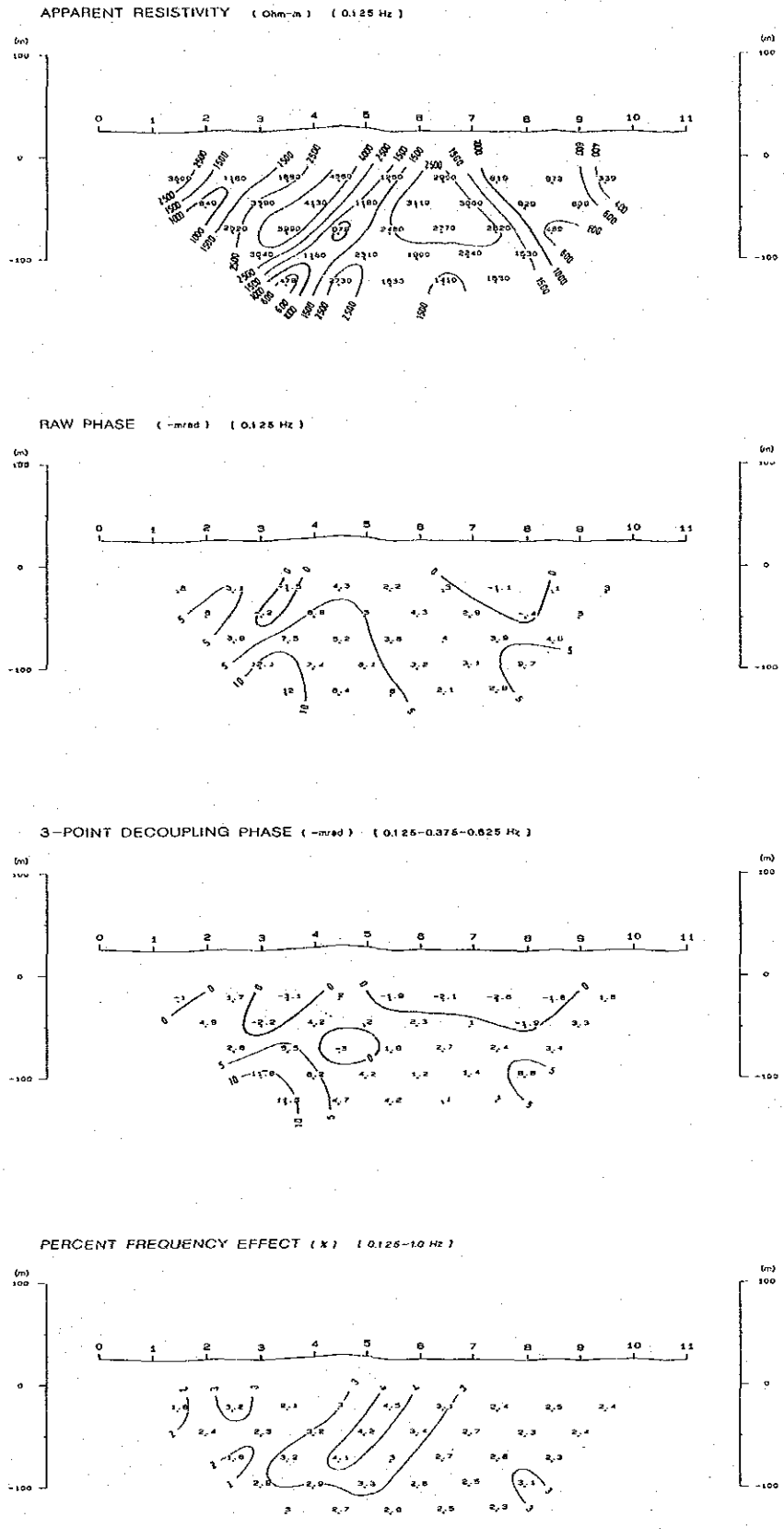

Fig. Ⅱ-22 Spectral IP Pseudo-Section of Line E

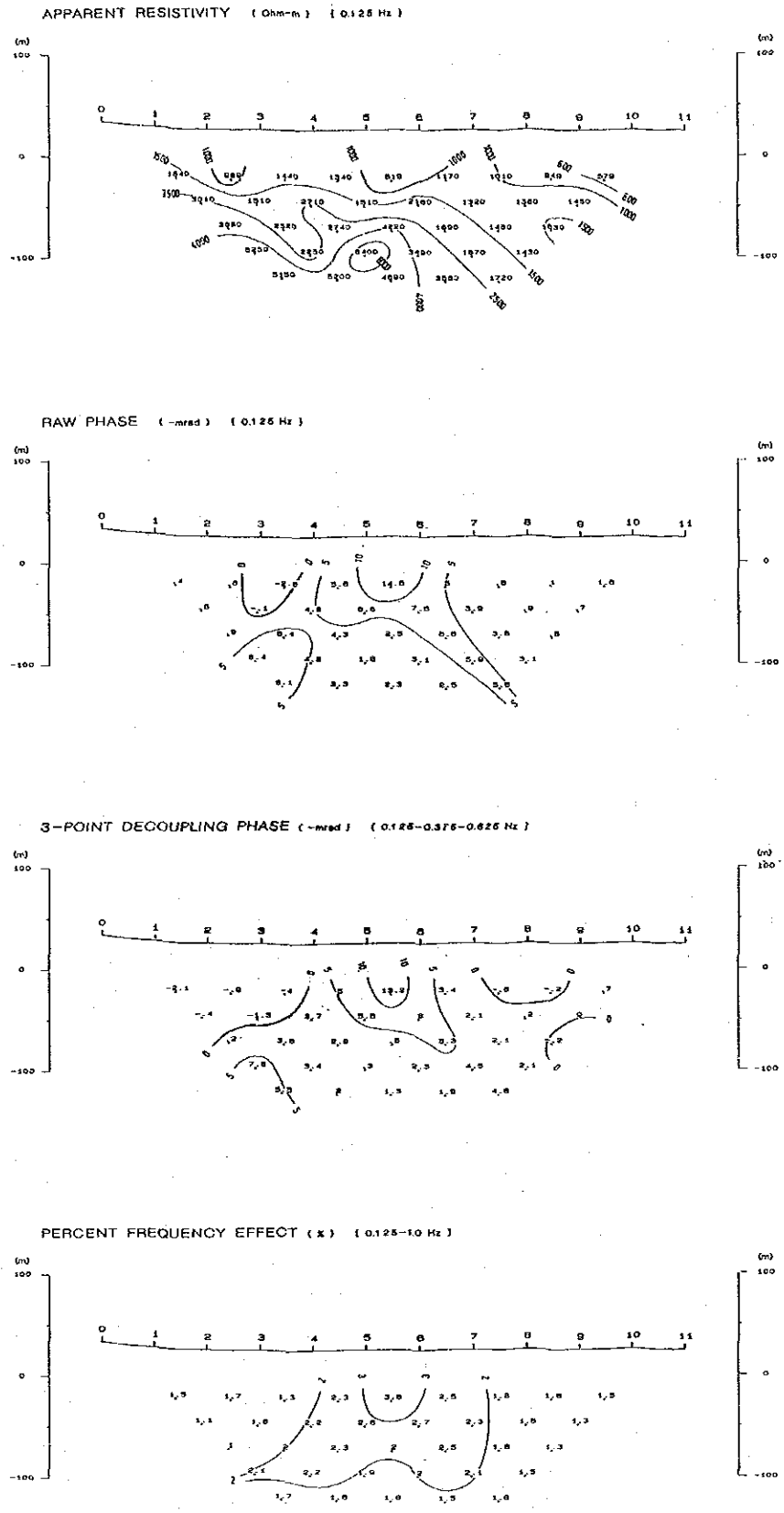

Fig. Ⅱ-23 Spectral IP Pseudo-Section of Line F

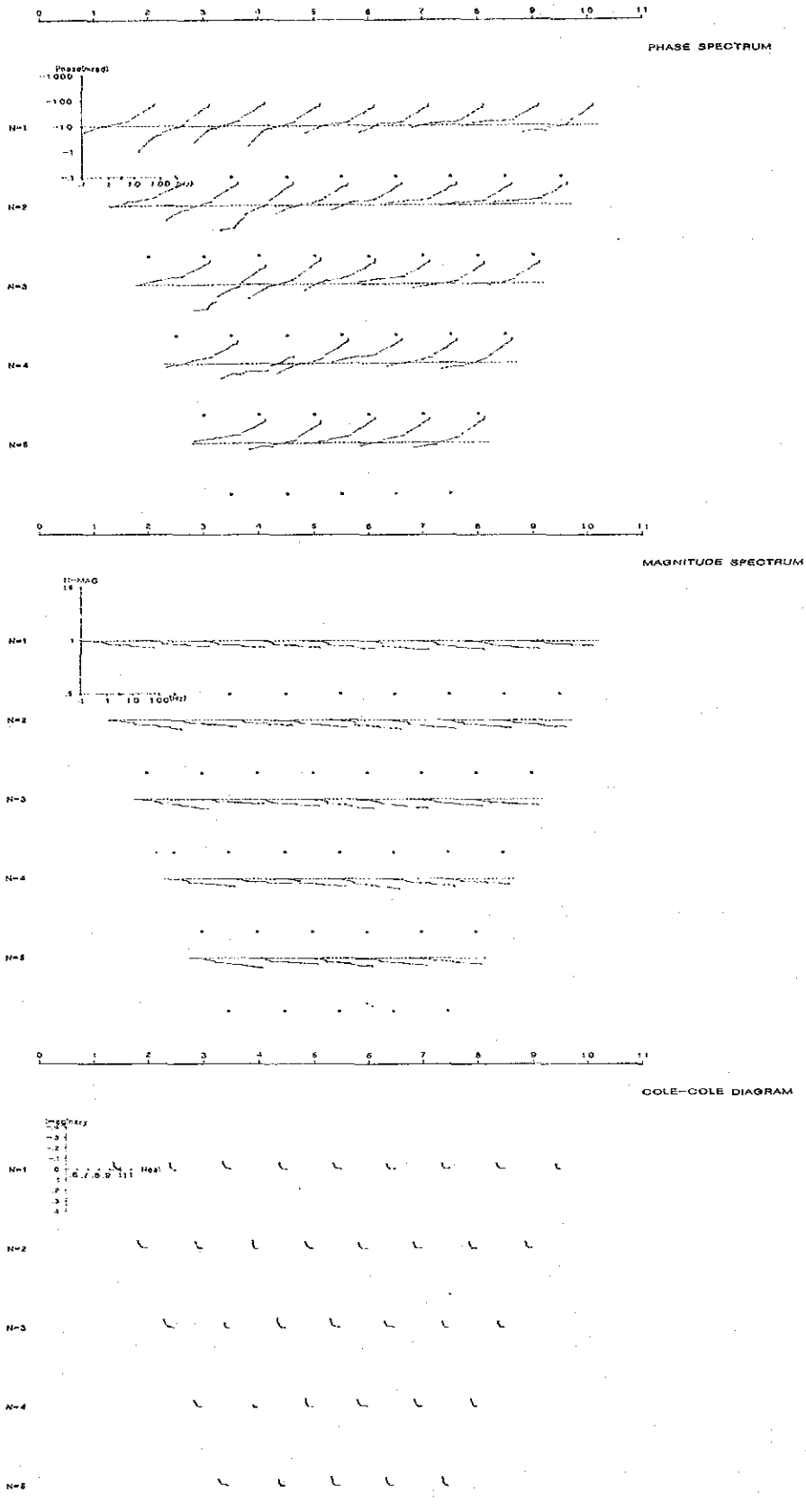

Fig. Ⅱ-24 Spectrum Diagram of Line D

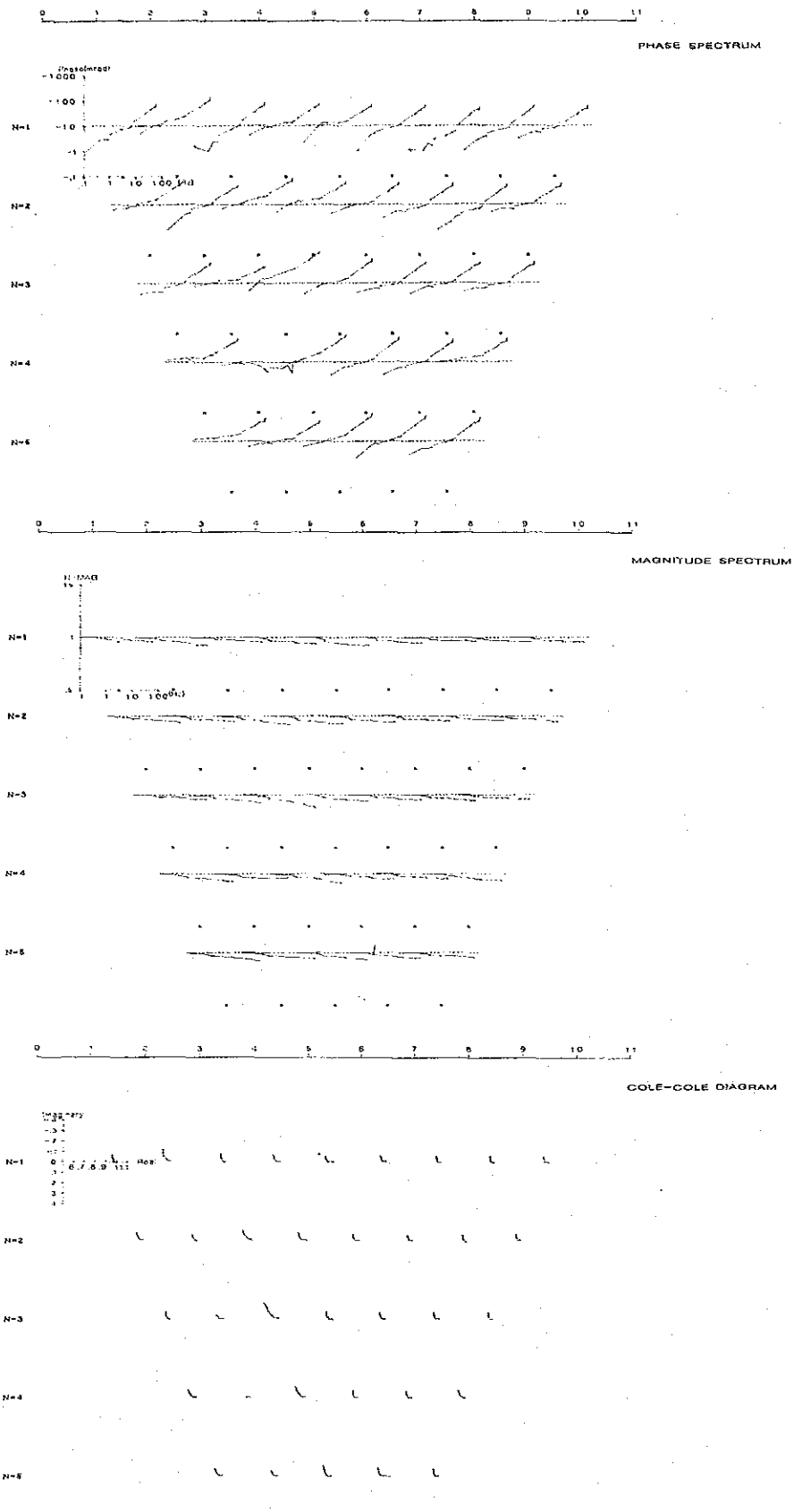

Fig. Ⅱ-25 Spectrum Diagram of Line E

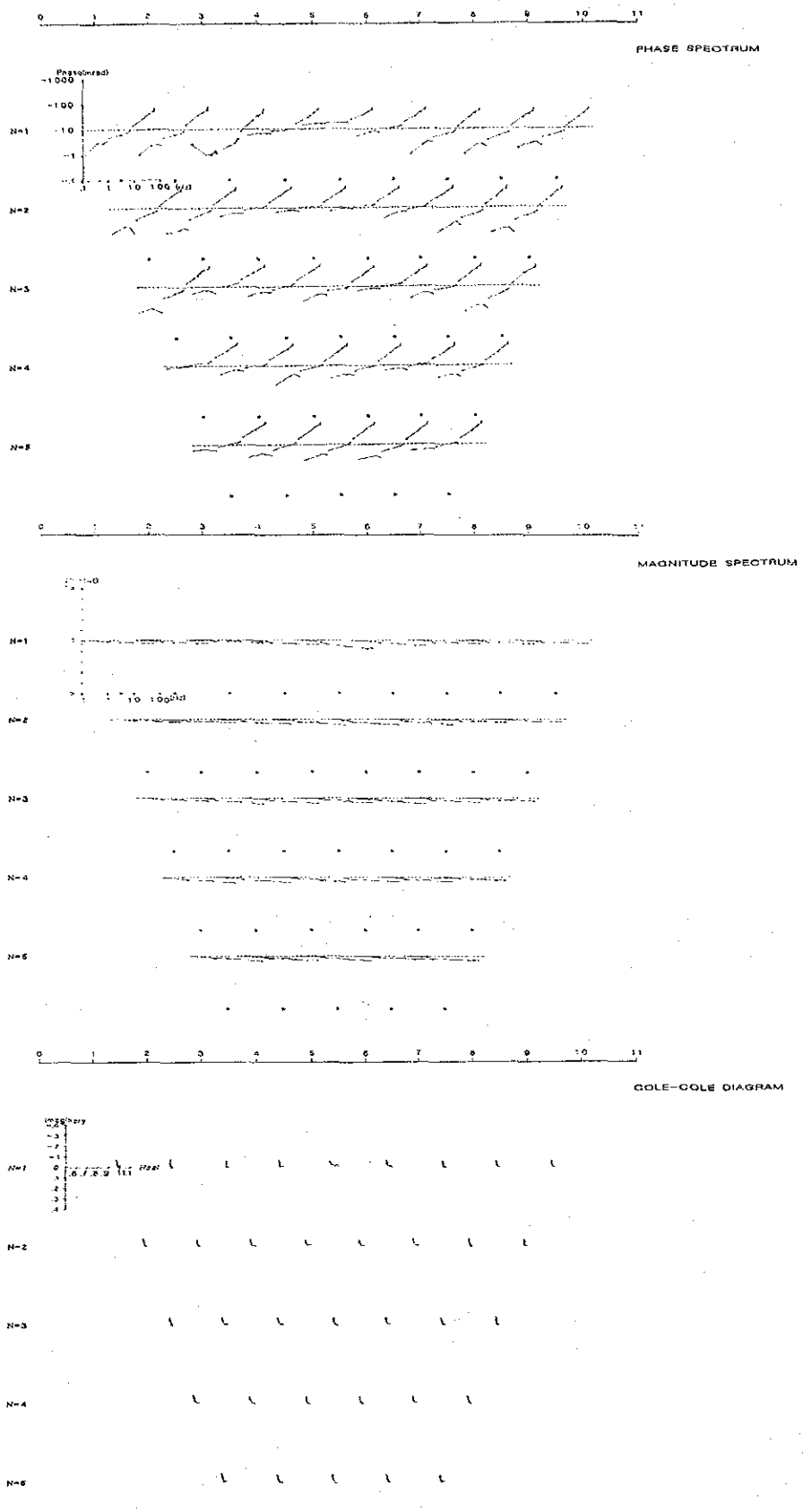

Fig. Ⅱ-26 Spectrum Diagram of Line F

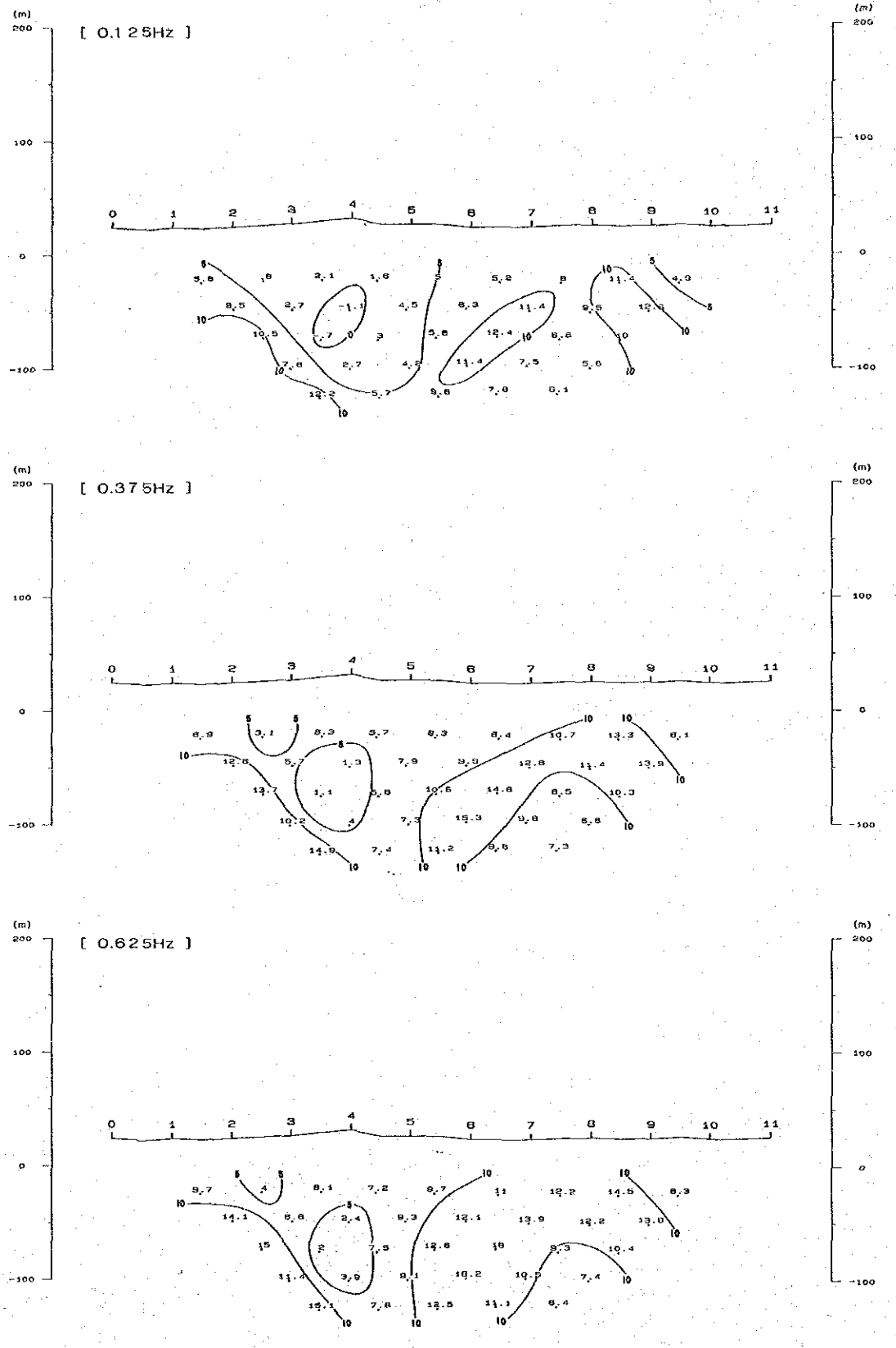

Fig. Ⅱ-27-1 Raw Phase Pseudo-Section of Line D (1)

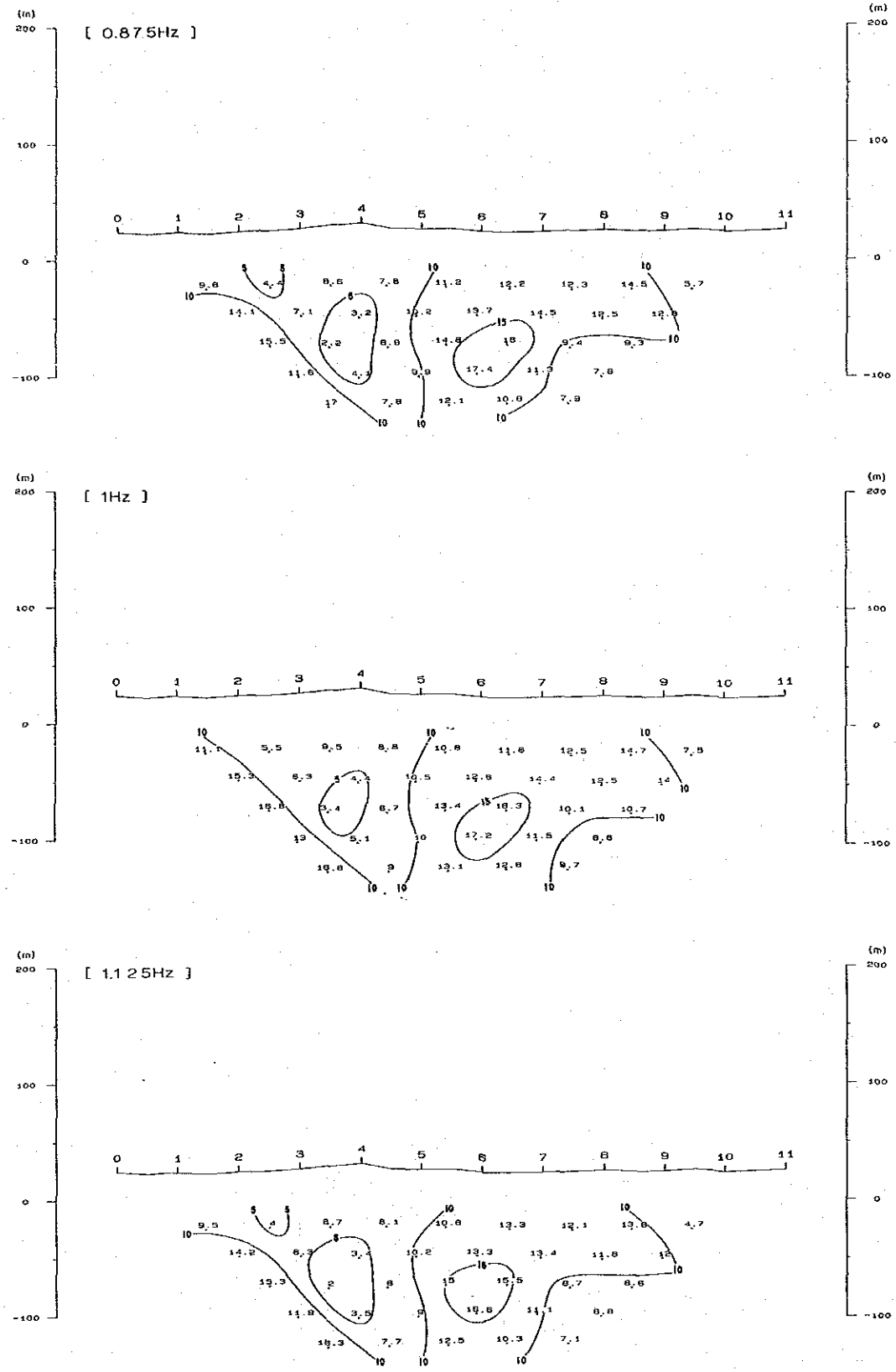

Fig. Ⅱ-27-2 Raw Phase Pseudo-Section of Line D (2)

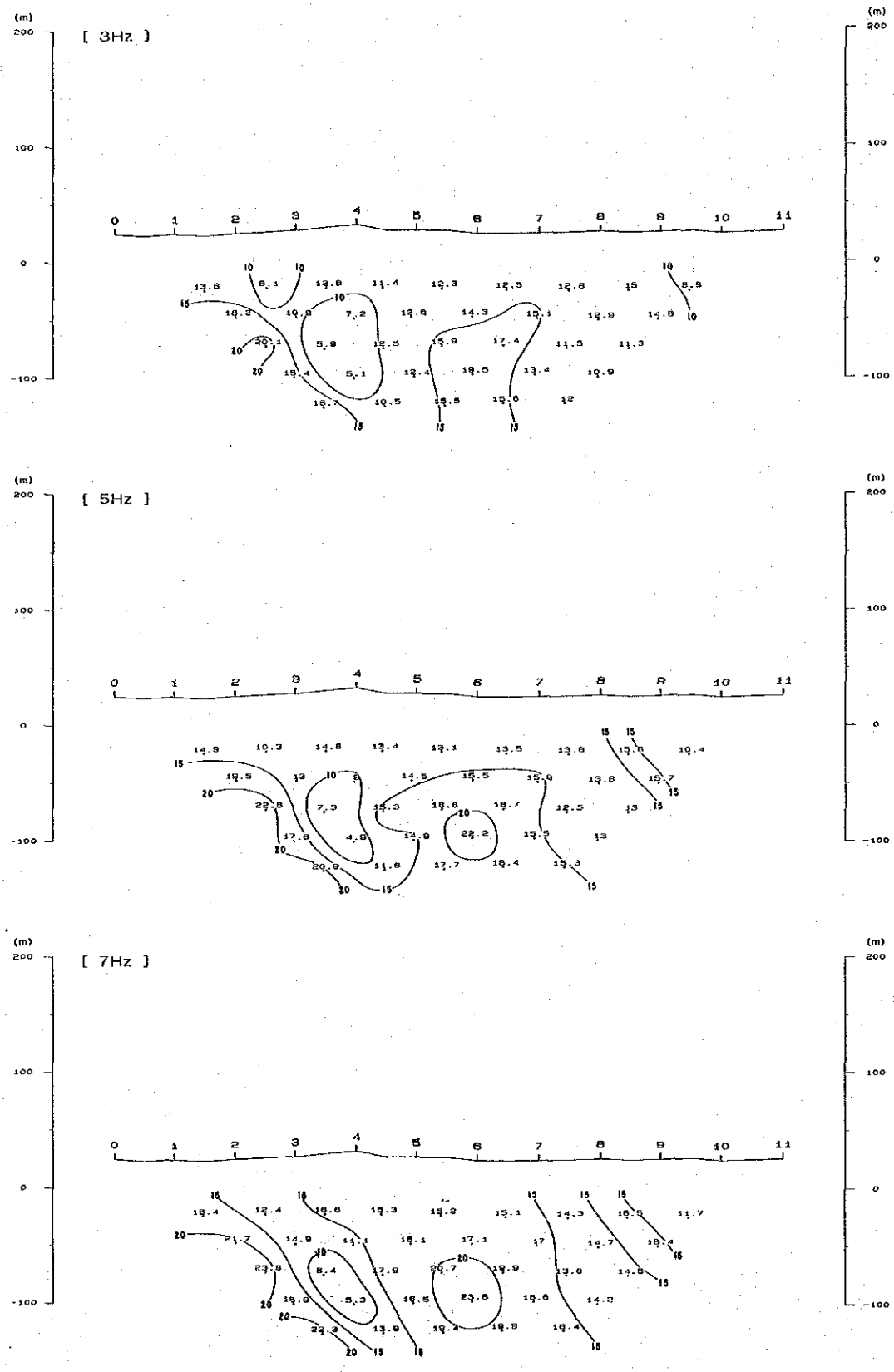

Fig. Ⅱ-27-3 Raw Phase Pseudo-Section of Line D (3)

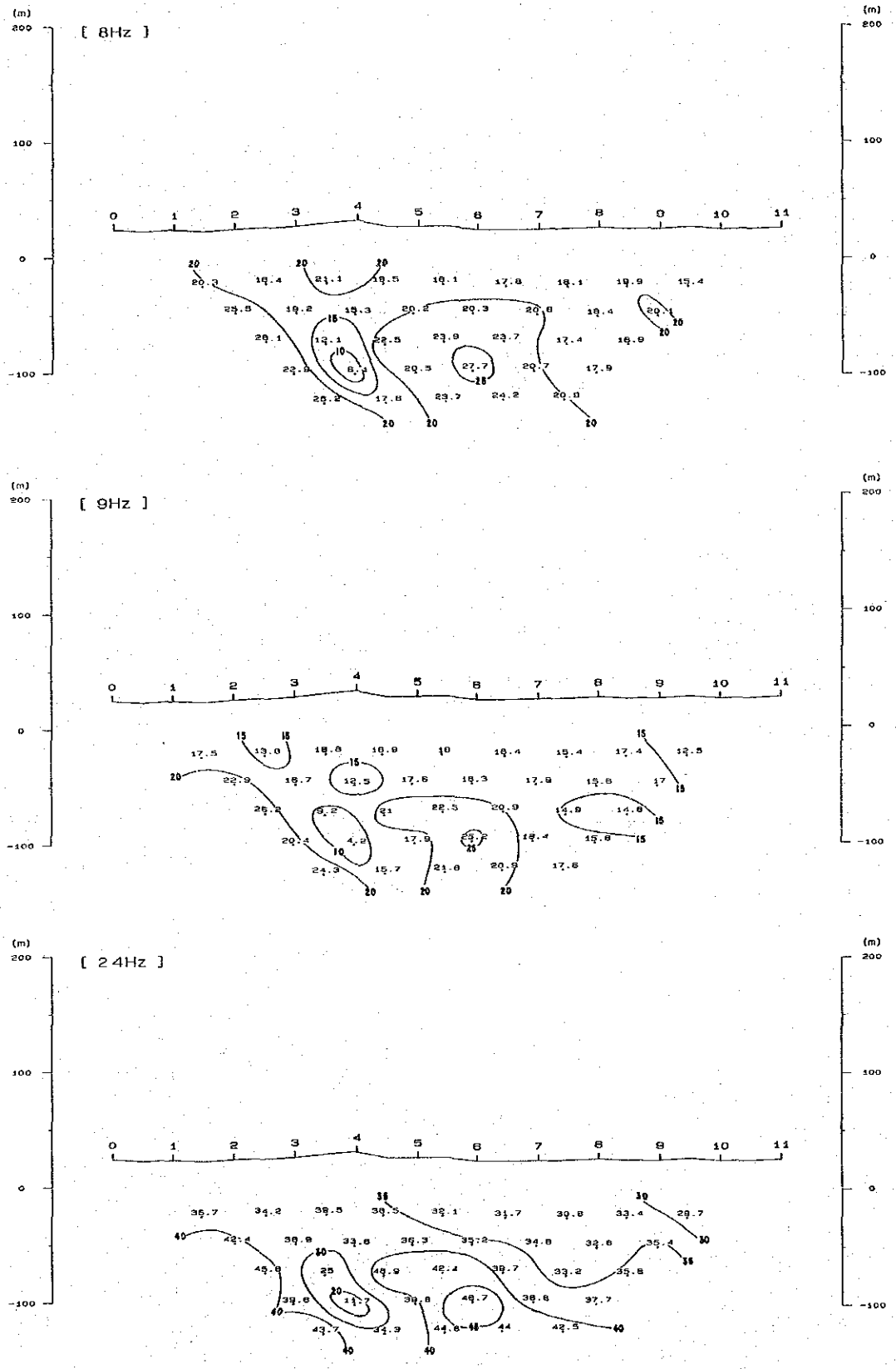

Fig. Ⅱ-27-4 Raw Phase Pseudo-Section of Line D (4)

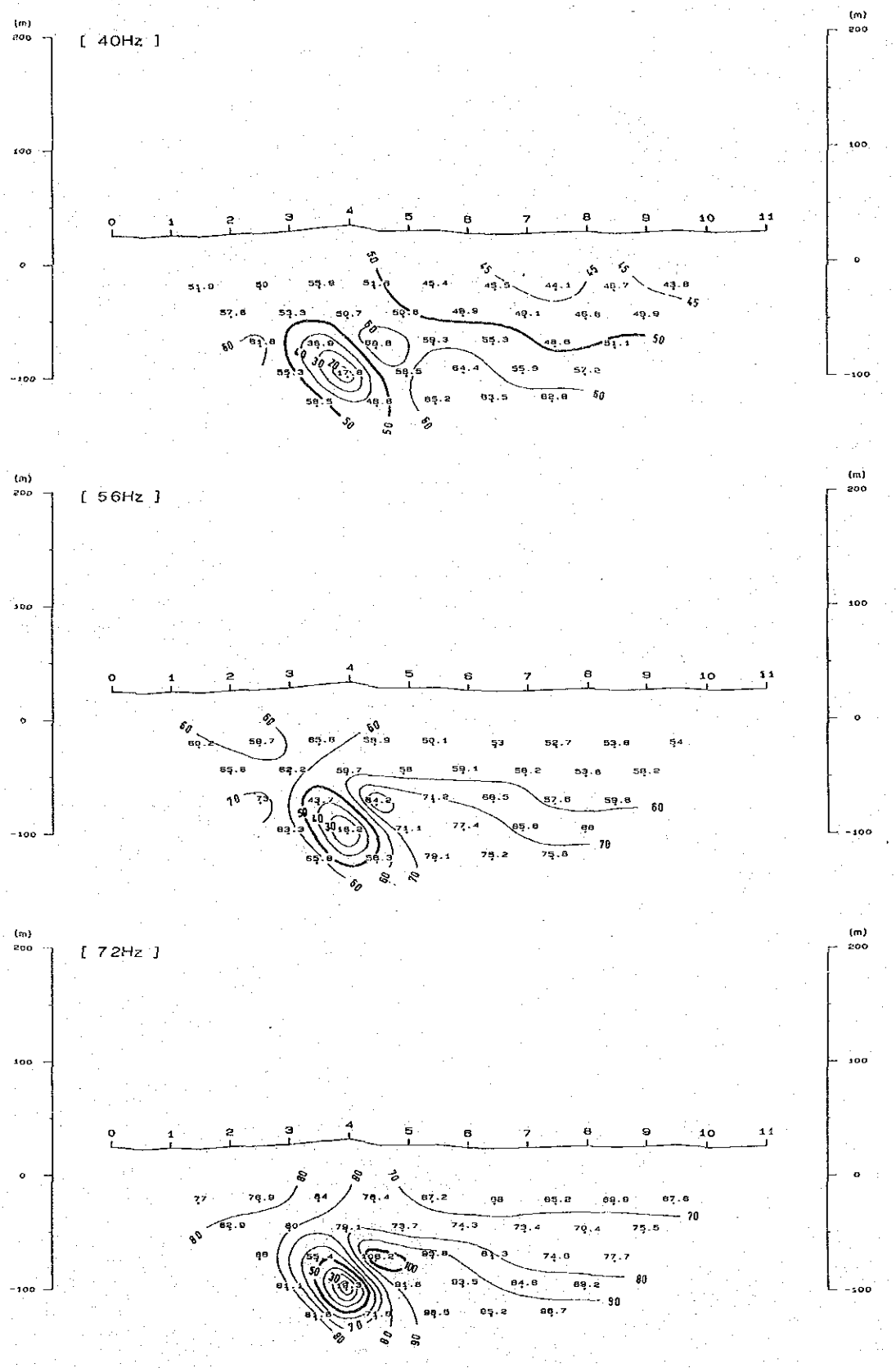

Fig. Ⅱ-27-5 Raw Phase Pseudo-Section of Line D (5)

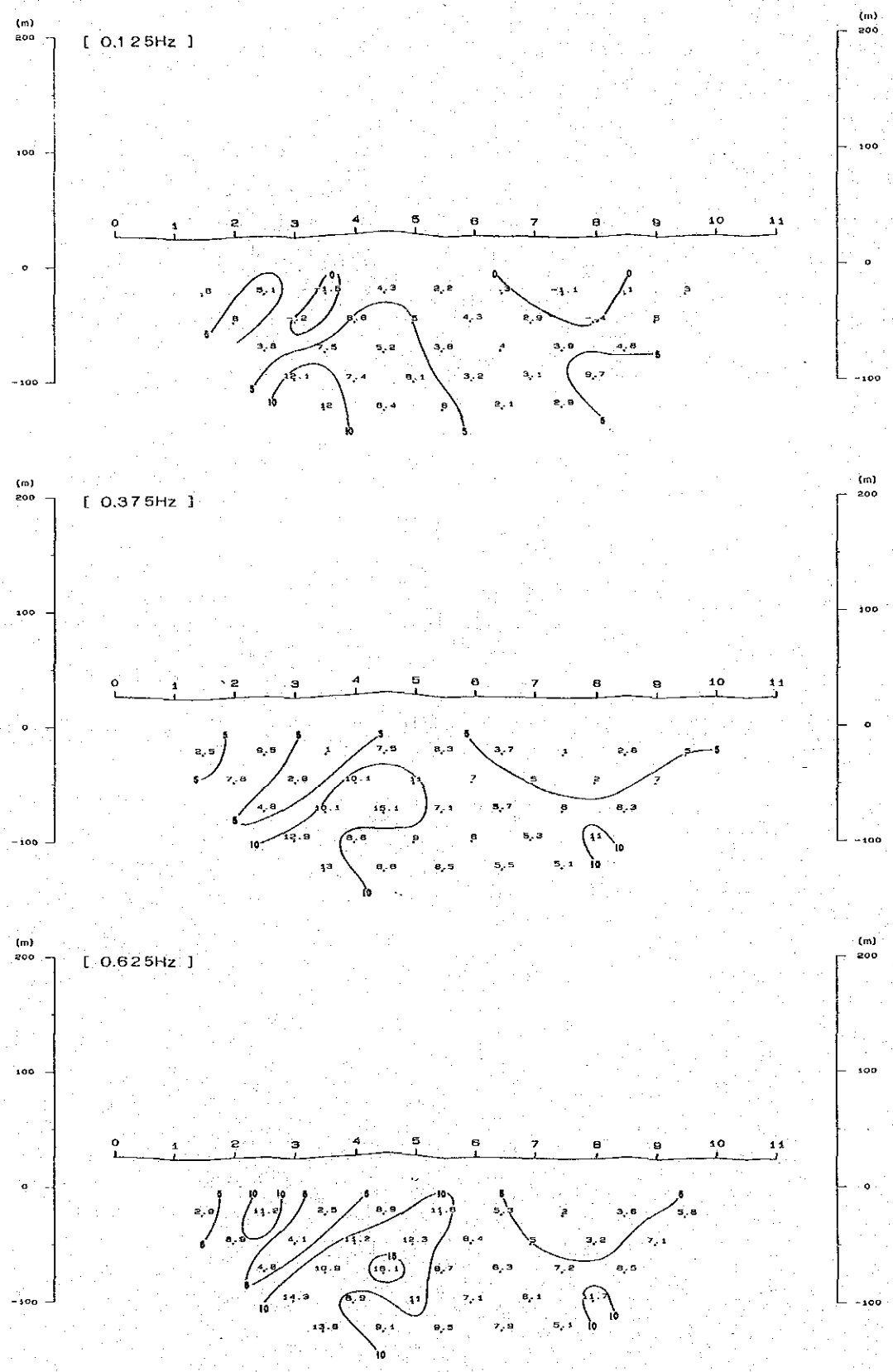

Fig. Ⅱ-28-1 Raw Phase Pseudo-Section of Line E (1)

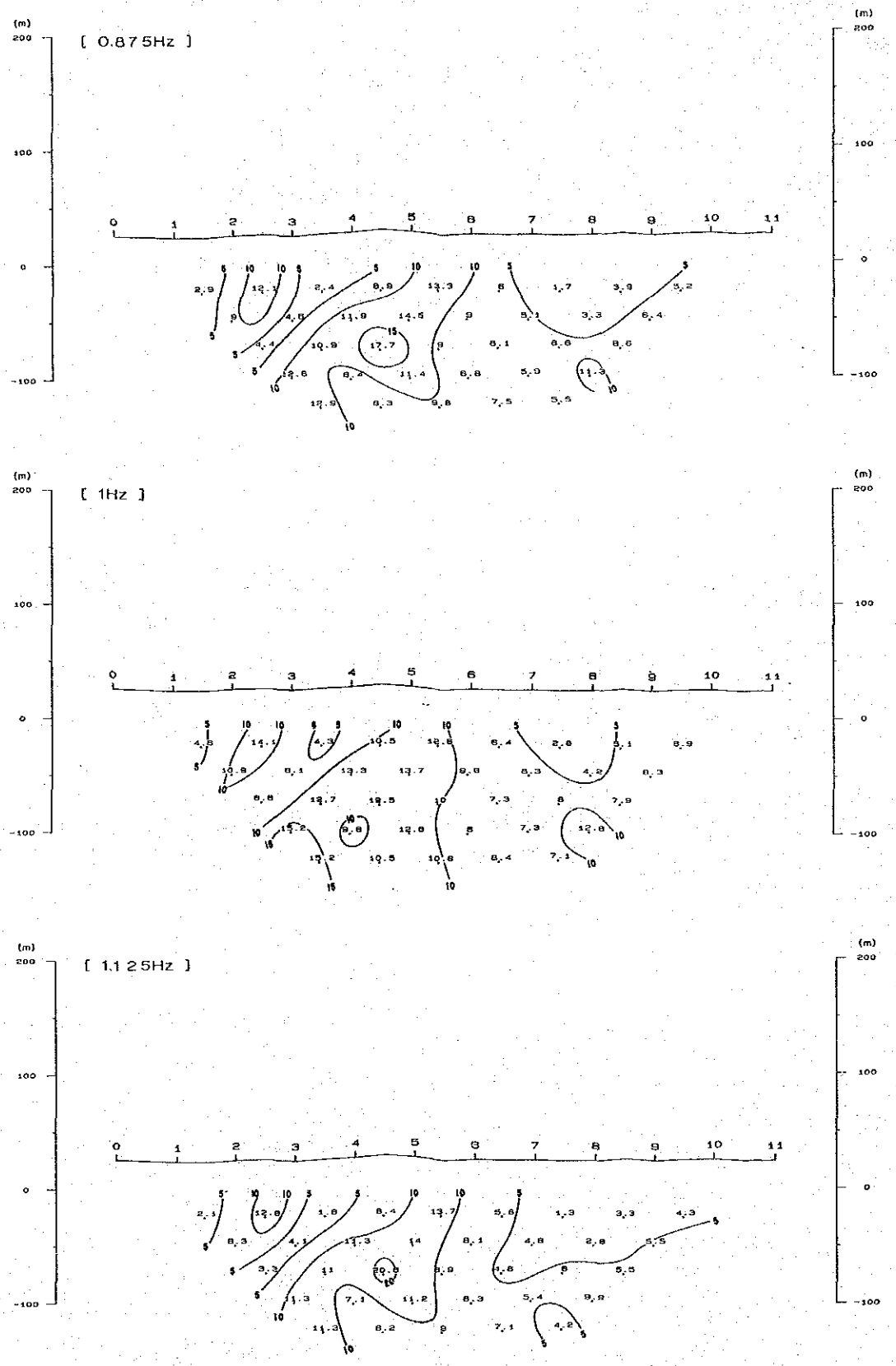

Fig. Ⅱ-28-2 Raw Phase Pseudo-Section of Line E (2)

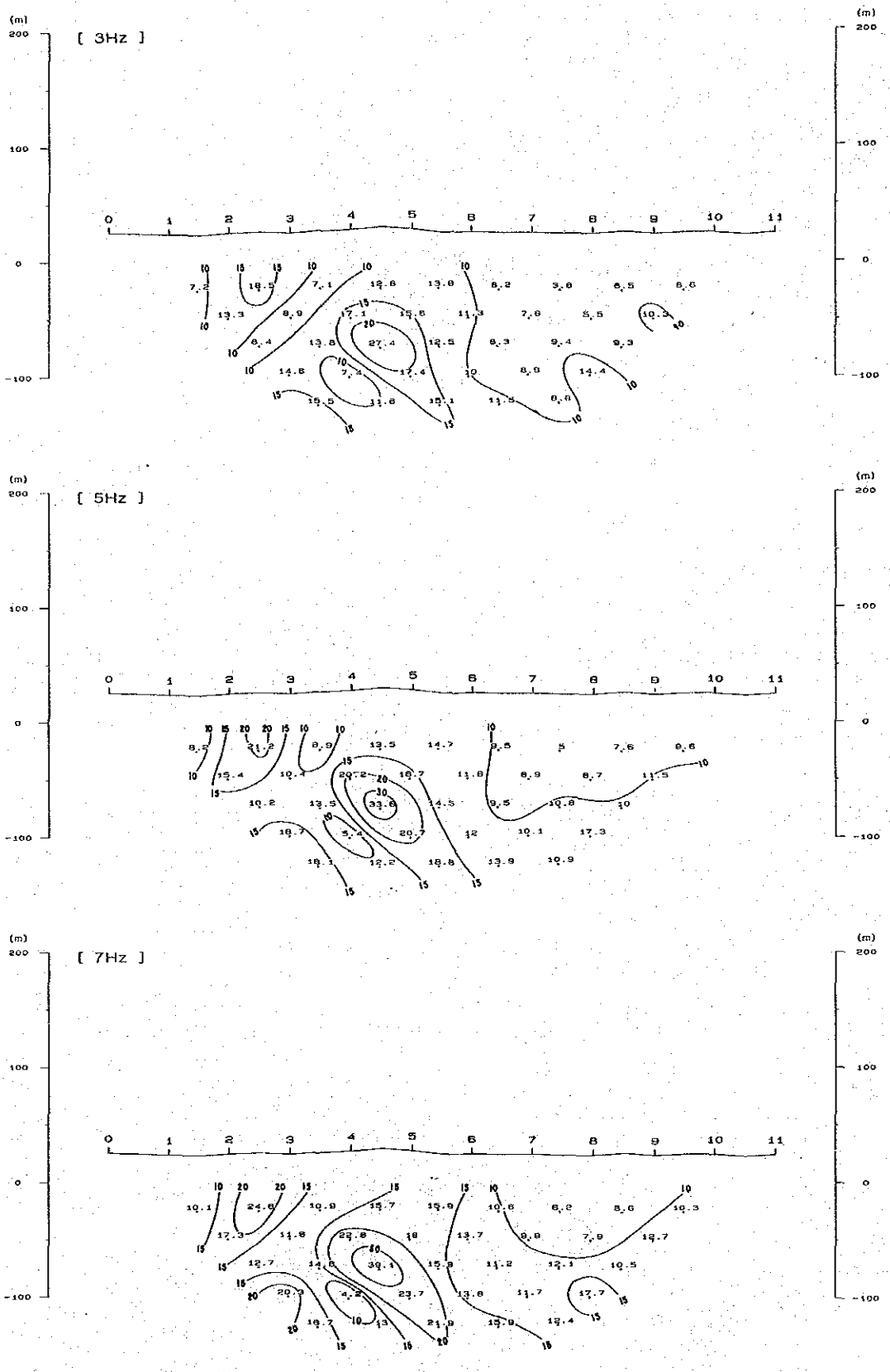

Fig. Ⅱ-28-3 Raw Phase Pseudo-Section of Line E (3)

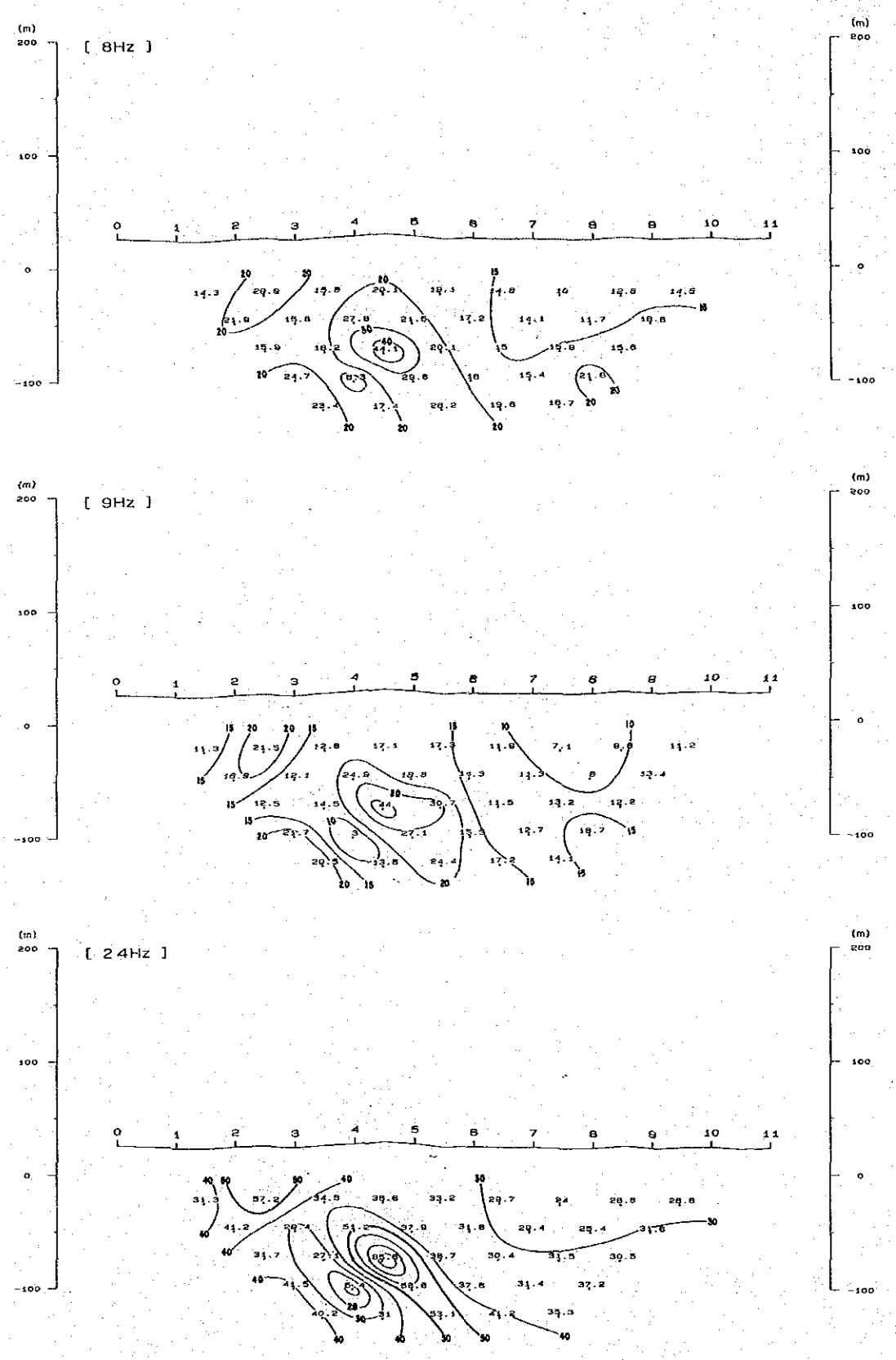

Fig. Ⅱ-28-4 Raw Phase Pseudo-Section of Line E (4)

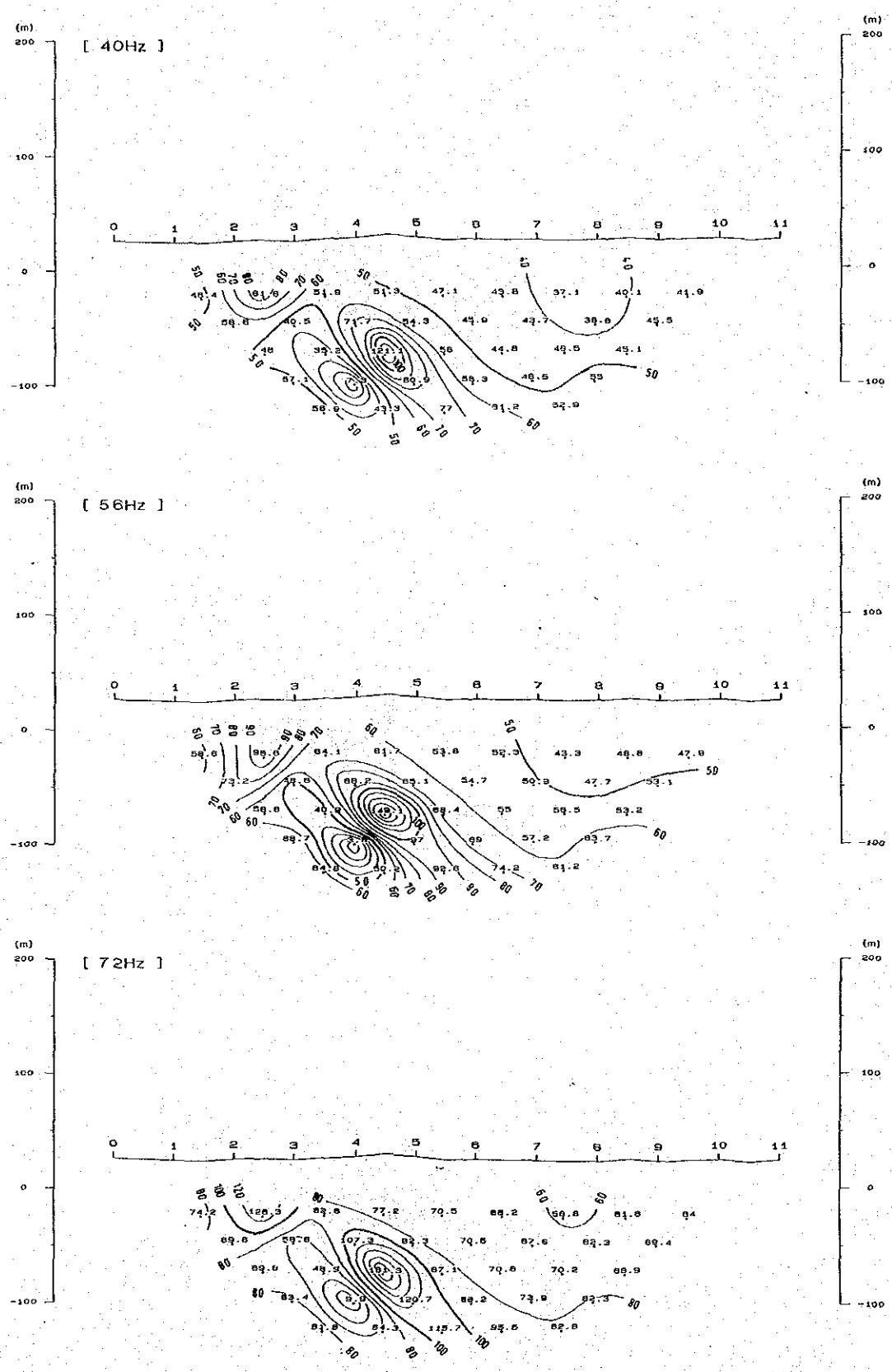

Fig. Ⅱ-28-5 Raw Phase Pseudo-Section of Line E (5)

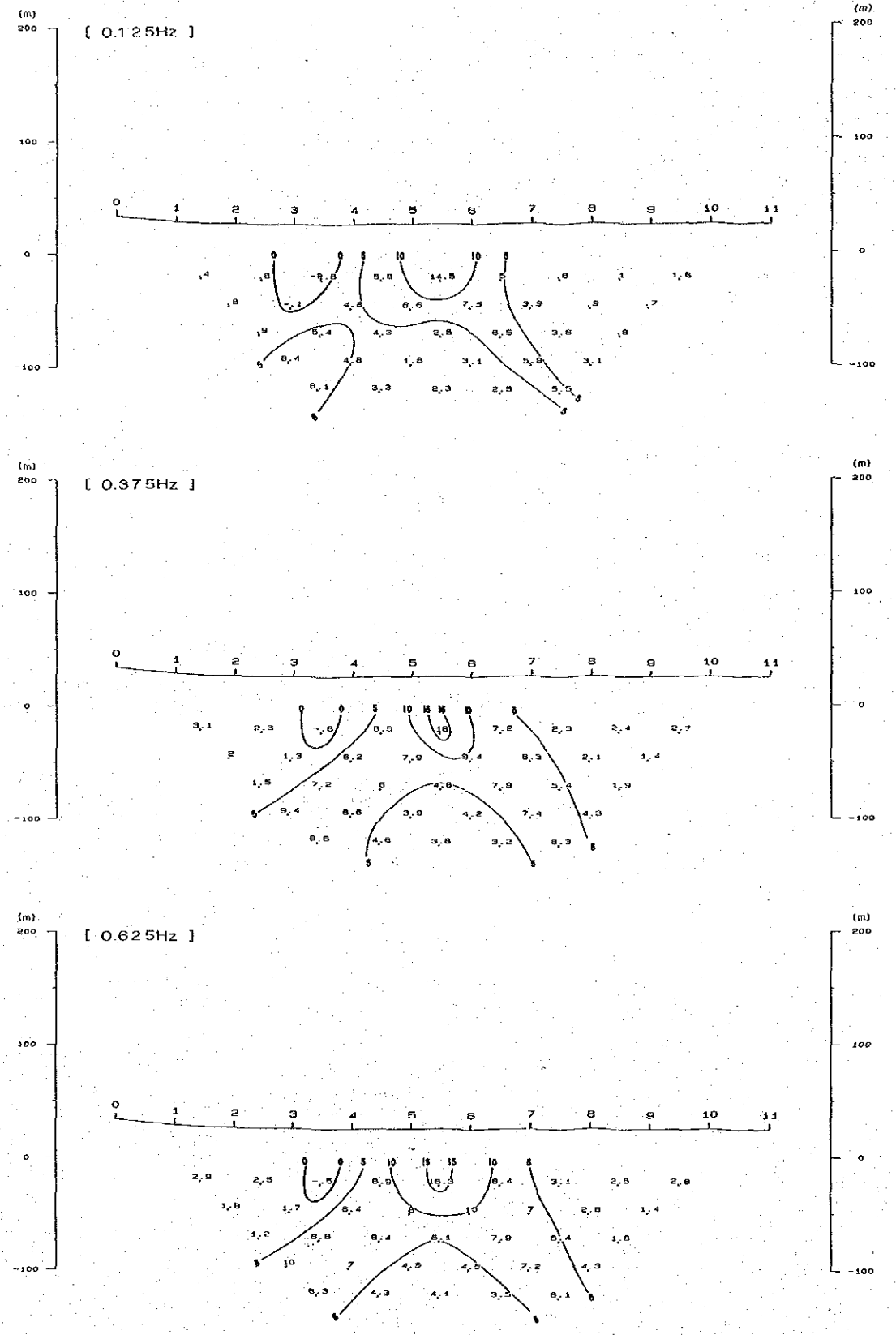

Fig. Ⅱ-29-1 Raw Phase Pseudo-Section of Line F (1)

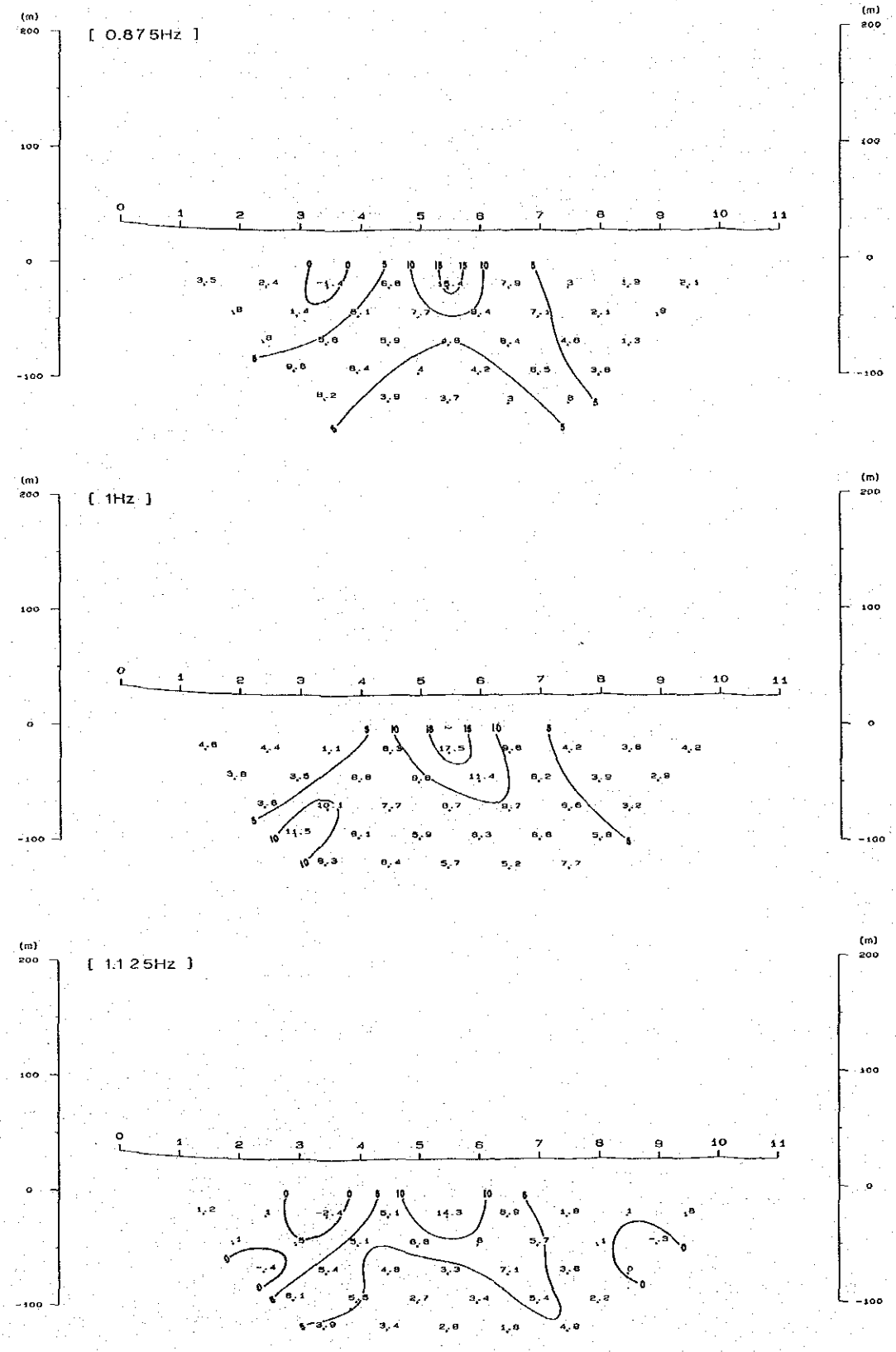

Fig. Ⅱ-29-2 Raw Phase Pseudo-Section of Line F (2)

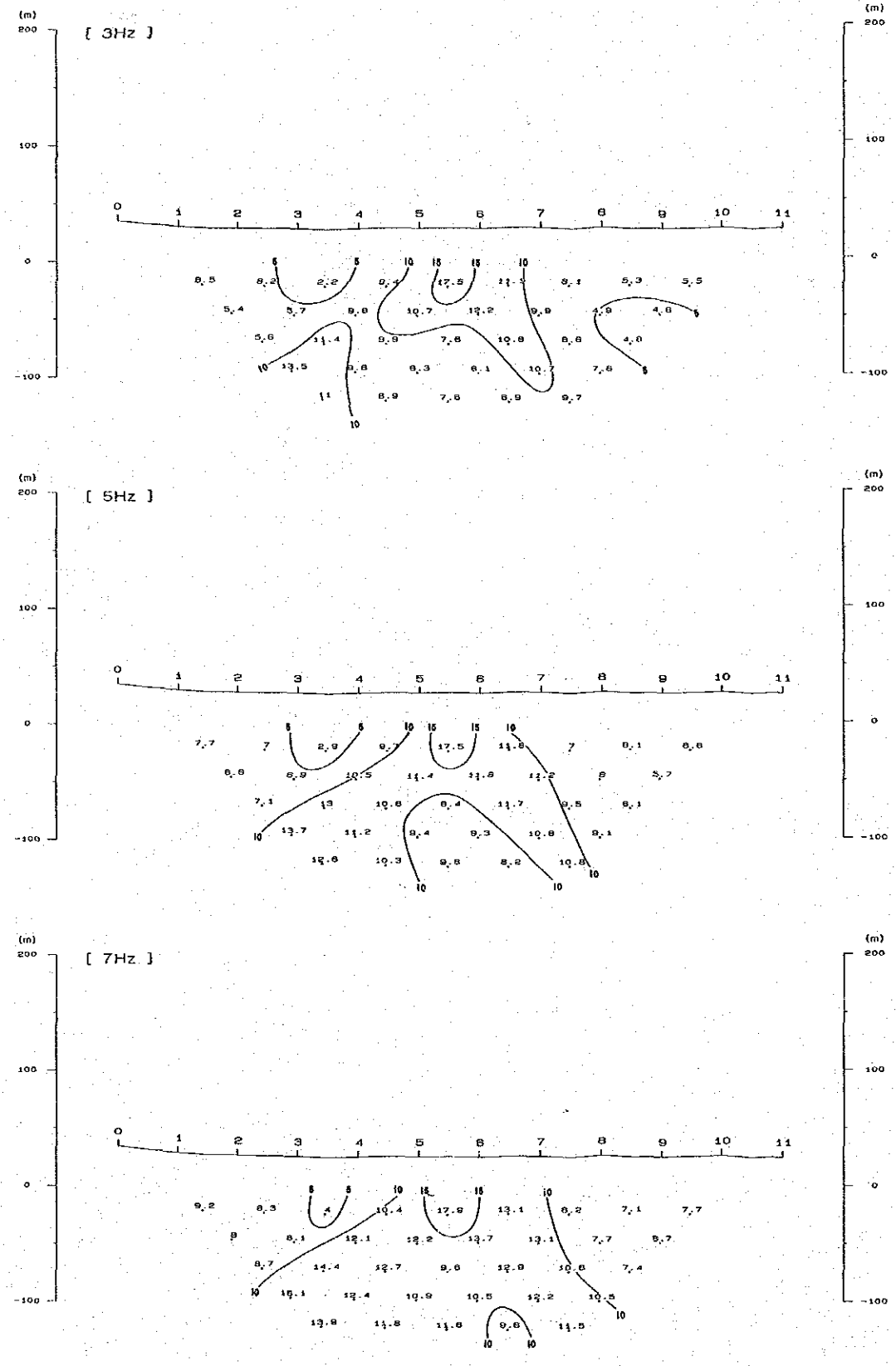

Fig. Ⅱ-29-3 Raw Phase Pseudo-Section of Line F (3)

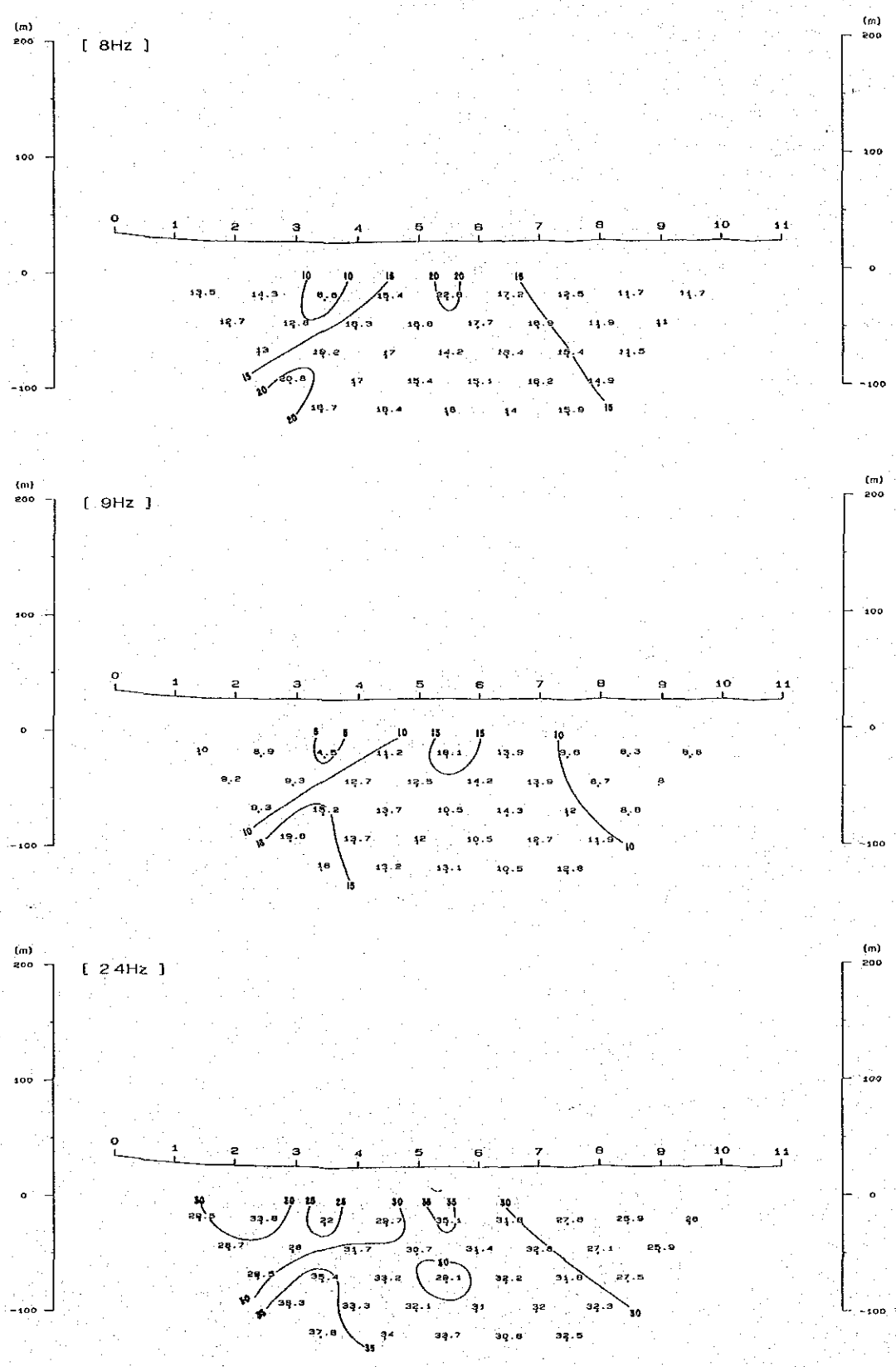

Fig. Ⅱ-29-4 Raw Phase Pseudo-Section of Line F (4)

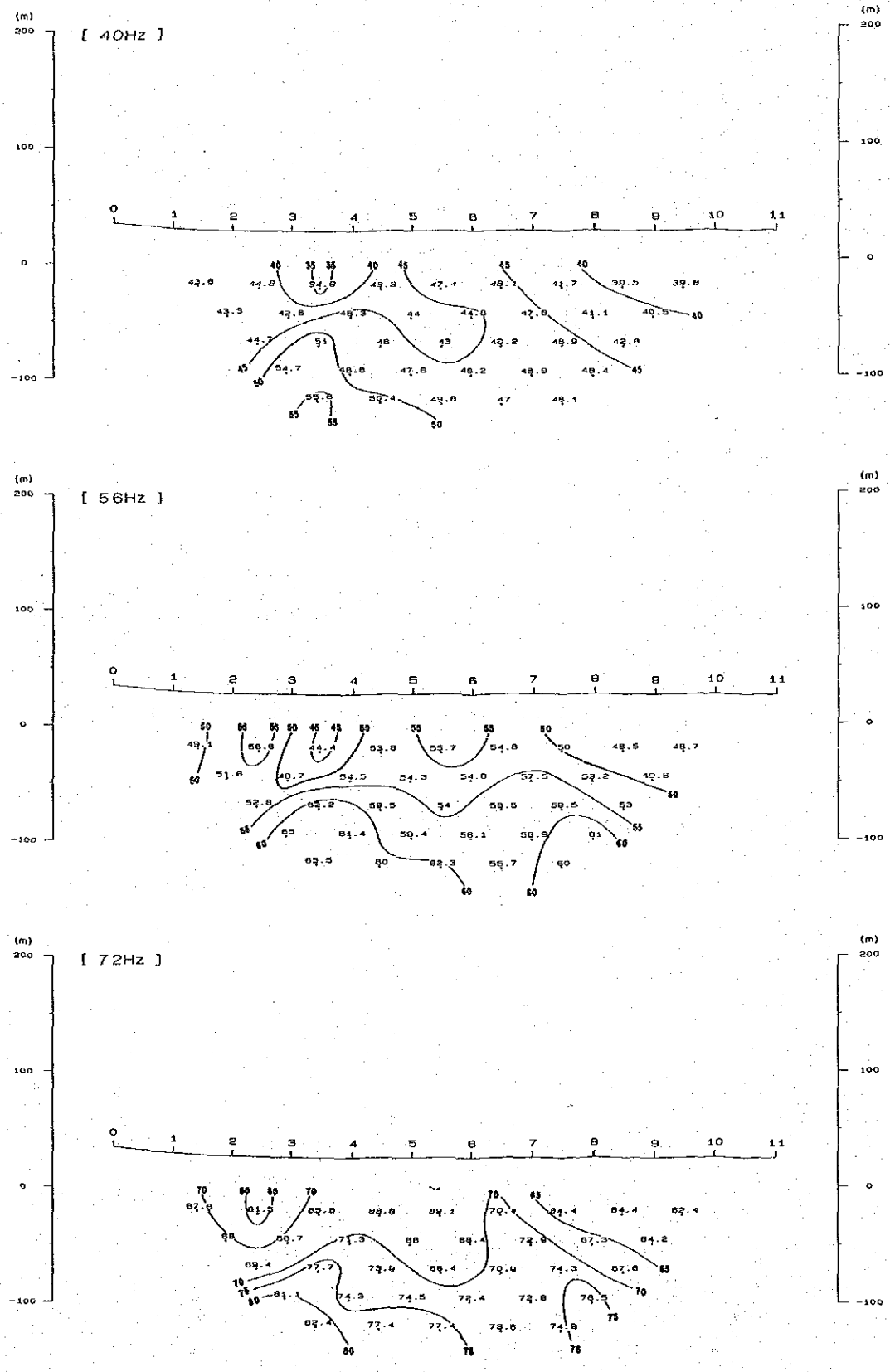

Fig. Ⅱ-29-5 Raw Phase Pseudo-Section of Line F (5)

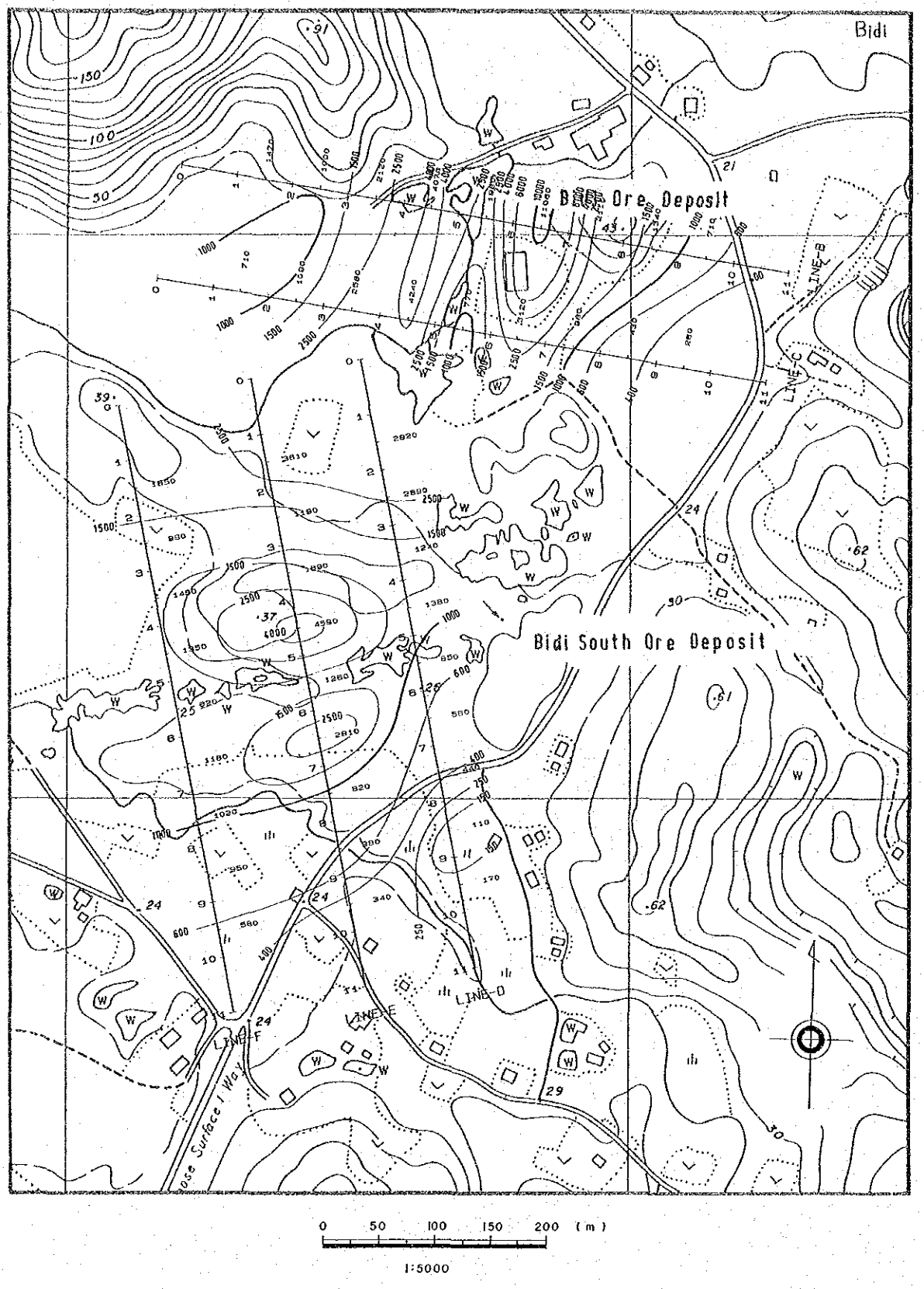

Fig. Ⅱ-30-1 Plan Map of Apparent Resistivity (n=1)

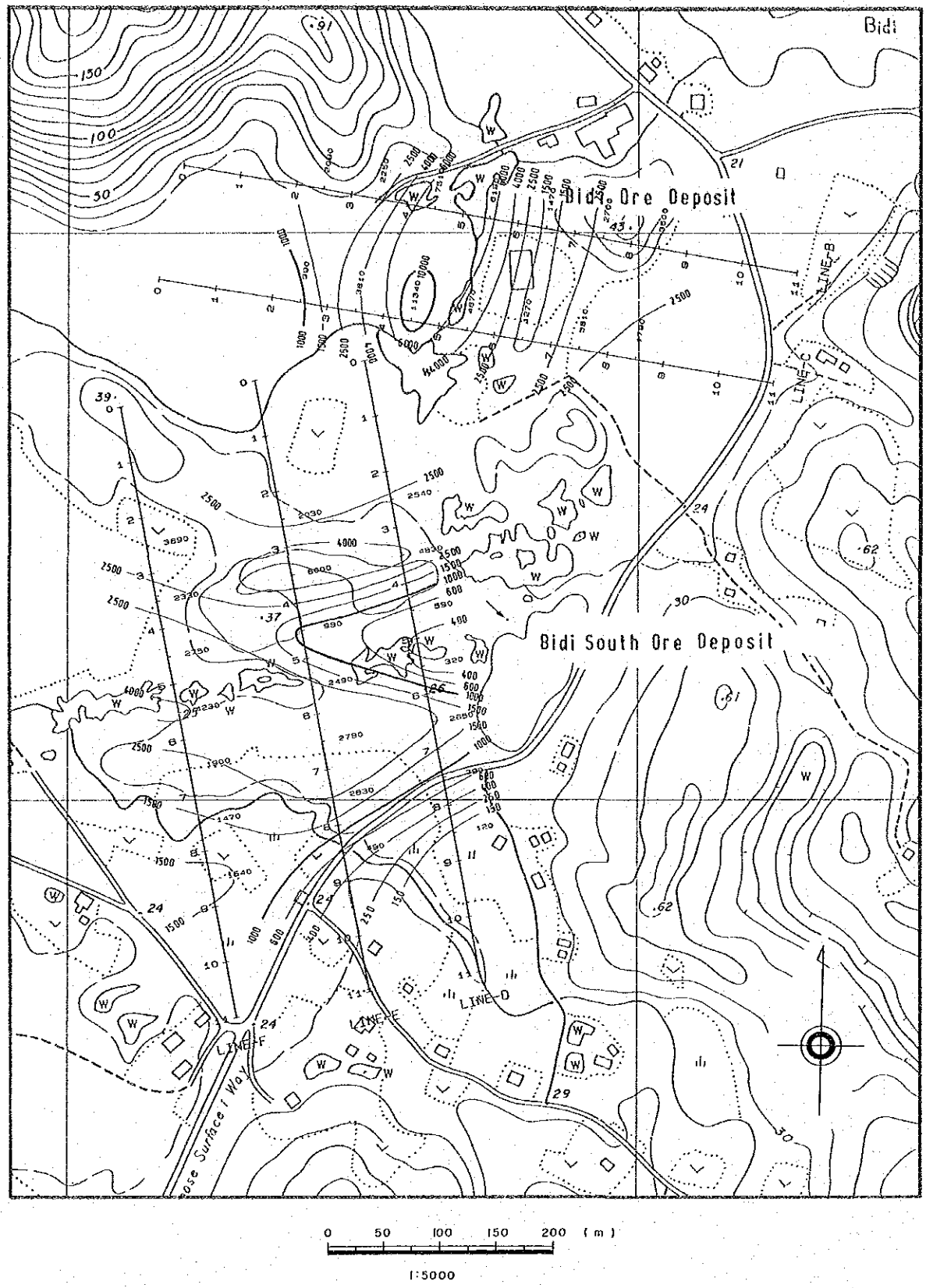

Fig. Ⅱ-30-2 Plan Map of Apparent Resistivity (n=3)

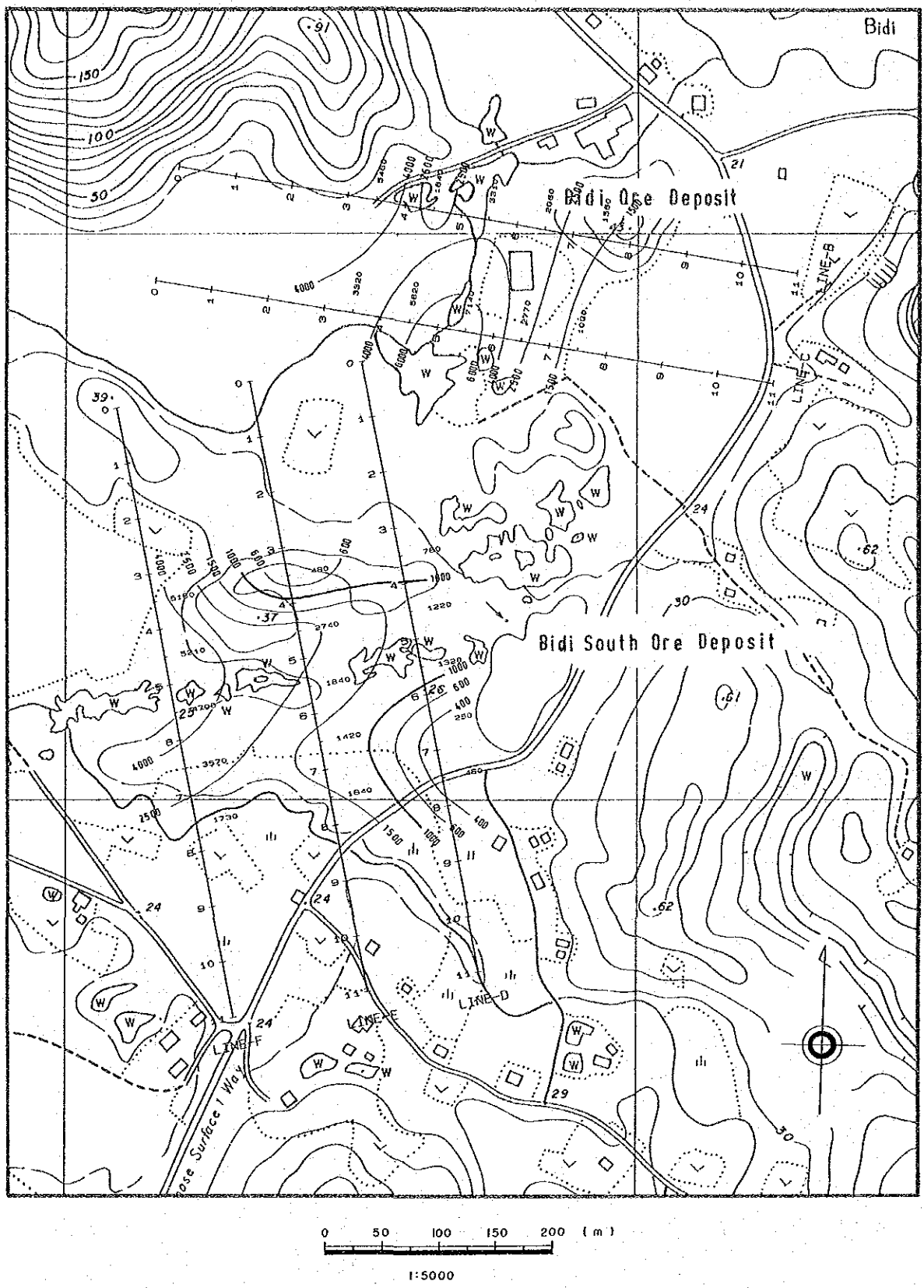

Fig. Ⅱ-30-3 Plan Map of Apparent Resistivity (n=5)

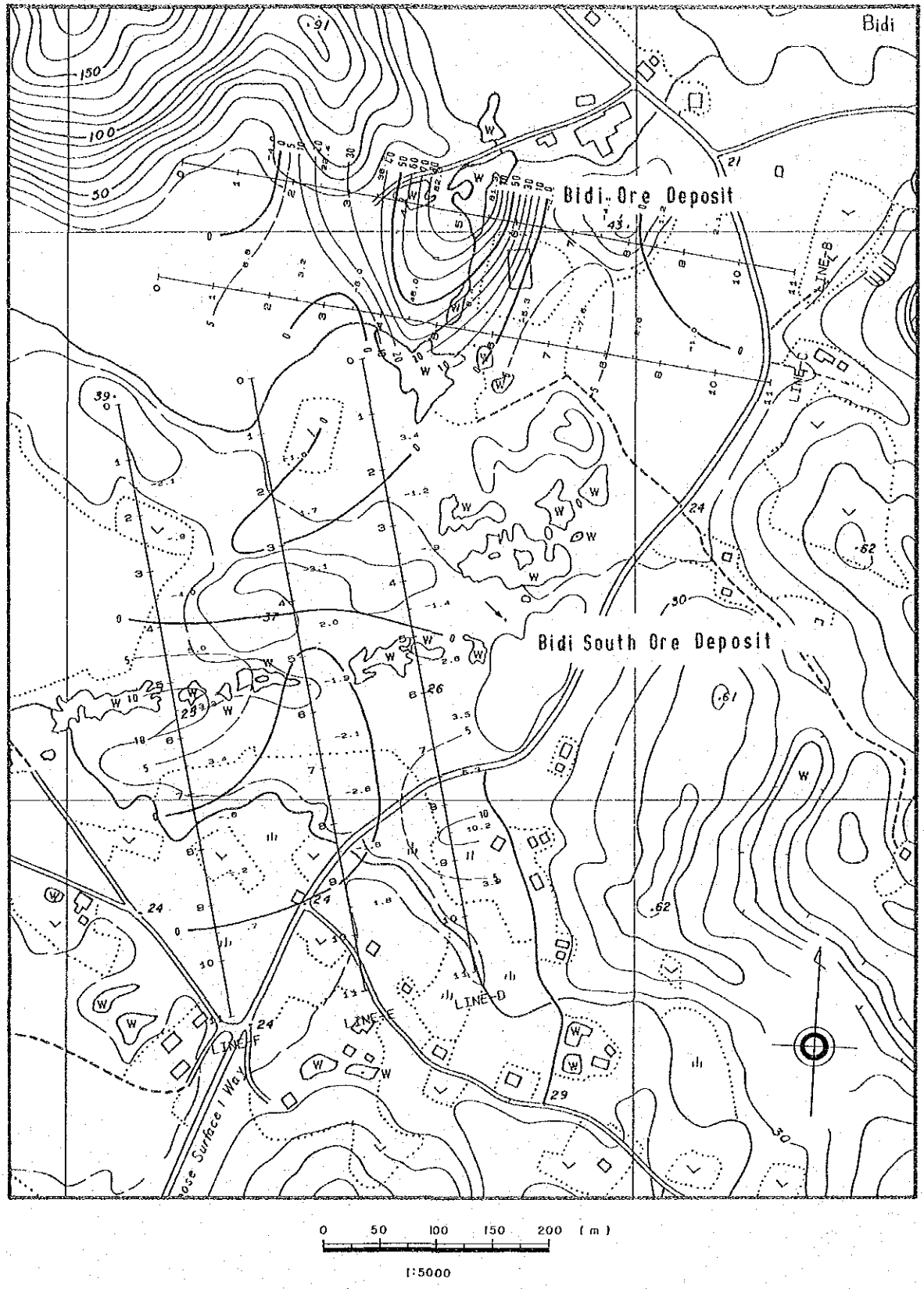

Fig. Ⅱ-31-1 Plan Map of Three-Point Decoupled Phase (n=1)

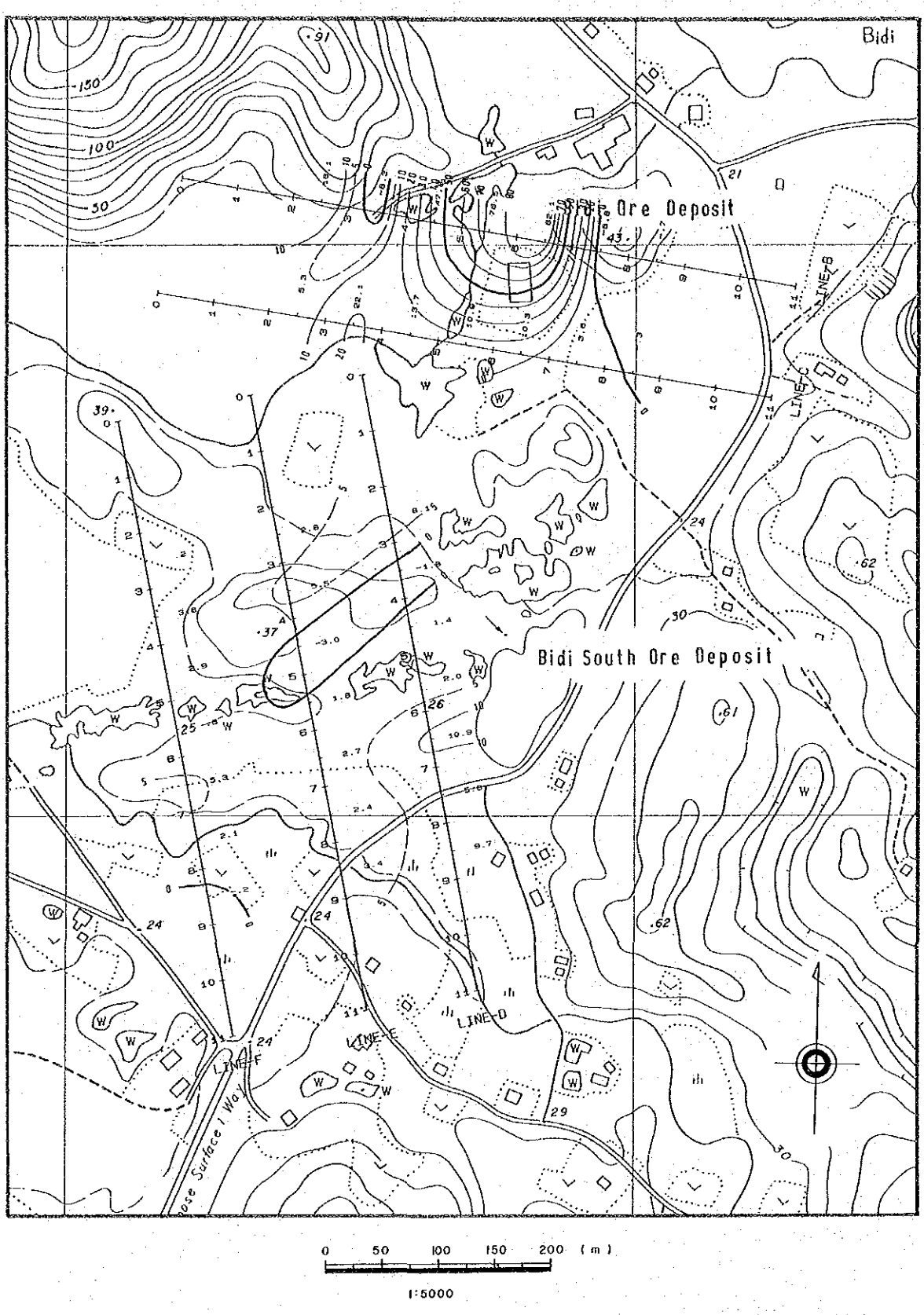

Fig. Ⅱ-31-2 Plan Map of Three-Point Decoupled Phase (n=3)

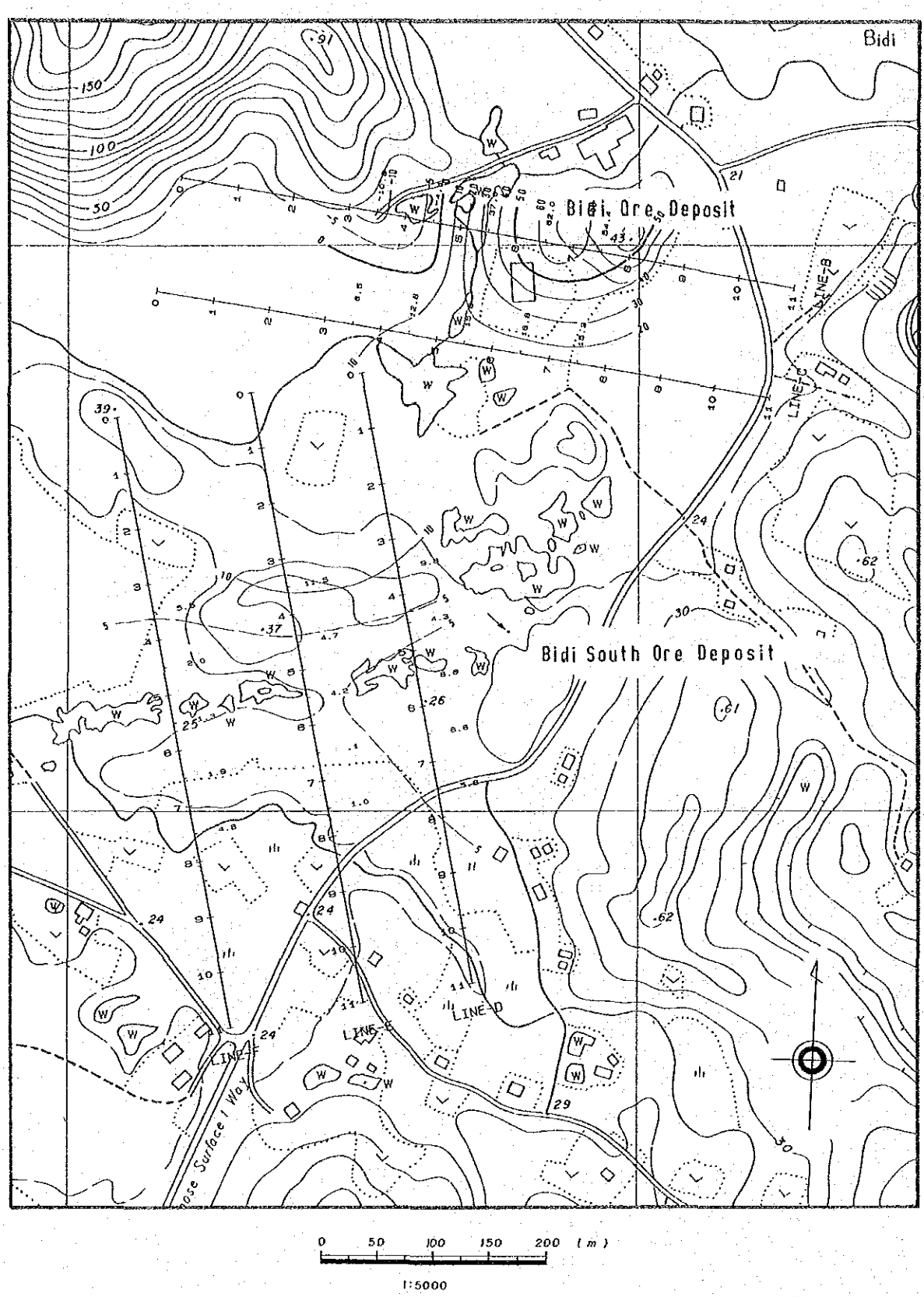

Fig. Ⅱ-31-3 Plan Map of Three-Point Dceoupled Phase (n=5)

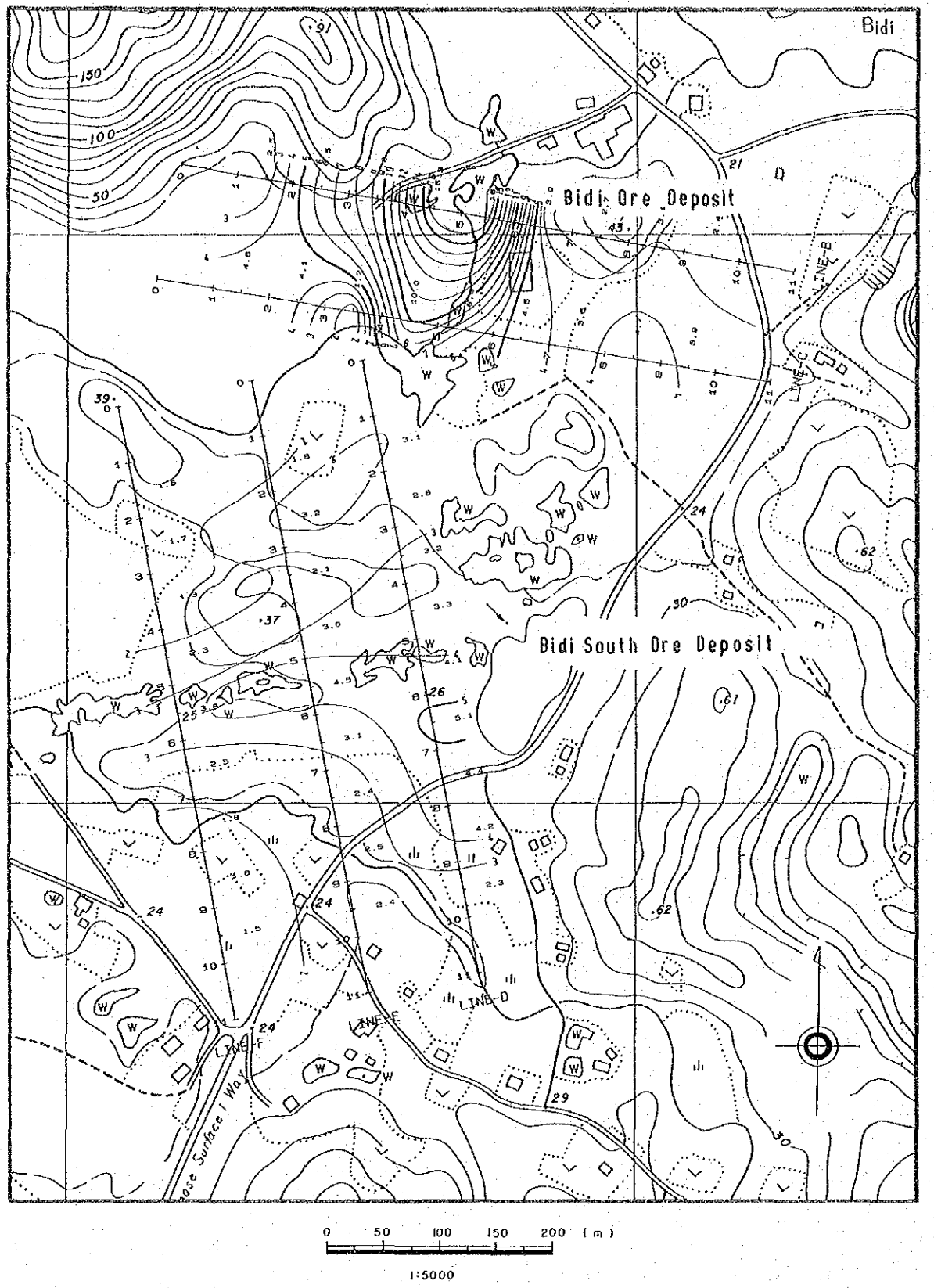

Fig. Ⅱ-32-1 Plan Map of Percent Frequency Effect (n=1)

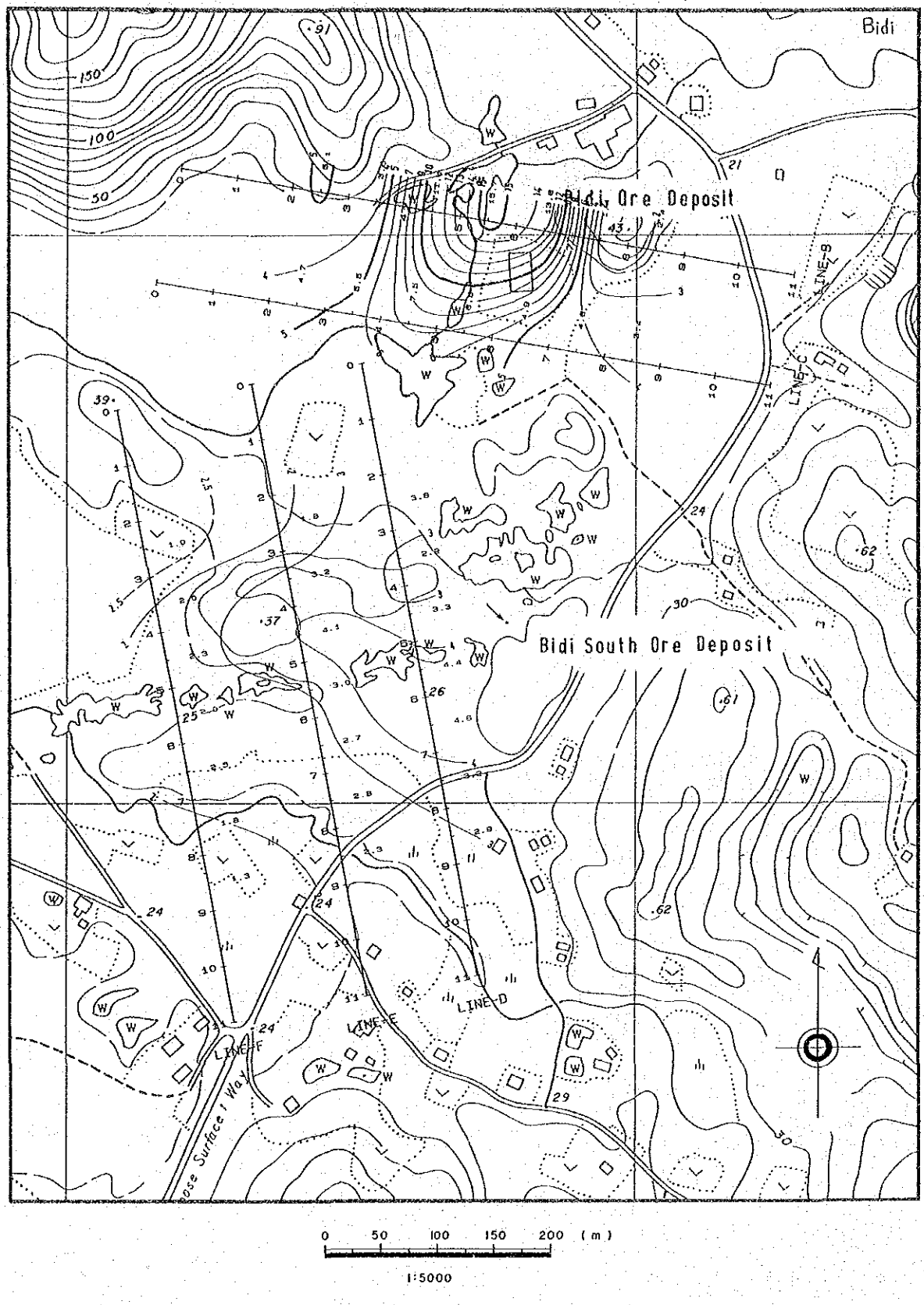

Fig. Ⅱ-32-2 Plan Map of Percent Frequency Effect (n=3)

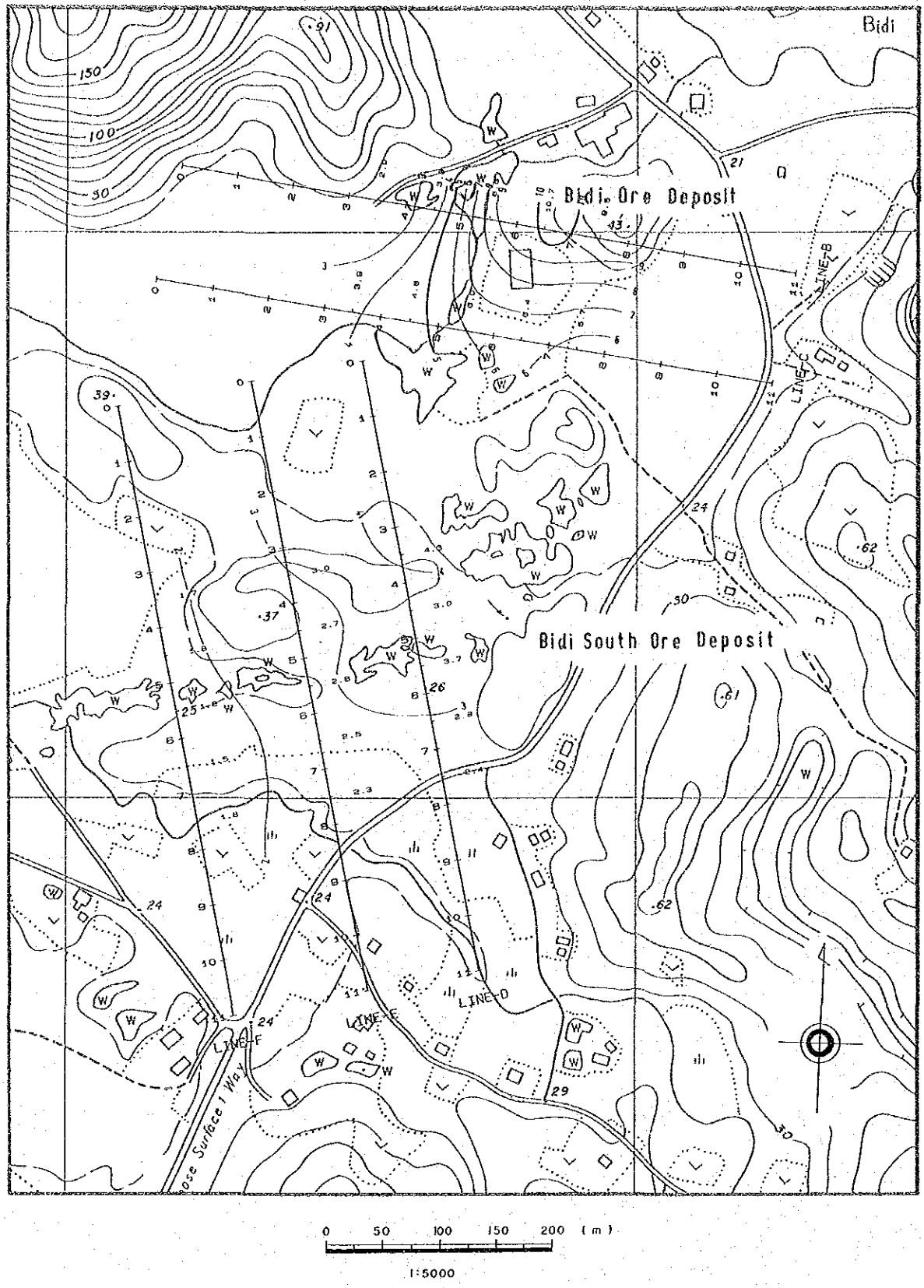

Fig. Ⅱ-32-3 Plan Map of Percent Frequency Effect (n=5)